POLITECNICO DI TORINO

Master of Science in Energy and Nuclear Engineering

Master of Science Thesis

Experimental evaluation of the reactivity of iron oxides in different reaction conditions for the splitting of carbon dioxide in a Chemical Looping process

Tutor
Massimo Santarelli
Domenico Ferrero
Davide Papurello

Candidate
Irene Gramaglia

Abstract

In this work, it is investigated one of the methods for reducing CO_2 emissions into the atmosphere precisely because the problem of climate change is becoming of great interest worldwide, since it affects both the health of the planet and human health. There are various processes for the capture of carbon dioxide such as the Carbon Capture Storage which involves the extraction of CO_2 from the flue gas of fossil fuels and then the storage of it, or the Carbon Capture Utilization which considers CO_2 as a raw material that can be recycled and used as a product or converted into a new product. It can be used, in fact, in the food and beverage industry, as a packaging gas or for the synthesis of pharmaceutical products, but above all it can be used to obtain CO which in turn leads to the production of a clean fuel, i.e. syngas. The carbon dioxide molecule is highly stable; therefore, a high energy vector is required to break one of the C=O bonds. It is of great interest when this energy vector is produced from renewable resources, an example can be CSP (Concentrated Solar Power). Different processes have been proposed for the dissociation of CO_2 but the one that is of greatest interest for research studies, especially for its large-scale application, is Chemical Looping. Today the Chemical Looping process is carried out with non-volatile cycles that use redox pairs of metal oxides, which generally are iron oxides, ceria, or perovskites.

In this work, the experimental investigation of the behavior of iron oxides during a Chemical Looping process is carried out with a focus on the oxidation phase with CO_2 to obtain CO. The production of CO is analyzed for a CO_2 concentration range from 20-40 vol% for a temperature range from 700°C to 1000°C. During the experimental investigation it was noted that the material shows a rapid deactivation with the formation of Fe_3C, namely carbon deposition, in the case in which only thermal reduction is performed, while a gradual deactivation occurs when the reduction is performed with hydrogen. This phenomenon is attributed to a sintering process on the surface of the material. In fact, during the reduction there is a loss of oxygen which leads to the creation of vacancies, while due to the sintering process there is less formation of vacancies which affect the yield of CO and the variation of iron oxide mass. Greater mass variation is a synonymous of greater release of oxygen during the reduction phase. Therefore, to obtain a good yield of CO, the temperature of the oxygen carrier must be between 800-1000 °C with a CO_2 concentration of 20-40 vol%, but first a reduction process with 5 vol% of hydrogen is needed, since this gas tends to reduce the formation of carbon deposition in the material. As a final experimental investigation, iron oxides reaction during the reduction phase with methane is investigated, with oxidation phase performed by carbon dioxide. This cycle shows H_2 formation by methane cracking in the reduction phase and CO_2 splitting with CO formation in the oxidation respectively, thus having the production of useful products in both the steps of the cycle.

Sommario

In questo lavoro è stato illustrato uno dei metodi per poter ridurre la CO_2 dall'atmosfera proprio perché il problema del cambiamento climatico sta diventando di grande interesse a livello mondiale, dal momento che incide sia sulla salute del pianeta e sia sulla salute umana. Esistono vari processi per la cattura di anidride carbonica come la Carbon Capture Storage che prevede l'estrazione di CO_2 dai fumi dei combustibili fossili, per poi stoccarla, oppure la Cabon Capture Utilization che considera la CO_2 come materia prima che può essere riciclata e utilizzata come prodotto o convertita in un nuovo prodotto, essa può essere utilizzata, infatti, nell'industria alimentare e delle bevande, come gas di confezionamento o per la sintesi di prodotti farmaceutici, ma soprattutto può essere utilizzata per effettuare lo splitting della CO_2 per ottenere produzione di CO che porta a sua volta alla produzione di un carburante pulito, detto syngas. La molecola di anidride carbonica si presenta altamente stabile, quindi per rompere uno dei legami C=O è necessario un vettore ad alta energia. Risulta di grande interesse quando tale vettore energetico viene prodotto da risorse rinnovabili, un esempio può essere la CSP (Concetrated Solar Power). Sono stati proposti diversi processi per la dissociazione della CO_2 ma quello che risulta di maggior interesse negli studi di ricerca, soprattutto per la sua applicazione su larga scala, è il Chemical Looping. Oggi il processo di Chemical Looping viene effettuato su cicli non volatili che impiegano coppie redox di ossidi di metallo, che in genere sono ossidi di ferro, ceria o perovskiti.

In tale lavoro viene effettuata l'indagine sperimentale del comportamento degli ossidi di ferro in ossidazione con CO_2 al fine di ottenere produzione di CO mediante un processo di Chemical Looping. Si è analizzata la produzione di CO per un intervallo di concentrazione di CO_2 che varia dal 20-40% in volume per una gamma di temperatura che va dai 700°C ai 1000°C. Eseguendo l'indagine sperimentale si è notato che il materiale mostra una rapida disattivazione con formazione di Fe_3C, ovvero deposizione di carbonio (carbon deposition), nel caso in cui viene eseguita sola riduzione termica, mentre una disattivazione graduale, nel caso in cui venga eseguito una riduzione con idrogeno. Tale fenomeno è attribuito ad un processo di sinterizzazione sulla superficie del materiale, infatti durante la riduzione si ha la perdita di ossigeno che porta alla creazione di vacanze, a causa di tale processo si ha minore formazione di vacanze che incidono sulla resa di CO e sulla variazione di massa. Maggiore variazione di massa è sinonimo di maggiore fuoriuscita di ossigeno durante la fase di riduzione per la creazione di vacanze, questo implica ad una maggiore resa di CO. Pertanto, per ottenere una buona resa di CO, la temperatura del vettore ossigeno deve essere compresa tra 800-1000°C con una concentrazione di CO_2 tra il 20-40% in volume, ed essere prima sottoposto ad un processo di riduzione con 5% in volume di idrogeno, dal momento che tale gas tende a ridurre la formazione di carbon deposition nel materiale. Come ultima indagine sperimentale, gli ossidi di ferro hanno reagito, durante la fase di riduzione con metano, mentre durante la fase di ossidazione con anidride carbonica,

ottenendo rispettivamente, il reforming del metano con formazione di H_2 e lo splitting della CO_2 con formazione di CO, avendo così la produzione di syngas.

Contents

List of Figures

List of Tables

Nomenclature

Abbreviation	
CO_2	Carbon Dioxide
CO	Carbon Monoxide
H_2	Hydrogen
N_2	Nitrogen
Ar	Argon
CH_4	Methane
H_2O	Water
SO_2	Sulfur Dioxide
CL	Chemical Looping
CSP	Concentrated Solar Power
Fe_3C	Iron Carbide
IPCC	Intergovernmental Panel on Climate Change
CCS	Carbon Capture Storage
CCU	Carbon Capture Utilization
MEA	Monoethanolamide
FCC	Fluid Catalytic Cracking
CLC	Chemical Looping Combustion
CLR	Chemical Looping Reforming
SRM	Steam Reforming of Methane
TR	Thermal Reduction
MR	Methane Reduction
WS	Water Splitting
OC	Oxygen Carrier
TGA	Thermogravimetric Analyzer

TPR	Temperature Programmed Reduction
TPO	Temperature Programmed Oxidation
XRD	X-Ray-Diffraction
SEM	Scanning Electron Microscope
OXI	Oxidation Reactor
RED	Reduction Reactor

Symbols

δ	Non-stoichiometry reached
$\dot{\omega}_{CO,oxi}$	CO rate production in oxidation phase
$X_{CO,out}$	Mole fraction of CO
$\dot{n}_{oxi,in}$	Molar inflow in oxidation phase
m_{OC}	Mass oxygen carrier
$\dot{V}^0_{oxy,in}$	Volume flow at standard conditions
P^0	Pressure at standard conditions
T^0	Temperature at standard conditions
K_p	Equilibrium constant of the reaction
$\dot{\omega}_{H_2,red}$	H_2 rate production in reduction phase
$X_{H_2,out}$	Mole fraction of H_2
$\dot{n}_{red,in}$	Molar inflow in reduction phase
$\dot{\omega}_{CO,red}$	CO rate production in reduction phase

Introduction

The world of energy is changing: new policies, technologies and sources suggest the beginning of a long journey towards a new era, an "energy transition" in search of a sustainable consumption model and solutions to combat global warming, climate change and provide, a growing world population, the energy needed to achieve an adequate level of development.

The Earth is overheating, and the scientific community is compact in attributing the cause to anthropogenic emissions of greenhouse gases into the atmosphere. The main of these gases, carbon dioxide, comes for 90% from the energy sector, from coal-fired power plants. To achieve this goal, the main tool is the energy transition, i.e. the transition from an energy mix centred on fossil fuels to one with low or zero carbon emissions, based on renewable sources.

This energy transition process is not new in history. In the past we have seen other great epoch-making changes such as that from wood to coal in the 19th century or from coal to oil in the 20th century. What distinguishes this transition from the previous one is the urgency to protect the planet from the greatest threat it has faced to date, and to do it as quickly as possible. This push has accelerated changes in the energy sector: in a decade (2010-2019) the costs of renewable technologies have decreased by 80% in the case of solar photovoltaics and by 60% of onshore wind. [1]

Solar energy is the one that has received much more attention due to its limitless and ecological characteristics: the Sun will continue to shine for billions of years and that is why solar energy, in addition to being abundant and well distributed, is also inexhaustible in our time scale. The Earth continuously receives from the Sun an immense amount of energy in the form of electromagnetic radiation, in almost all areas of the planet, although with different intensities depending on the latitude.

As a result of the gradual depletion of fossil fuels, combined CO_2 and H_2O dissociation processes have been developed and perfected to produce synthetic gas (syngas), based on the exploitation of heat from solar origin and iron oxide. The latter has established itself as a reference redox material for the realization of two-phase thermochemical cycles and the consequent generation of sustainable fuels. Molecular hydrogen gas is in fact a clean fuel with the highest energy content per unit of mass compared to all other fuels but it is not a primary resource, unlike fossil fuels, extracted from natural deposits: this means that to generate hydrogen from water by electrochemical or thermochemical means it will be necessary to spend energy. The energy sources used to produce syngas play a fundamental role: using a synthetic gas deriving from methane and other carbon-containing substances as fuel does not offer any advantage in terms of environmental impact, as the process would involve the generation of the same amount of CO_2 produced by directly burning the hydrocarbon mixture. The prospect changes completely if an abundant, renewable, and

non-polluting energy source such as solar is used. The thermochemical splitting of CO_2 and H_2O can use the full spectrum of solar radiation to produce CO and H_2. [2]

The objectives of the present work are to study the Chemical Looping the CO/syngas production systems driven by Iron Oxides and are listed as:

- Provide the state of the art on the technologies and reactors that have been explored in the two-step thermochemical conversion of CO_2 and H_2O to produce syngas.
- Illustrate the various physico-chemical characteristics of the materials used, paying close attention to the different behaviors of iron oxides
- Investigate thermochemical dissociation using a moving bed reactor for the reduction and oxidation of a chemical loop CO_2 cleavage unit and to explore the effect of temperature and carbon dioxide concentration in the reduction step and in the efficiency of the entire CL process in order to obtain optimal CO/syngas producibility.

CHAPTER 1
Climate change and techniques to reduce CO_2

The climate change is a problem that today really exist, that turns out to be the enemy of humanity due to of large emissions of pollutants injected into the atmosphere by man. Today we must think to safeguard our planet for the life of future generations.

1.1. Climate change

In recent decades, man has witnessed a sudden climate change, in fact, it has been possible to observe a significant increase in the climatic temperature in the area where he lives with an adjoining shift of the seasons.

The increase in temperature is generally the cause of natural and anthropogenic phenomena. Classically, natural climatic variations occur on a year-to-year or even decade-to-decade scale, maintaining the climate fluctuations that occur over centuries and millennia. Nature, in particular: the earth, the sun, the biosphere and the oceans, continuously exchange CO_2 with the atmosphere, but in addition to the emissions naturally produced by the earth, we must add those deriving from fossil fuels. [3]

Scientific studies show that the rapid warming of the atmosphere is mainly the cause of anthropogenic effects, in fact the increase in the concentration of carbon dioxide in the atmosphere is the result of the combustion of fossil fuels or forest fires that have persisted for years. As shown in Figure 1, the terrestrial environment is capable of exchanging carbon dioxide with the atmosphere, but since CO_2 concentrations have increased over time, carbon dioxide together with other pollutants have created a gas barrier that hinders the exit of terrestrial radiation, the so called greenhouse effect, which causes a rise in the earth's temperature, melting glaciers, risk of flooding and consequences for human health. [4]. The more GHG (Greenhouse Gases) are emitted and accumulated in the atmosphere, the more the earth's temperature increases precisely because as the GHGs released into the atmosphere increase, it becomes more difficult for the earth to evacuate the radiation due to the selective entrapment effect of GHG towards infrared radiation. [5]

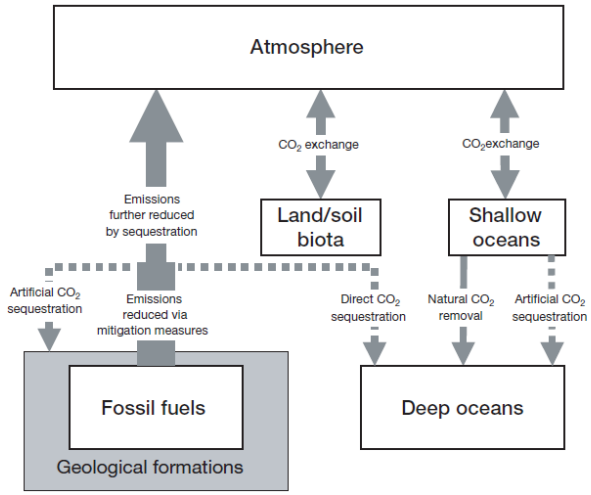

Figure 1 - Carbon dioxide exchange cycle between earth and atmosphere [4]

According to the IPCC (Intergovernmental Panel on Climate Change), human influence on the climate system tends to increase and it is for this reason, that there are the highest greenhouse gas emissions in the history of the world. Earth's surface temperature is expected to rise, and heat waves will occur more often and last longer, while extreme rainfall will become more intense and more frequent in some areas. For this reason, through the Paris Agreement, the overall goal is to strengthen the response to the impending global threat of climate change. One of the goals is to try to keep the global temperature below 2°C above pre-industrial levels and try to combine efforts to limit the rise in this temperature to 1.5°C.

The disastrous effects on earth lead us to understand how important it is today to mitigate these effects. To be able to stabilize the concentrations of greenhouse gases in the atmosphere, it is necessary to try to reduce the consumption of fuels from fossil sources by using fuels from renewable sources, or to remove and sequester carbon dioxide and store it in the oceans or in the soil. [6].

However, there is no doubt that one of the main causes of the global temperature increase is linked to the emission of CO_2 due to the combustion of fossil fuels. In this regard, thanks to scientific innovations, some plant engineering methods come into play to try to reduce CO_2 in the atmosphere. [5]

1.2. Carbon Capture Storage (CCS)

One of the methods to capture CO_2 is CCS (Carbon Capture Storage), initially this technique was designed for carbon extraction and proposed in the late 1970s to improve oil refining after the global crisis, today, the use of CCS aims to extract CO_2 from fossil fuels to fight against climate change. [7]

CCS technologies are part of the supply chain that separates the carbon dioxide emitted by fossil fuel power plants and permanently neutralizes it by removing it from the atmosphere. The solution currently used involves underground storage in geological formations, but other methods for reuse of CO_2 are also being sought. The CCS can contribute for a 20% to reduce emissions by 2050, in the hypothesis of a scenario that foresees, by 2050, a 50% reduction in emissions compared to current levels, as shown in the following diagram Figure 2. [8]

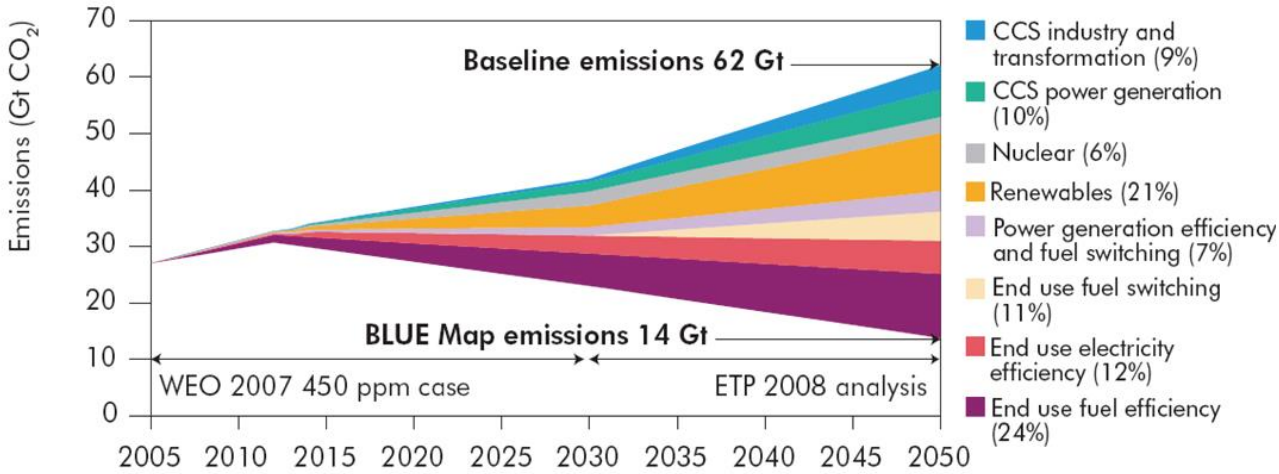

Figure 2 - Forecast of CO_2 reduction by 2050 if CCS were used in combination with other efficient systems [8]

There are currently 26 integrated CCS systems that avoid CO_2 emissions above 30 Mtpa. CO_2 produced in an electrical or industrial system is pre-captured, conditioned, transported via pipelines, railways, or highways, and stored in a suitable body for decades. Depending on the destination of the CO_2 captured by the CCS, the fuel is referred to as oxidized fuel before or after combustion, as shown in Figure 3. [7]

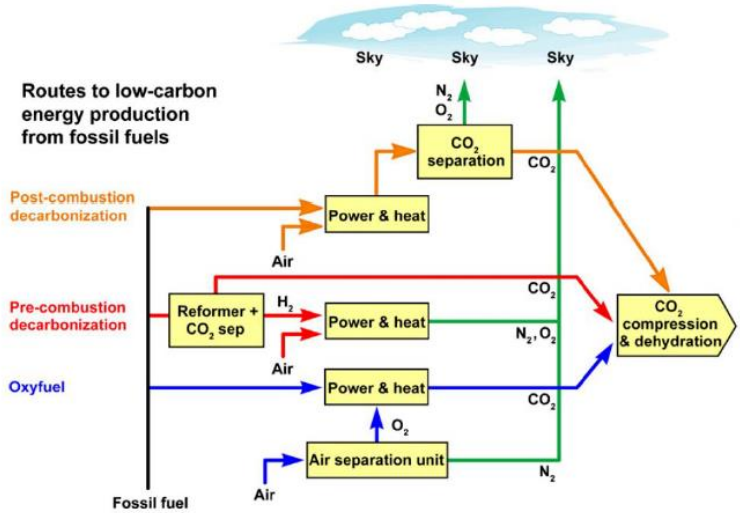

Figure 3 - Different uses of CO_2 in the three methods of oxyfuel, pre combustion and post-combustion to send only N_2 and O_2 into the atmosphere [7]

Today, CCS technologies are already available, even if at very high cost, for industrial applications to demonstrate the possibility of generating electricity from fossil fuels with almost zero CO_2 emissions. [8]

In relation to the capture of CO_2 there are basically three methods, applicable to power plants fueled by various fuels, mainly coal and also gas, as shown in the Figure 4:

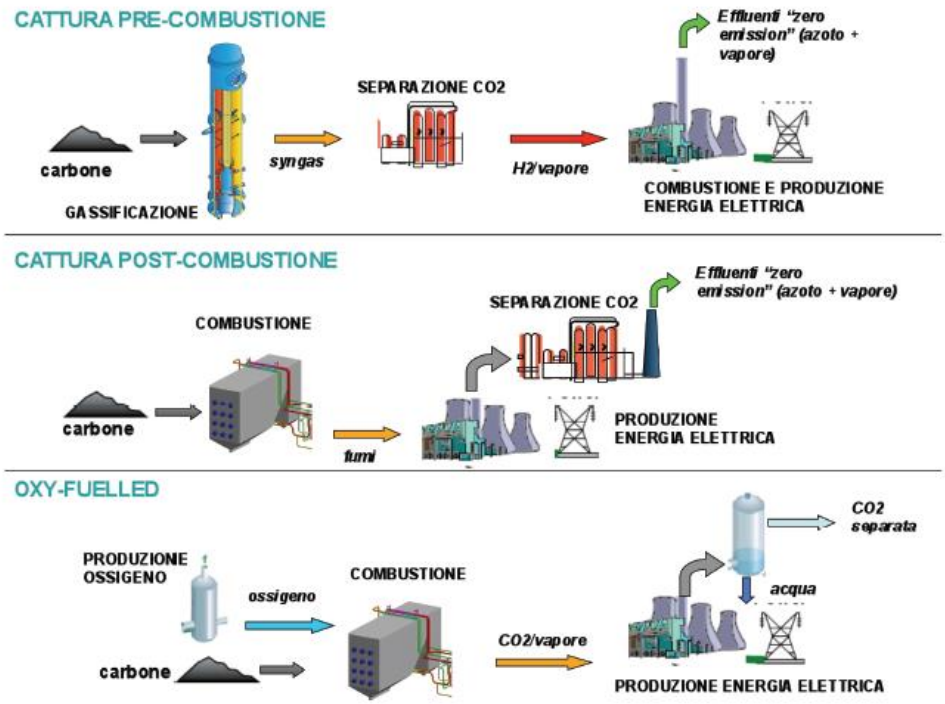

Figure 4 - Illustration of the various steps of the methods applicable to plants for the production of CO_2 from coal or gas [8]

1. *Post-combustion*. It involves the capture of carbon dioxide from the flue gases, therefore at the end of the cycle; with this technique it is necessary to make substantial changes to the plant, but these are expensive and very complex procedures.

2. *Oxy-combustion*. It is a technology studied for coal which, when introduced in pulverized form into the boiler, does not burn with air but with oxygen (or very enriched air). In this way the concentration of CO_2 in the flue gases is enormously increased, making it less difficult to capture carbon dioxide.

3. *Pre-combustion***.** It is the most promising in the medium to long term and consists in capturing CO_2 before combustion. The fuel (coal or gas) is previously treated by transforming it first into syngas (synthesis gas) and subsequently separating two gaseous streams: a gas with a high concentration of hydrogen destined for combustion (or other uses), and carbon dioxide.

As for the transport and storage of CO_2, the preferred option is that of geological confinement carried out by injection in deep aquifers, injection in exhausted oil or gas wells or injection in non-exploitable coal beds. However, there are technologies that can use CO_2 that is injected into active wells to increase the production of extracted hydrocarbons. [8]

An alternative is to store CO_2 in the oceans, some studies attest that by injecting carbon monoxide at a depth of more than 3 km it can be stored for centuries thanks to the higher density of CO_2 compared to the surrounding environment. Furthermore, the oceans cover

70% of the earth's surface which implies the possibility of having a reservoir for an enormous amount of CO_2 to be stored. In addition to the advantages just outlined, there are some disadvantages, there are, in fact, some controversies about the fact that there may be the possibility that the water will acidify due to the storage of CO_2, which would be disastrous for the marine ecosystem. For this reason, despite the high potential, ocean storage is not seen as a short-term possibility. [7]

Finally, CCS remains one of the most interesting and promising solutions to solve the problem of climate change, especially in the medium term, where fossil fuels are unfortunately still the main source of energy production. However, it has some drawbacks, such as a decrease in the energy efficiency of the system when it is integrated. It is estimated that the energy penalty can vary from 7-15% effectively depending on the carbon capture technology. Additionally, storage due to potential leakage, earthquakes, global capacity, engineering feasibility, and economic expenditure are a controversial and critical part of the CCS network. For this reason, more than a pollutant to be stored, CO_2 can be as a carbon material feedstock to produce new chemicals and green fuels. This idea opens a new branch called Carbon Capture and Utilization (CCU). [7]

1.3. Carbon Capture and Utilization (CCU)

The use of CO_2 as an alternative to storage has received a lot of resonance in recent years in both science and industry. Through the Carbon Capture and Utilization (CCU), the concept of cleaner fuel at the same time sustainable energy savings is established. The advantage of using CO_2 is that it can be recycled and used as a product or converted into a new product. Carbon dioxide is now used in the food and beverage industry but can also be used as a packaging gas or for the synthesis of pharmaceutical products. However, the use of CO_2 in these sectors does not show a sustainable solution to significantly reduce carbon dioxide emissions into the atmosphere.

Today, an attractive sector is the conversion of CO_2 into chemicals and fuels, since through this mechanism it is possible to create a closed cycle, like the one shown in Figure 5, and reduces capture costs.

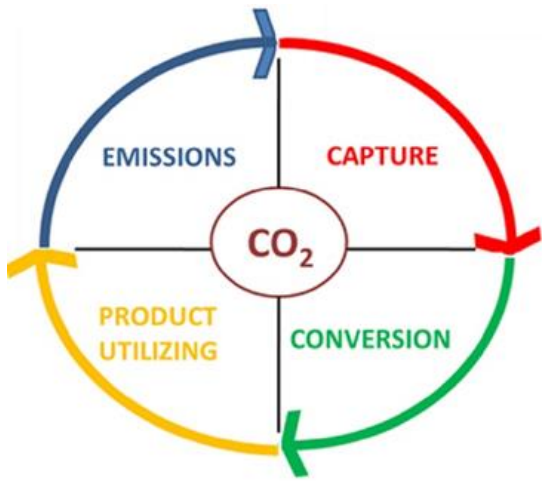

Figure 5 - Closed cycle to reduce emissions into the atmosphere [9]

Initially, this technique was strongly criticized since it is possible the presence of an open cycle if the CO_2 is not captured. CO_2 is used to generate fuel which in turn generates carbon dioxide during the combustion phase which returns to the atmosphere if not recovered.

Today it is estimated that CO_2 recycling helps to reduce 7% of total waste but one of the main disadvantages of CO_2 is that being a very thermodynamically stable molecule and it requires a high amount of energy. Carbon dioxide can be used in carboxylation reactions to carry out the carbonation of the mineral, to generate fertilizers or polymers. As an alternative to carboxylation, it can be decided to further reduce CO_2 by breaking, one or both, the C=O bonds, for the synthesis of new species such as syngas which can be used in several processes for the production of chemical products, and energy. All possible uses of CO_2 are shown in Figure 6.

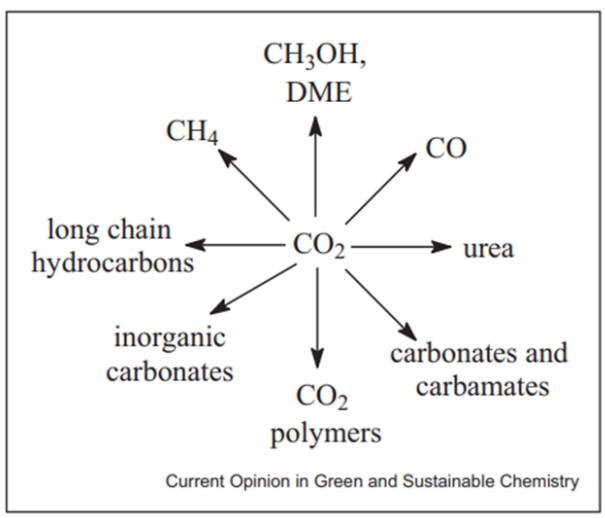

Figure 6 - Areas in which it is possible to use CO_2 as a raw material [9]

However, as already stated, CO_2 is a highly stable molecule, so a high energy carrier is needed to break one of the C=O bonds. Of great interest is when this energy carrier, heat, electricity, high energy reagents (H_2, CH_4 etc.) are produced from renewable resources, an example could be CSP (Concentrated Solar Power) this would make the dissociation reaction a chemical deposit of a renewable source. Several processes have been proposed for the dissociation of CO_2 but one that has received great consideration in research, especially for its large-scale application, is Chemical Looping. [10]

CHAPTER 2
Chemical Looping Technology

Chemical Looping technology is a new indirect combustion process that allows oxygen to be transferred from the combustion air to the fuel. Advances in this area of technology are proving extremely important to reduce CO_2 emissions and to combat global warming. This technology exploits the different oxidation states of a solid-state metal oxide which, circulating in a reactor or between different reactors, transports oxygen atoms and making oxidation possible.

2.1. Chemical Looping

There are two methods for thermochemical CO_2 conversions:

- Direct dissociation
- Chemical Looping

Direct dissociation occurs at extremely high temperatures of 1900-2400°C and this process allows the production of about 6% of CO_2 in CO, but due to the very high reaction temperature at the moment the dissociation of CO_2 is considered a difficult and unprofitable reaction, for this reason the chemical looping method is preferred. [11]

Chemical Looping is based on a principle of a series of chain reactions that take place inside reactors, in which one of the reactants constantly circulates inside the reactor creating a closed circuit. In general, depending on whether the individual reactions are exothermic or endothermic, these systems do not work in isothermal conditions since they have thermal oscillations. [11].

Today, the Chemical Looping is used in both energy and petrochemical engineering, one of the tools is the Fluid Catalytic Cracking (FCC) that is used to break higher order hydrocarbons into shorter chains.

An example of chemical looping used on an industrial level is the monoethanolamine rector (MEA) for carbon capture and storage systems using Carbon Capture Storage (CCS) but it is a system used on a small scale due to lack of economic resources. MEA is used as a post-combustion method for CO_2 separation.

As can be seen in the Figure 7, the exhaust gas is cleaned with monoethanolamine and subsequently cooled and sent to the counter-flow reactor where the amines absorb CO_2, SO_2 and other oxides if present, these then leave the reactor where they are cooled and conveyed to the scrubber.

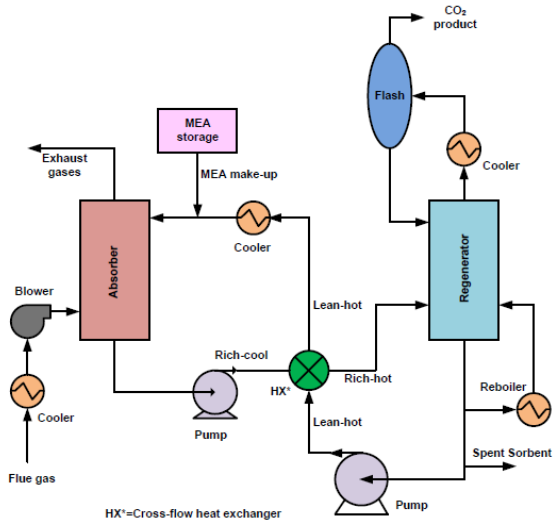

Figure 7 - Monoethanolamine based carbon capture chemical loop diagram [11]

However, new approaches to carbon capture are currently under study, so much so that one of the recent developments has led to the separation of exhaust gases from an oxidant through a Chemical Looping Combustion (CLC) process. [11]

The advantage of using CLC lies in the fact that it has emerged as an interesting solution for CO_2 capture since carbon dioxide is intrinsically separated from other components of the fumes, namely: N_2 and O_2, so no energy is spent on the separation of the gas and is not necessary to implement. The CLC system consists of two fluidized bed reactors, as shown in Figure 8, interconnected, where there is an air reactor and a fuel reactor. Metal oxides are used as oxygen carriers to transfer oxygen from one reactor to another. To date, the CLC study has focused mainly on gaseous fuels but in recent years it has also tried to focus attention on solid fuels such as iron oxides. [12]

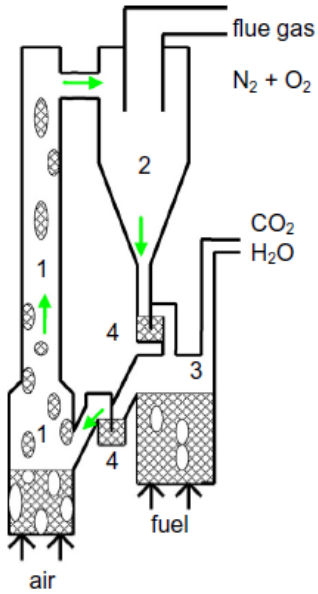

Figure 8 - Example of CLC reactor system for gas (1) air reactor and riser, (2) cyclone, (3) fuel reactor and (4) loop seals. [12]

Most oxygen carriers are low-cost and are highly reactive in respect of syngas released from the gasification phase. Complete conversion of all gas produced is difficult to obtain for this reason CO and H_2 produced by the coal gasification reaction must be converted to allow oxidation, it is necessary to insert oxygen. In this system the oxygen needed for the combustion process is transported by metallic oxides. [12]

Through the process of Chemical Looping, lectured in this paper, we will see the dissociation of CO_2 that requires energy anyway but on a large scale not supplied by fossil fuel but by solar energy, useful in the reduction process. [11]

2.1.1. Chemical Looping Reforming

The abundance of natural gas compared to oil and its lower emissions, have brought considerable interest in the conversion of methane into products with added value. Various studies are currently underway for the conversion of methane that aim to understand the reliability and economic feasibility. In processes like Steam Methane Reforming, methane is converted in a reforming phase into syngas, i.e. a mixture of carbon monoxide and hydrogen, and as we know syngas can be further processed to products with superior added value such as, hydrogen, liquid fuels through various conversion and purification steps.

At present, the processes are carried out in the presence of a catalyst that uses an oxidant such as oxygen (partial oxidation), steam (steam reforming) or carbon dioxide (dry reforming) which can generate deactivation problems due to the formation of carbon on the surface.

An innovative and ecological technology can be the Chemical Looping Reforming (CLR) process which is performed in two interconnected reactors with the presence of a solid oxygen carrier, generally metal oxides, also known as a redox catalyst. The redox catalyst releases its oxygen network (O_2−) to partially oxidize the methane to syngas in the reducer (fuel reactor); the metal oxides, depleted of oxygen, are then transferred to the oxidant to regenerate with a gaseous oxidant. [13]

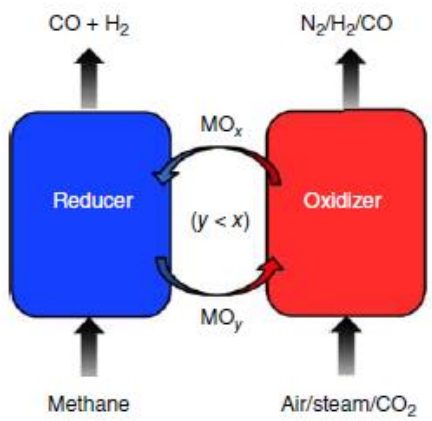

Figure 9 - Schematic of chemical looping reforming; various regeneration options are shown [13]

As shown in the Figure 9, gaseous oxidants that are studied and tested in CLR are air, vapor, and carbon dioxide. The use of steam and/or CO_2 for the regeneration of the redox catalyst, on the other hand, leads to the production of hydrogen and/or CO respectively. The added value of these products can increase the overall efficiency and economy of the process. In these cases, however, the CLR process requires external heat input. The required heat can be met by burning additional fuels or concentrated solar energy. Despite its potential, CLR is still in the early stages of development and faces many challenges to obtain a more active, selective, and stable, more effective redox catalyst and improve gas-solid interaction. [13]

2.2. CO_2 Splitting in Chemical Looping process (CL)

The production of syngas from chemical Looping is an innovative technology based on the splitting of CO_2 or H_2O, to produce CO and H_2 respectively. Generally, there are two interconnected reactors, one acts as a reactor for reduction and one for oxidation. The reactors contain particles of metal oxides that circulate within a closed circuit, alternating the phases of oxidation and reduction.

The operating principle is based on exploiting the two phases of the cycle. During the reduction phase, which generally occurs at temperatures above 1300 °C, a spontaneous release of oxygen is observed from the crystal lattice of the metal oxide, this release of oxygen leads to the creation of vacancies within the lattice of the material . After the

reduction phase, the oxidation phase follows, where the metal oxide is re-oxidized at low temperature with the use of CO_2 or H_2O.

Thermal reduction can be carried out using the solar energy produced by CSP, in fact the redox cycles can work both at atmospheric pressure and in isothermal mode. [11]

In the thermal reduction phase, we will have the reaction illustrated in the equation 2.1

$$MeO_x \rightarrow MeO_{x-\delta} + 0.5\delta O_2 \tag{2.1}$$

Where δ represents the non-stoichiometry factor which is defined as the ratio between the completely reduced form of metal oxide and the still unreacted form.

In the oxidation phase, therefore, the splitting of CO_2/H_2O we will have the reaction illustrated in the equation 2.2 and 2.3:

CO_2 splitting →

$$MeO_{x-\delta} + \delta CO_2 \rightarrow MeO_x + \delta CO \tag{2.2}$$

Water splitting →

$$MeO_{x-\delta} + \delta H_2O \rightarrow MeO_x + \delta H_2 \tag{2.3}$$

A CO_2 / H_2O splitting scheme in a chemical looping using solar thermal is represented by the following scheme at Figure 10:

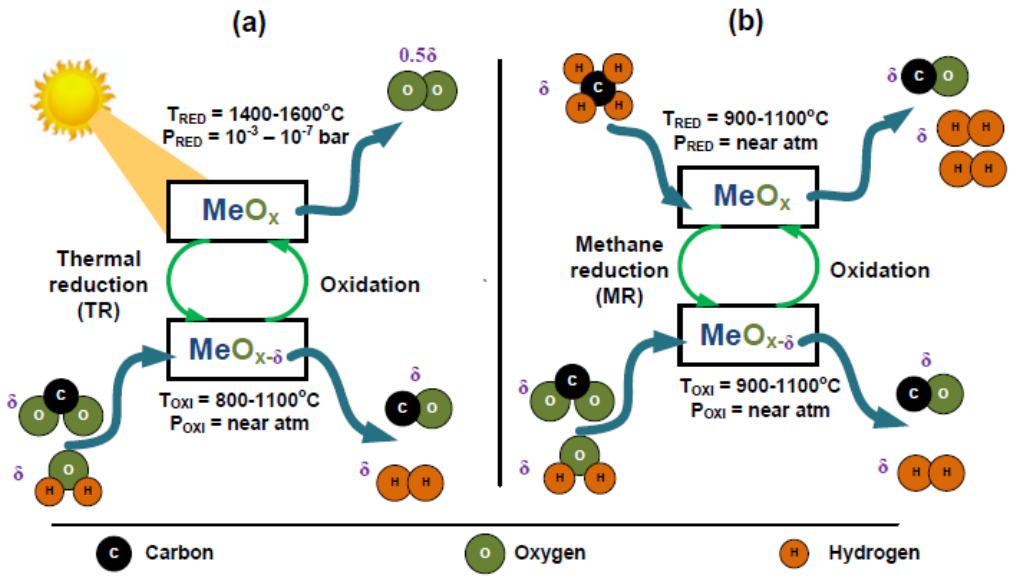

Figure 10 - (a) Solar thermochemical redox cycle for syngas production (b) methane-reduction chemical looping CO_2/H_2O splitting for syngas production [11]

As already seen, this cycle works at very high reduction temperatures, it is however possible to make the cycle work at lower temperatures by also reducing the oscillation between reduction and oxidation temperatures, combining the redox cycle with methane reforming. In SMR it is possible to use the natural gas that you already have locally from land reserves, or to use synthetic gas or methane obtained from renewable resources. The advantage of obtaining syngas from chemical looping lies in the fact that a continuous and non-intermittent production would be obtained, which instead occurs with the use of solar sources. A general scheme of the two-phase thermochemical cycle for chemical dissociation by heat solar power is shown in Figure 11. [11]

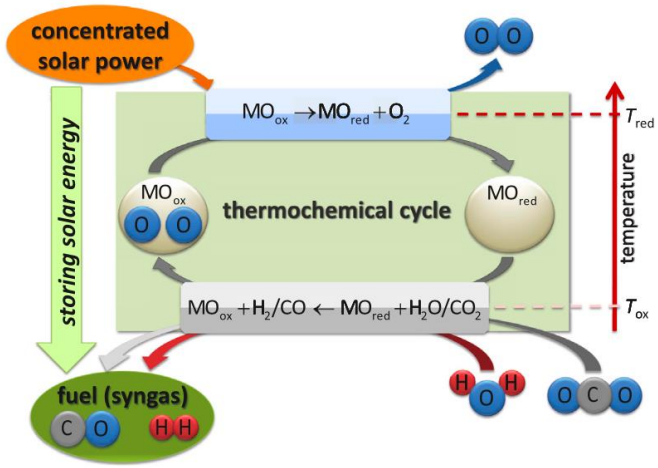

Figure 11 - General scheme of the two-phase thermochemical cycle for chemical dissociation by heat solar. Thanks to the redox reactions, the splitting of CO_2 and H_2O into CO and H_2 is achieved respectively (syngas) [2]

Although the use of solar sources leads to an intermittent productivity disadvantage, the major advantage lies in the fact that thanks to the use of solar reactors it is possible to reach the high temperatures necessary in the reactions to obtain syngas. By choosing appropriate materials and an appropriate thermochemical reactor, the redox processes can be performed separately from each other, producing a separate flow of H_2 and CO. The yield of oxygen during the first phase at high temperature depends on the extent of the reduction: the oxidized form of the material, with the metal cation at its maximum valence, can be reduced to a metal oxide of lower valence or completely reduced to obtain the respective metal with zero valence. Metal/metal oxide systems (ZnO/Zn) or metal oxide/metal oxide systems such as: Fe_3O_4/FeO, Mn_3O_4/MnO and CeO_2/Ce_2O_3, can be used for the generation of hydrogen/syngas, through thermo-chemical processes of oxide reduction. In this case, starting from a multivalent metal oxide in the higher valence state and assuming that all the metal cations change their valence from the highest to the lowest state during the reduction phase, and vice versa, during the oxidation the relative reactions to the Fe_3O_4/FeO system can be written as:

$$Fe_3O_4 \rightarrow 3FeO + 0.5O_2 \tag{2.4}$$

$$3FeO + 2H_2O \rightarrow Fe_3O_4 + H_{2\,(g)} \tag{2.5}$$

Thermodynamic calculations have shown that systems working with metal oxides, which could be thermally reduced at atmospheric pressure and moderate temperatures, have yields of hydrogen, during the hydrolysis phase, too low to be of economic interest, for this reason it is use high reduction temperatures which can be achieved by using CSP.

Most experimental reactors use inert gas to remove oxygen from the reaction chamber and to keep the environment at low oxygen partial pressure, even if the use of inert gas involves additional energy costs, to avoid these costs it could be reduced in "vacuum" conditions.

The thermochemical processes are the distinction of "volatile" from "non-volatile" cycles according to whether the chemical species containing metal or not in the solid state during the whole process.

The ***VOLATILE CYCLES*** occur in ZnO/Zn redox pairs, in this pair two-step cycles are carried out, in the reduction process there is a solid-gas phase transition by all chemical species other than oxygen which are the metal itself or the oxide at a low level of valence. This phase transition is thermodynamically advantageous, since it offers a considerable contribution in terms of entropy. On the other hand, there are problems due to the recombination of the dissociation products with oxygen to form the initial reagent, or the oxidized metal, in the product gas stream again.

The ***NON-VOLATILE CYCLES*** employ redox pairs of metal oxides which remain in the solid state throughout the process, thus avoiding the recombination problem encountered for volatile cycles. Physico-chemical characteristics, such as particle size and porosity, become important for carrying out the reaction with steam and CO_2. However, it should be borne in mind that the problem of redox materials in thermochemical cycles is to maintain as much as possible the properties of the high surface area, porosity and reduction effectiveness, during the actual operating conditions encountered in "real" operation, with solar energy, which involve very high temperatures and repeated thermal cycles. [2]

2.3. Coupling Redox Chemistry to Solar Energy: Heat Transfer issues

Once the type of redox composition, the next step is to couple the chemical reaction to solar energy. One of the first steps is to try to channel the reflected and direct solar energy using heliostats or solar collectors. Today CSPs are often used to produce electricity, exploiting the sun's rays, for this reason mobile reflectors (mirrors) are used that follow the sun's rays, namely: the Parabolic Trough Collectors (PT). Also used are Fresnel Linear Reflectors and central receivers, well known for their central tower shape.

All these systems can reach very high temperatures in the process, precisely because the solar energy is concentrated in a single central focal point thanks to mirrors. Inside the CSP there is a heat exchanger called "receiver" which has the purpose of absorbing concentrated solar radiation and transferring it to the carrier fluid for heat transfer which can be: water, air, or molten salts. The carrier fluid heated by the sun's rays is then used to drive a conventional cycle (Rankine, Brayton, or Stirling). Using a second heat exchanger, the heat of the carrier fluid is transferred to the water which is heated, evaporated, and then superheated to be sent to the turbine, which is connected to an alternator to produce electricity, as shown in the Figure 12. [14]

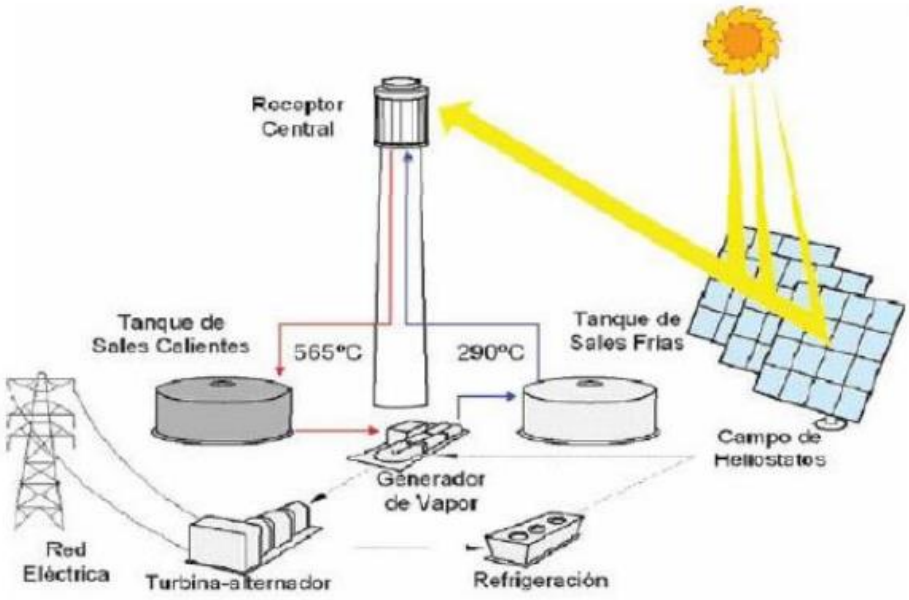

Figure 12 - Central tower plant to produce electricity [15]

Solar thermochemical applications use the same technology illustrated above. The only difference, lies in the fact that, in the case of thermochemical reactions, the solar radiation is conveyed into a receiver-reactor where the thermochemical reactions are carried out, for this reason the choice of the receiver to use becomes of great importance. For the thermochemical reaction to take place it is necessary that very high temperatures are reached around 2300 K and only solar towers and solar dish can reach this temperature.

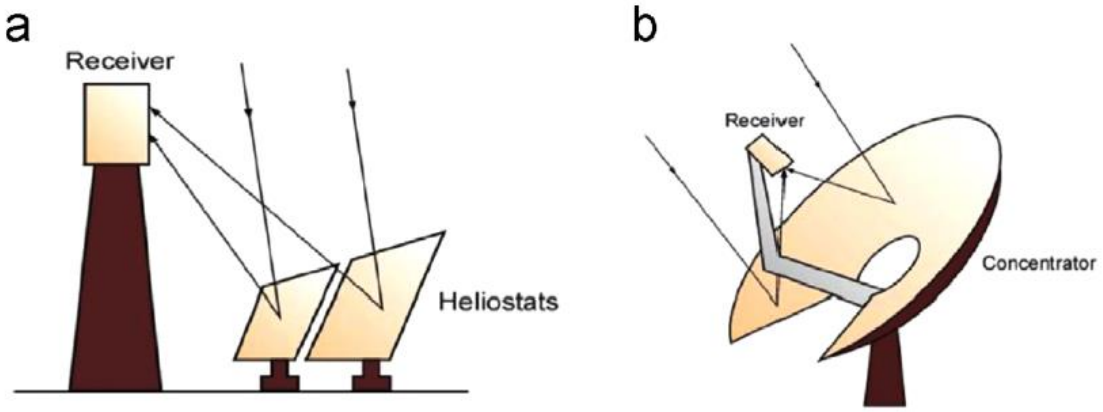

Figure 13 – a) Solar tower b) Solar dish [14]

Generally the pre-development tests with solar heat are performed on a scale starting from a solar simulator or furnaces as in the case illustrated in the thesis, and then move on to

solar towers, preferably in the "beam-down" variant which creates a second hyperboidal reflector placed on top of the tower to direct sunlight to the reactor, because they require very large dimensions for hydrogen or syngas production plants. [14]

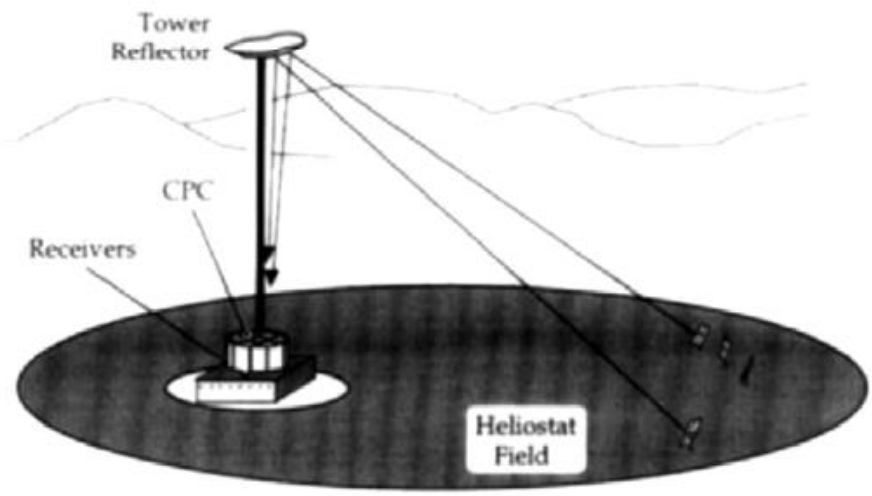

Figure 14 - Beam-down solar tower receiver [14]

2.3.1. Solar receiver – reactor concepts

The solar receivers suitable to be used in chemical looping processes and to withstand high temperatures are essentially external receivers and cavity receivers.

External receivers concentrated solar radiation affects the external surface of the system. These receivers consist of absorbent surfaces exposed to concentrated solar radiation, through whose walls the heat is transferred to the thermal fluid. [2]

Cavity receivers consist of a container-like structure, where solar radiation enters through an opening, which often has a window of glass or some other transparent material. [16]

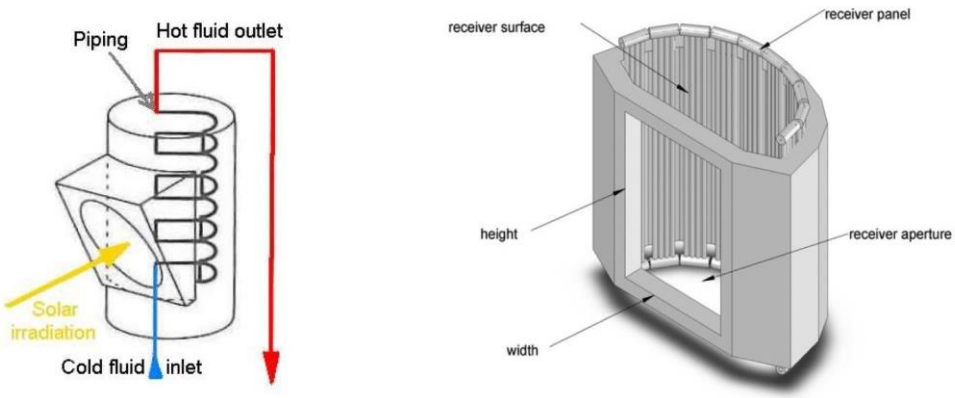

Figure 15 - Cavity receiver [2]

The choice of the receiver in this respect is also linked to the type of arrangement of the heliostats. In fact, cavity receivers have angular constraints and therefore are better suited to be used in structures with heliostats north or south of the tower, while external ones are more used in installations with the tower at the center of the solar park. Another classification is to distinguish *tubular receivers* from *volumetric receivers*.

In *tubular receivers*, the heat transfer fluid flows inside small tubes, which touch the surface on which the radiation affects, and thus absorb the heat. The heat exchange takes place through the wall of the pipes, therefore it becomes difficult, with this type of receivers, to have good performance for radiation values that go beyond a certain limit (about 600 kW/m^2), except in the case in which fluids such as high thermal conductivity, such as, for example, liquid sodium. [16]

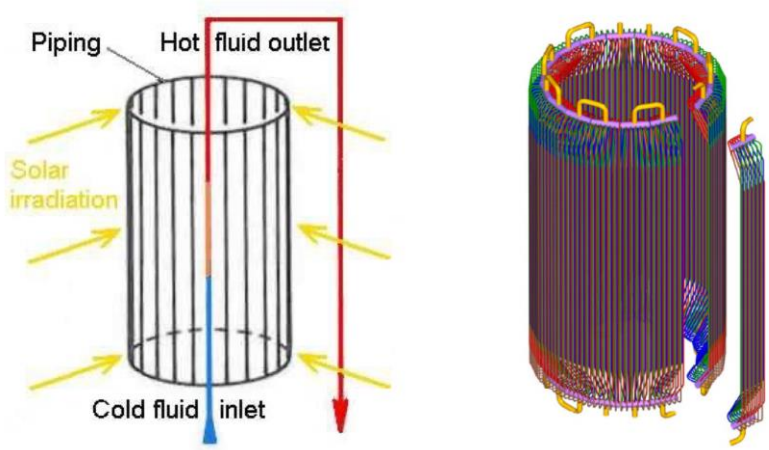

Figure 16 - Tubular receiver [2]

Volumetric receivers, on the other hand, are made of materials with a porous structure, so the concentrated radiation penetrates inside the volume of the receiver, where the heat exchange takes place with the fluid, generally air or other gas, which is forced to pass

through the pores of the material. In volumetric receivers, during the heat exchange, a phenomenon known as the volumetric effect occurs, which consists in the fact that the gas leaving the receiver has a higher temperature than the external wall of the latter. [16]

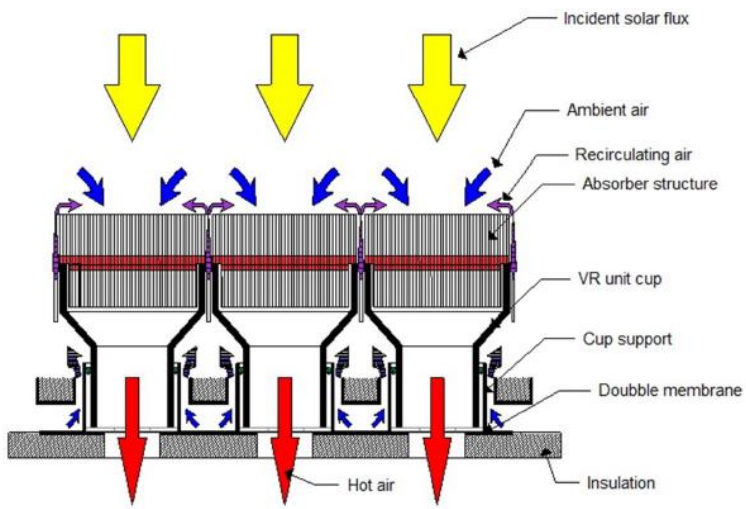

Figure 17 - Volumetric air receiver [2]

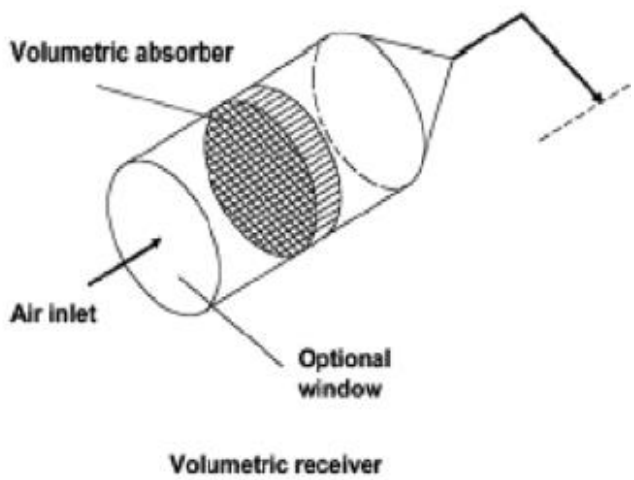

Figure 18 - Volumetric receiver with porous absorber [14]

2.3.2. Solar reactors for thermochemical experiments

For the design and optimal operation of reactors combined with solar receivers, sufficient heating must be ensured to allow reductions in chemical looping processes.

In general, catalytic reactors can be divided into two categories based on the type of particles that enter the reactor, in fact there are unstructured fluidized bed reactors and or honeycomb, foam and membrane catalytic reactors. With reference to conventional

applications, both categories can be adapted to operate as solar chemical reactors operating with solid oxide redox materials.

The solid particles can be inside tubular receivers exposed to the sun (IIR) or be directly irradiated by rays (DIR). In directly irradiated receivers (DIRR) the catalytic particles absorb concentrated solar radiation and heat the reacting gases up to the reaction temperature. Generally in solid-gas reactions, the reactant, which can be a metal oxide, is not present in lower quantities than the gaseous reactants, but has a non-negligible mass which is exhausted with the progress of the reactions and for this reason must be reintegrated. The thermal reduction phase is facilitated by the high temperatures and low partial pressures of oxygen while the splitting by the low temperatures and high partial pressures of H_2O/CO_2.

Most of the reactors are DIRR and use solid particles or structures directly exposed to concentrated solar radiation. Two types of reactors can be differentiated based on the redox chemistry relating to volatile and non-volatile cycles.

In volatile cycle reactors, during the thermal reduction phase, a gaseous mixture composed of the reduced phase occurs, in the form of oxide or metal, which together with oxygen requires a treatment to avoid a recombination that leads it to the starting oxidized form . Generally, such systems consist of two separate reactors, in the first the reduction process takes place and in the second the oxidation process. The decoupling of the two reactions makes it possible to carry out the reduction during the day to yield the solar radiation and oxidation to produce syngas during the night. [2]

Among the most important reactors, unstructured and operating with direct radiation, which only carry out the thermal reduction phase with solid particles in motion, there is the so-called ROCA: "Rotary Cavity Reactor". It is a rotary cavity reactor developed for the dissociation of zinc oxide (ZnO) and for the subsequent production of syngas. It has a rotating cavity equipped with a quartz window, for the entry of solar radiation, fixed to a non-rotating and water-cooled structure. The reactor exploits the action of centrifugal forces generated by rotation to move the ZnO plates towards the external walls to form a coating of ZnO directly exposed to concentrated solar radiation on them. With this arrangement, the ZnO powders simultaneously perform the functions of radiative absorbers, thermal insulators, and chemical reagents. The process is constantly fed with a gaseous flow for cooling and cleaning the quartz window, while the reaction products (Zn and O_2) are continuously removed and directed towards a device for cooling. [2]

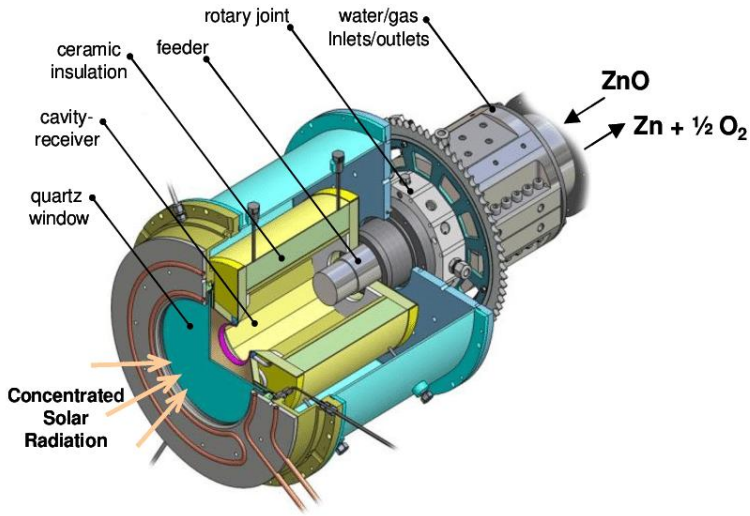

Figure 19 - Operating diagram of a rotary cavity reactor for the thermal dissociation of zinc oxide (ZnO) [2]

Reactors employing non-volatile redox pairs perform both phases of the cycle. An example of these reactors can be those illustrated in Figure 20 which can work with porous ceramic foams produced entirely with redox materials. In the cavity of these receivers there is a porous metallic cylinder composed of ceria oxide, the walls of which are affected by concentrated solar radiation entering through a window opening. The reacting gases are introduced radially through the porous structure until they reach the internal cavity while the gases produced exit axially from the cavity through an outlet located at the bottom of the reactor. With this methodology, installing a volumetric reactor in the focus of the solar paraboloid would allow to generate flows of CO, H_2, and O_2 starting from a flow of steam and CO_2. Referring to ceria oxide, the thermal reduction occurs around 1873 K and subsequently there is a significant release of oxygen. During the oxidation phase, which is carried out in the first phase, the production of hydrogen with complete oxidation takes place. [2]

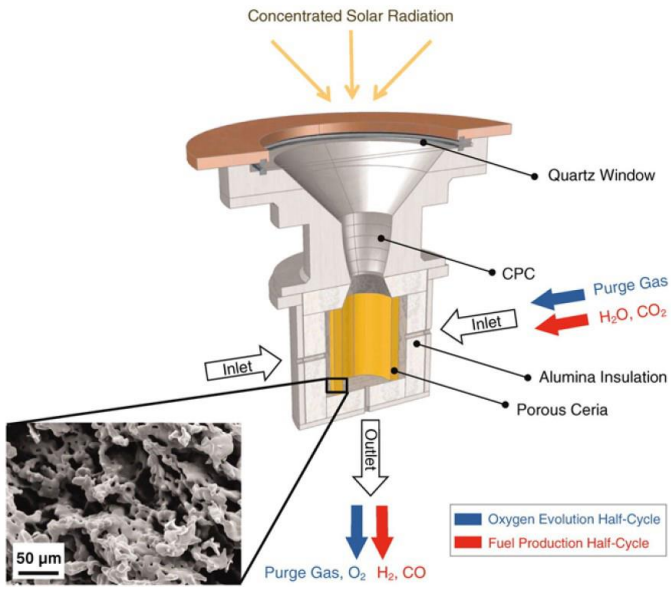

Figure 20 - Operation diagram of the first solar reactor designed to operate using ceramic foams, containing a monolithic cylinder based on ceria oxide [2]

The evolution of CeO_2-based reactors for the thermochemical production of solar energy fuels is an interesting and promising option, although some refinements are needed and for this reason a cavity solar receiver containing porous CeO_2, directly exposed to concentrated thermal radiation from a solar simulator. A further optimization of the solar reactor for the combination of the two thermochemical splitting cycles for the synthesis of solar syngas and the production of aviation fuels was proposed by SOLAR-JET. It is shown in Figure 21 the configuration created for the production of solar kerosene from H_2O and CO_2 through a redox cycle based on CeO_2. [2]

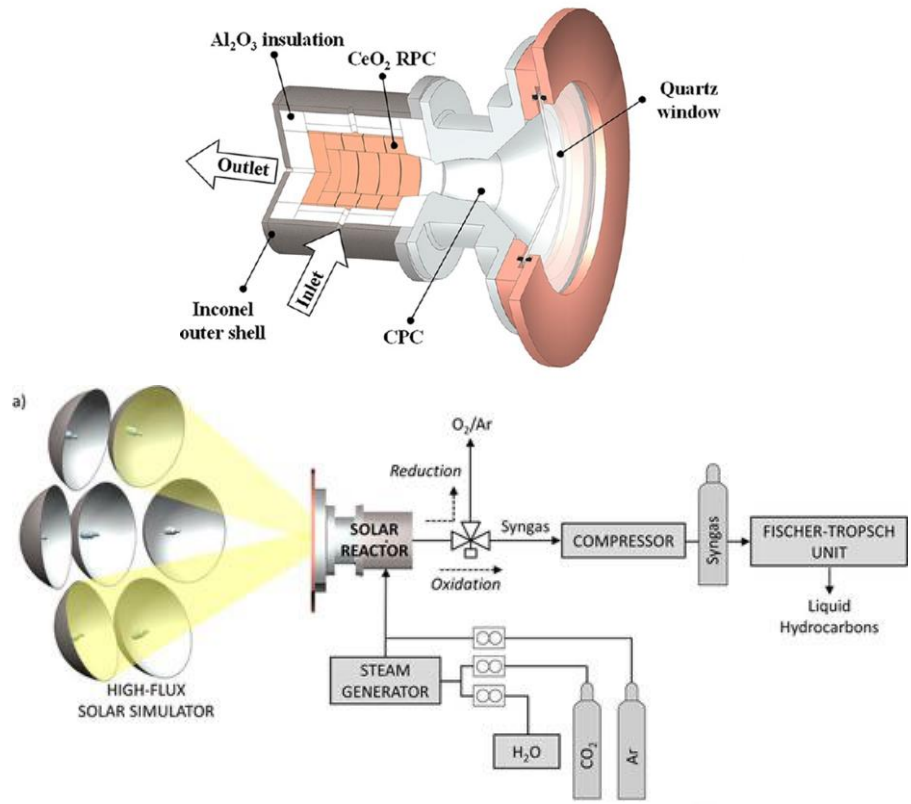

Figure 21 - General description of the aviation fuel (kerosene) production plant built by SOLAR-JET, consisting of the solar simulator (High Flux Solar Simulator) and the cavity reactor working with CeO_2-based ceramic foams [2]

CHAPTER 3
Materials for Chemical Looping Processes

The materials used, and which are preferred, in the chemical looping processes are those that use non-volatile cycles, precisely because the metal oxides remain in the solid state throughout the process and avoid recombination problems. In general, to understand how the materials behave during the entire process, we focus on observing the structural variation of the material in the thermal reduction and splitting phase (of CO_2 or water). Reduction tests are very important to understand the ability of a material to release oxygen, generally hydrogen can be used as reducing agent, while nitrogen, argon as purge gas in the thermal reduction phase. The hydrogen is often used as a reducing agent in a procedure like that which in catalytic studies it is called "Temperature Programmed Reduction - TPR". However, there is no guarantee that a chemically reduced material will exhibit similar oxygen release performance as when it is thermally reduced. On the other hand, it is not guaranteed that a material reduced by chemical or thermal means is capable of completely regaining the oxygen lost by CO or H_2O in the second phase of the cycle, or oxidation. For this reason, to understand the full operability of the material, screening is carried out by observing the materials in conditions of thermal reduction in H_2, CH_4 or CO.

To date, the materials of great interest in chemical looping processes are precisely metal oxides and in particular: iron oxides, ceria and perovskite. [14]

3.1. Iron Oxides

Among various metal oxide candidates, iron oxide is the one that stands out as a promising oxygen carrier for CO_2 utilization due to the fact that it is environmentally friendly, low cost and reliable towards CO_2 reduction, in fact, it thermodynamically contains a high oxygen content. However, pure iron oxide is prone to sintering during the redox cycle, especially at high temperatures causing rapid deactivation, i.e. a sharp slowdown in reduction/oxidation. The key to success in chemical looping processes lies in its ability to resist sintering and therefore maintain its thermal stability. [17]

Iron oxides typically occur as fine powders. Tests carried out on the oxides have shown that the suitable temperatures for which thermal reduction occurs are around 1600-1700 K, however this could cause significant sintering of the iron oxide. Typically, to test materials, thermal programmed oxidation/reduction (TPO/TPR) tests are performed using a thermogravimetric instrument, TGA, and then an XRD (X-Ray-Diffraction) is performed to observe the structure of the material. [14]

a)

b)

Figure 22 – a) Iron ore [18] b) Iron oxide powder [19]

Iron oxides may contain traces of other metals such as nickel, zinc, or manganese. Among the various ferritic materials tested for chemical looping, it was noted that those materials containing traces of Zn have volatilization problems, while there are stability problems in those containing traces of Mn. [20]

A very important concept to be introduced is that of sintering, with this term we mean the ability of a powdered material to aggregate into a single more grainy and brittle component at high temperatures but below the melting temperature. [21] It is useful for us to understand this concept precisely because the improvement of the sintering resistance is fundamental for the application of iron-based oxygen carriers in chemical looping and this prompts research to look for the origin of the sintering of iron oxide during redox cycle. [17].

Some tests based on a thermodynamic analysis, carried out by Hu, on the Fe_2O_3 material by means of a support of ZrO_2, considered as an impartial support in ferrous species, since it does not alter either the thermodynamics of the system or the kinetics; showed how the material behaves through an XRD analysis. In the test a redox cycle was carried out where H_2 at 5% and CO_2 were used respectively as a reducing and oxidizing agent. Looking the Figure 23, it is possible to notice how the three reduction peaks with maximum consumption of H_2 at about 350°C, 460°C and 550°C, lead to a gradual reduction of Fe_2O_3/ZrO_2. [17]

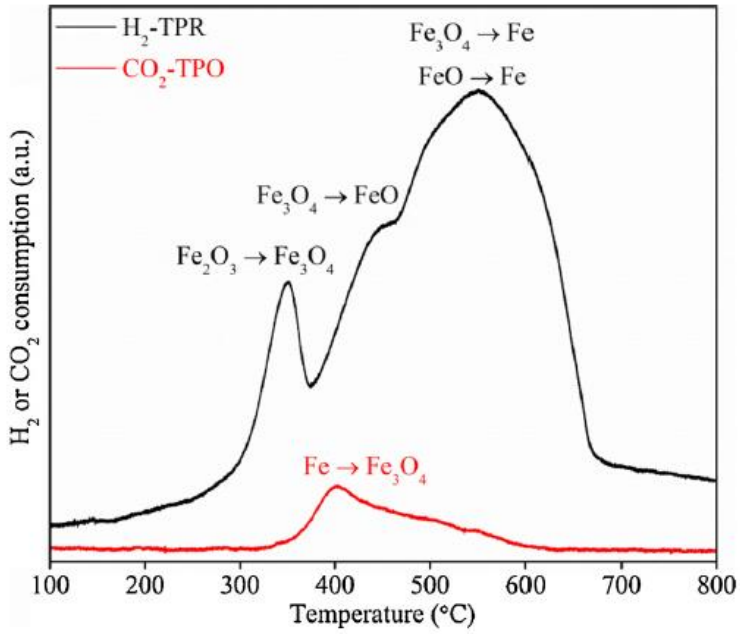

Figure 23 - Conventional H_2-TPR and Fe_2O_3/ZrO_2 CO_2-TPO. Test carried out with reducing gas: 5 vol% H_2 in Ar; Oxidizing gas: pure CO_2; Gas flow rate: 60 Nml min^{-1}. Samples were heated from room temperature to 800 ° C with a ramp rate of 20°C min^{-1}. [17]

In the first reduction performed at low temperature, the transformation from Fe_2O_3 to Fe_3O_4 takes place, followed by two strongly superimposed peaks in a wide temperature range, the reduction of Fe_3O_4 into metallic Fe occurs with the presence of the intermediate FeO. The uneven size distribution of iron oxide particles and the similar reduction mechanism of Fe_3O_4 and FeO, the reduction of Fe_3O_4 could lead to the formation of larger particles simultaneously within the temperature range. The reduction of FeO leads to an unclear transition between the second and third peaks, which obviously cannot reflect the formation of the intermediate FeO. [17]

However, it was detected by XRD-2D models, see Figure 24, that during H_2-TPR a three-stage reduction of the iron oxide Fe_2O_3/ZrO_2 is clearly evident, in fact we have that:

$$Fe_2O_3 \rightarrow Fe_3O_4 \rightarrow FeO \rightarrow Fe \tag{3.1}$$

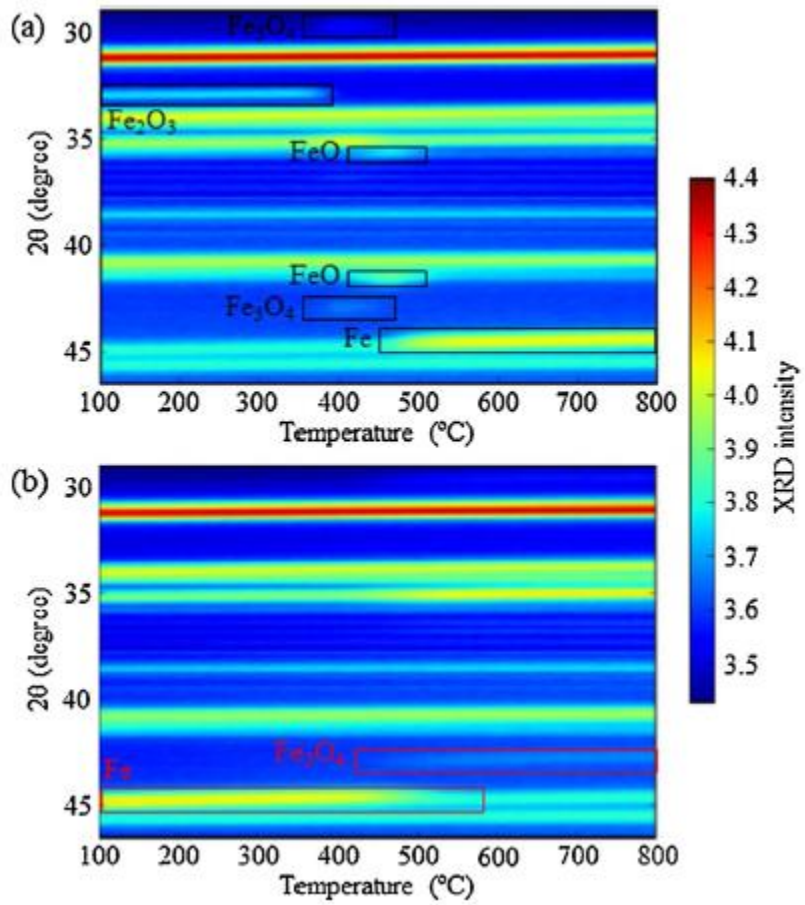

Figure 24 - XRD-2D models, in the 2ϑ range from 29.5 ° to 46.5 ° recorded during (a) H_2-TPR and (b) CO_2-TPO of Fe_2O_3/ZrO_2. Reducing gas: 5 vol% H_2 in He; Oxidizing gas: pure CO_2; Gas flow rate: 60 Nml min^{-1}. Samples were heated from 100 to 800 °C with a ramp rate of 20 °C min^{-1}. In XRD iron peaks at different redox states are marked with rectangles and the unlabelled ones are the characteristic peaks of crystalline ZrO_2. [17]

The results reveal that the iron oxide sintering in the redox cycle originates from the formation of FeO as an intermediate product during the reduction phase and the longer FeO persists, the more important the sintering becomes. A sintered iron oxide shows a deactivation and therefore a decrease in the yield of CO, see the Figure 25, during reoxidation by CO_2. Therefore, the improvement of the sintering resistance of the iron-based oxygen carrier should focus on suppressing the formation of the FeO intermediate during reduction. Feasible approaches are adjusting the operating conditions or limiting the particle size to increase the rate of oxide reduction. [17]

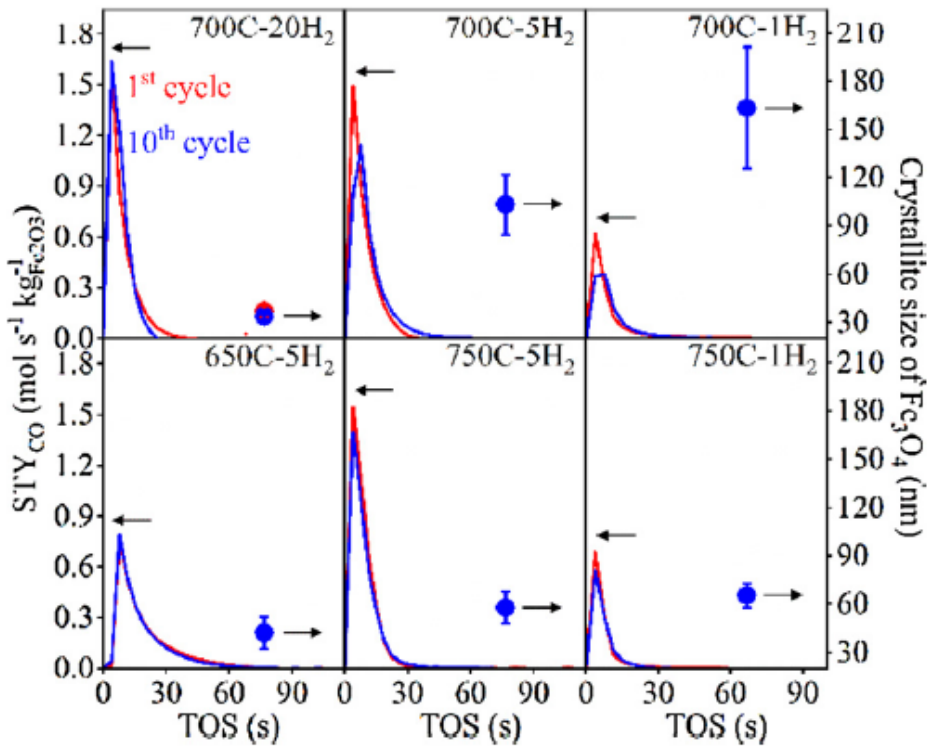

Figure 25 - Deactivation studies: space-time yield of CO (STY_{CO}, mol s^{-1} kg_{Fe2O3}^{-1}) during the reoxidation phase of the 1st (red curve) and 10th (blue curve) and the crystallite size of the Fe_3O_4 phase after 10 redox cycles (blue-spherical symbol) at different H_2 treatments [17].

Observing SEM images of reduced samples, from other studies, at different reduction temperatures they show how larger particles are always formed as the temperature increases and the reduction time increases. Larger particles were formed following the coalescence of smaller particles due to the high surface energy that the iron oxide possesses. In general, the migration rate of the material is sensitive to changes in temperature and sintering occurs faster at higher temperatures. The formation of larger particles can be clearly seen in (b) and (c) of the Figure 26. [22]

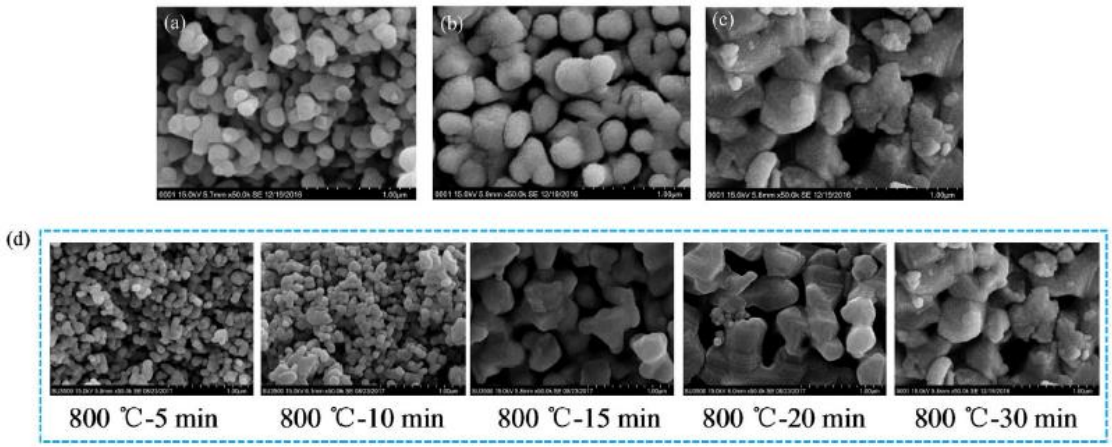

Figure 26 - SEM images of reacted iron oxide reduced by 5% H_2 under different reduction conditions. (a) 700 °C-30 min, (b) 750 °C-30 min and (c) 800 °C-30 min, (d) consecutive images at different reduction time below 800 °C. [22]

The greater sintering led to a greater likelihood of the formation of larger particles which decreased the surface area of the iron oxide. Thus, it can be concluded that in general the sintering processes take place at a high temperature and strongly depend on the temperature.

The sintering process is an irreversible thermodynamic phenomenon that changes unstable particles with superfluous free energy into larger particles with a stable state. By elevated temperatures, these particles become larger and more abundant, effectively reducing the surface area of the iron oxide.

In Figure 27 the evolution of the surface morphology of iron oxides is shown for fresh and reacted samples. During the reduction reaction, oxygen loss occurs which would lead to the creation of vacancies, the aggregation of oxygen vacancies causes the formation of a porous structure. [22]

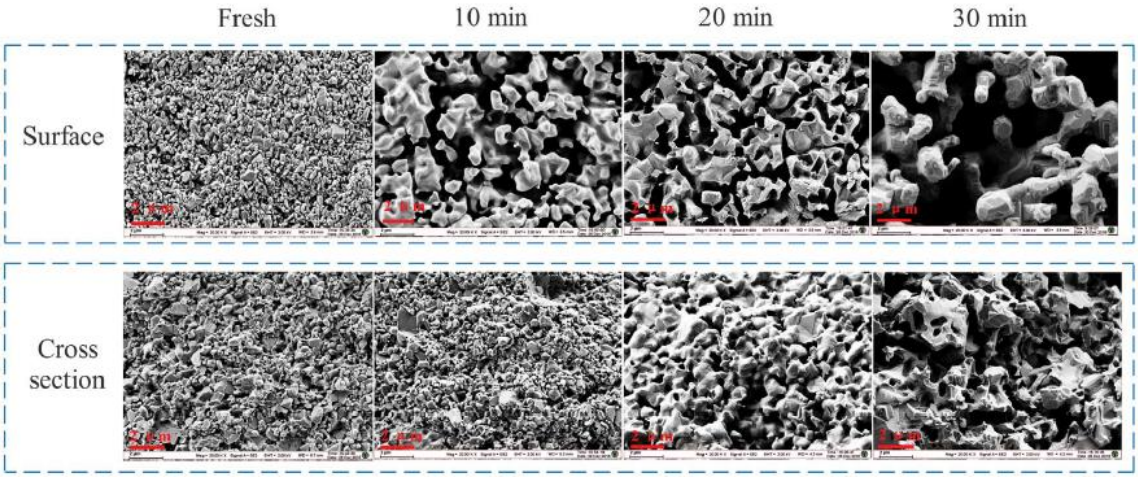

Figure 27 - Morphology of fresh and reacted samples after reduction below 800 ° C with 5% H2. [22]

Due to the different oxidation of the outer surface of the iron oxide compared to that of the inner core, the degree of reduction of the interior was lower than that of the outer surface. This difference in the degree of reduction allowed the coalescence of the particles and the formation of porous structures to occur with less speed.

There are then two causes that lead to the evolution of the microstructure: the creation of coalescence or the growth of the particles by sintering which leads to a smaller surface area of the iron oxide and the creation of vacancies due to the loss of oxygen during the phase of reduction which leads to the formation of a porous structure. [22]

3.2. Cerium Oxides

Cerium oxides, also known Ceria, in addition to iron oxides, are considered one of the most promising materials to be oxygen redox carriers due to its fast chemistry, high ion diffusivity and large oxygen storage capacity. [23]

They are solid at ambient temperature and if very pure the compound has a white to pale yellow color and is odorless; the rawest product, on the other hand, has a color from pink to brick red due to the presence of other lanthanides and rare earth oxides. [24]

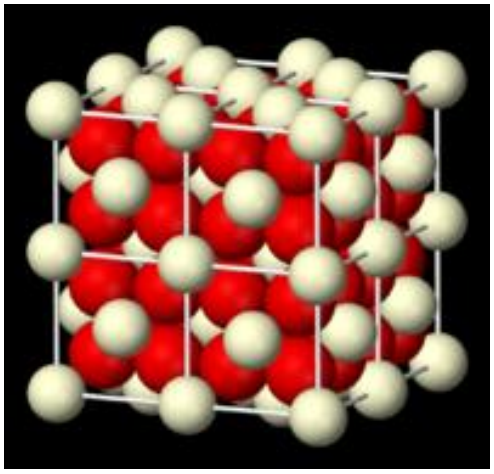

a)

b)

Figure 28 – a) Molecular structure of cerium oxide [24] b) Powder of cerium oxides [24]

Figure 29 – Cerium oxide with coarse grain size

Redox reactions can also be carried out on cerium oxides as it is a metal oxide and belongs to the class of non-volatile cycles. Ceria offers numerous advantages, compared to alternative metal oxide systems, since in lack of oxygen it shows excellent reactivity with water and a satisfactory yield in the production of H_2. However, complications are not absent: the most relevant is given by the high temperatures required for thermal reduction, to achieve a significant dissociation efficiency. At these temperatures, above 1800 K, in addition to the compatibility and resistance problems of the reactor materials, a partial

sublimation of the cerium oxide may occur, which therefore gradually decreases its effective predisposition to reduction. [2]

As was also the case for iron oxides, oxidation is strongly linked to temperature. Some studies have shown, however, that at different concentrations of CO_2 during the oxidation phase, more vacancies are created as this concentration increases. [23]

By carrying out XRD analysis of cerium before and after the reaction cycle, where H_2 is sent as a reducing agent and CO_2 as an oxidant, the presence of a cubic structure of fluorite is observed in both cases. [23]

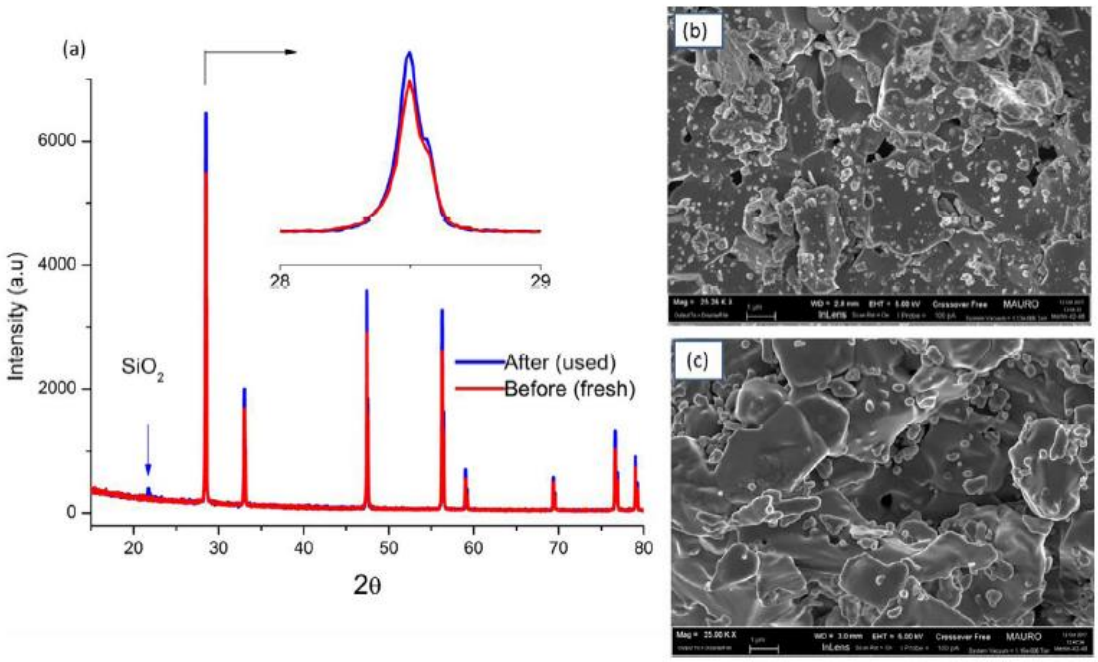

Figure 30 - XRD patterns of ceria before and after the reaction cycle. (b) FE-SEM images of fresh and (c) cycled ceria with traces of silica due to quartz wool to fix oxides in the fluid bed [23]

Looking at the XRD patterns prior to cycling, the peaks appear more intense after cycling, indicating that crystalline growth occurred during the high temperature process. The size of the larger particles is not significantly affected by the reaction, while the smaller ceria particles, due to sintering, appear larger after the reaction. [23]

3.3. Perovskite

Perovskite is a material consisting mainly of calcium titanate, they are mineralogical components of sectors of the lithospheric mantle, but generally synthetic perovskites produced with calcination processes or overheating of mixtures of mineral salts are used. [25]

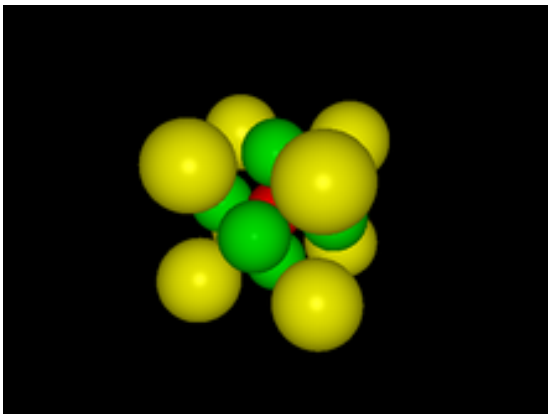

a)

b)

Figure 31 - a) ABO_3 structure typical of a perovskite. The alkali metal is represented in yellow, the transition metal is in red, and oxygen is in green. [25] b) Mineral of Perovskite [25]

Figure 32 – Perovskite powder inserted inside an alumina boat

In recent years, perovskites have proved to be of great interest for chemical looping purposes, as they are structures composed of a combination of metal oxides with different characteristics, which gives us a wide range of elements to choose from and adjust the properties of perovskites. in relation to their intended applications. Perovskites have a general formula of ABO_3, where A and B are both cations, with A being the larger cation than B. The transition metals are usually located at site B, while larger cations (such as Na^+, K^+, Ca^{2+}, Sr^{2+}, Ba^{2+}) will be found on site A.

The most promising perovskite material that has been widely used in the last decade is $CaMnO_3$. In this structure, the release and capture of oxygen are due to the transformation of Mn^{4+}–Mn^{3+}, thus facilitating the release of oxygen to the inside the fuel reactor. This

structure is subject to changes in Ca_2MnO_4 and $CaMn_2O_4$, which could cause a decrease in the efficiency of the perovskite during the oxidation reduction cycles at high temperatures. According to the literature, to solve this problem, transition metals such as Ti, Fe, Zr and Cu can be doped with the cation of the B site (Mn), leading to a more stable structure during the process. [26]

The ideal structure of the perovskite is cubic, the small ion radius of the doped ions, compared with the voids between the octahedral, will result in a cooperative inclination of the shared octahedral angle.

Chemical-structural changes affect the properties of perovskites which strongly depend on the synthesis conditions. To date, several synthetic methods have been introduced to produce perovskite, which strongly influence the physicochemical properties of the surface, surface area, porosity, purity, stability, and size of the crystals. Of all the techniques proposed, the solid-state reaction, the sol-gel method, the combustion method, the mechanical-chemical processing, and the microwave path are the most common. An important feature of the method of preparation is its ability to expand. Most of the preparation methods mentioned above are developed for laboratory-scale production. Currently, the planned preparation methods for the preparation of the oxygen carrier in large-scale production are spray drying and impregnation. Extrusion is an important forming technique in the ceramic industry due to its ability to provide complex shapes with dimensional accuracy and its flexibility for mass production. One of the main objectives of the proposed method is to use the mass production capacity from the extrusion technique. [26]

CHAPTER 4
Experimental Methods

In the following chapter the experimental method will be described to obtain CO through a process of Chemical Looping on iron oxides following a reduction and oxidation. Will be described in detail the various components and instrumentation used. Description of experimental procedures and results with relevant considerations, in the various experimental tests carried out.

4.1. Furnace and Gas Analyzer Description

The experimental tests were performed in a furnace installed in the laboratory of the Environment Park, inside which the reactors loaded with the material to be tested were inserted.

Observing the section diagram of the furnace, illustrated in Figure 33, it is clear how at the entrance to the furnace, inside the alumina reactor, where the powders of iron oxides are placed, there is the passage of gas flows. It is also noted that inside the furnace there is a resistance (red lines), activated by an external power supply, this allows the localized temperature to rise in the center of the reactor.

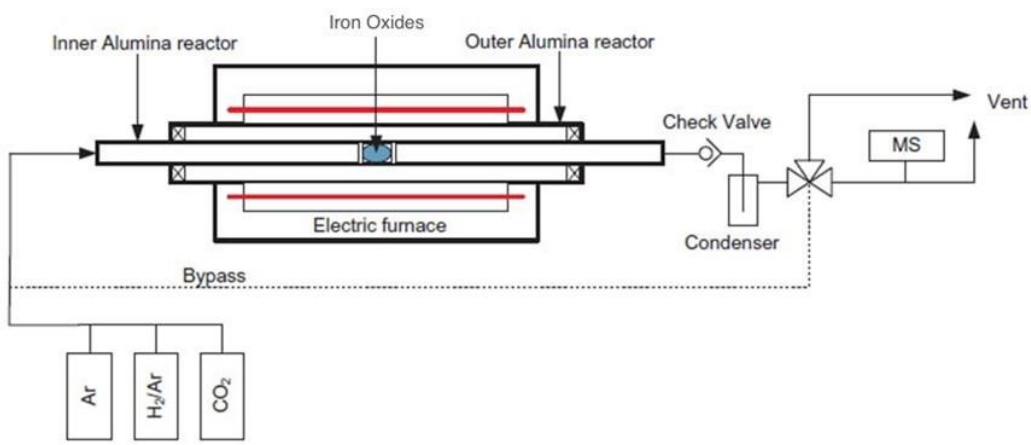

Figure 33 – Diagram of the furnace section

The micro-reactor, also called micro-channel, is a tubular-shaped reactor in which chemical reactions take place in a restricted area. The furnace used in this study, shown in Figure 34, belongs to the manufacturer Carbolite Gero and could work in the temperature range of 30°C to 1700°C, in condition of atmospheric pressure.

Figure 34 – Furnace Carbolite Gero

It is a continuous flow reactor; this means that the chemical reactions take place in a flow that movements continuously in the micro-channels of the microreactor. These microchannels may be alumina (Al_2O_3) tubes, shown in Figure 35, or they can also be presented as small boats, Figure 36.

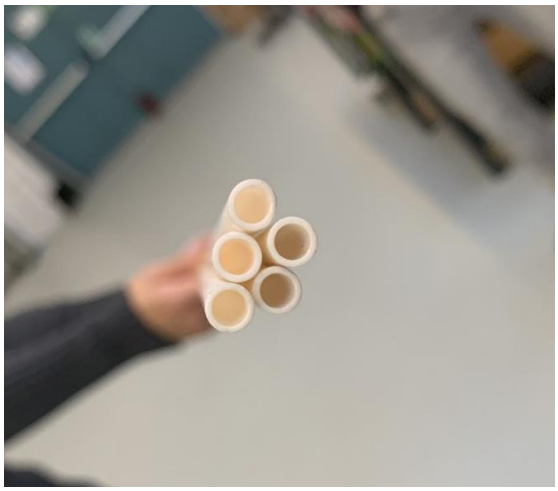

a)

b)

Figure 35 - Micro-channels/Micro-reactor in alumina

Figure 36 - Alumina boat reactor

For the tests executed inside the tubular micro-reactor, iron oxide powders were inserted in the center of the 8 mm tubes and kept in position thanks to the presence of quartz wool, moreover, to avoid the entrainment of these particles due to the continuous flow of the reagents, they were blocked by a second micro-reactor with a 6.4 mm diameter about 40 cm long.

For the tests executed through the boat reactor it was only sufficient to cover the bottom of the reactor with iron oxides, see Figure 37.

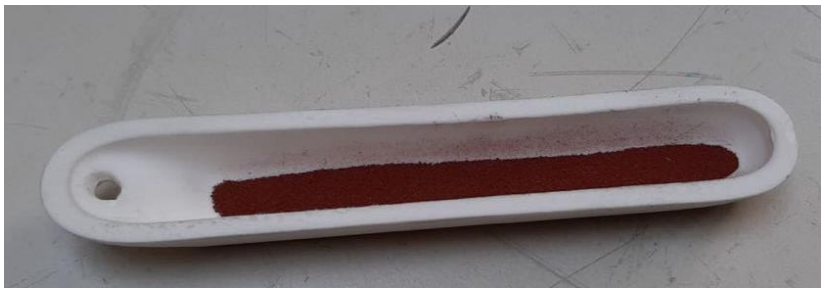

Figure 37 – Alumina boat loaded with iron oxides

The reactors are inserted inside the tubular section indicated in Figure 38. In Figure 39, it can be seen the position of the boat inside the tubular section of the furnace.

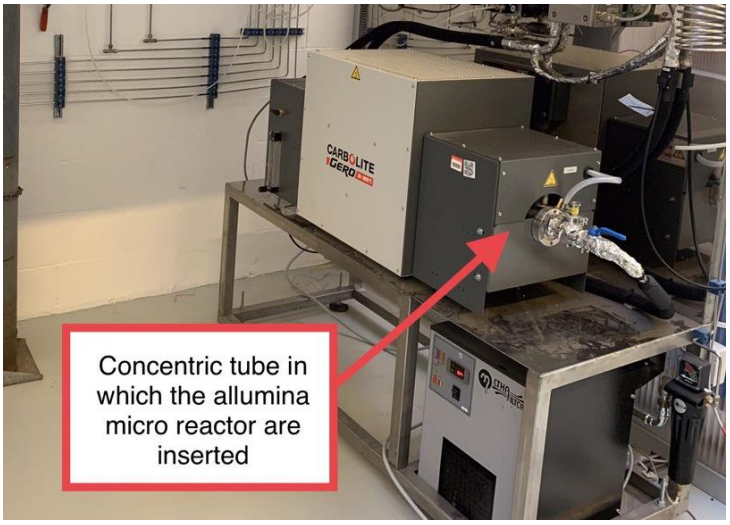

Figure 38 - Position of furnace where reactors loaded with iron oxides are inserted

Figure 39 – Boat position inside the tubular section of the oven

The mass of the powders placed in the reactors is measured through an electronic precision balance sensitive to the order of micrograms, shown in Figure 40. The filling of the reactors is performed inside the hood, shown in Figure 41, for safety reasons.

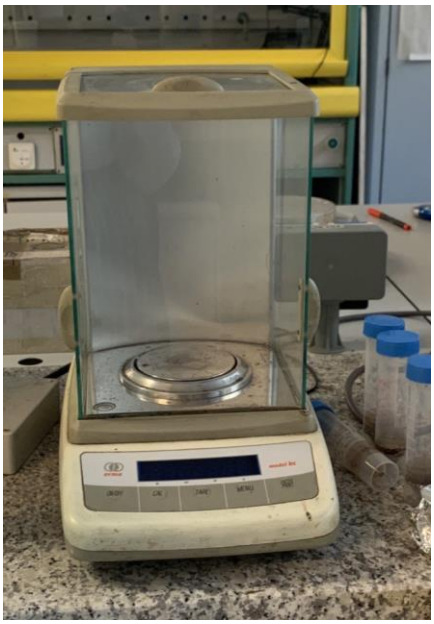

Figure 40 – Precision balance

Figure 41 - Hood

The composition of the furnace output flows is analyzed in the gas analyzer Emerson, shown in Figure 42.

Figure 42 – Gas Analyzer Emerson

This component is used to analyze the physical properties of input flow with the properties of a reference material. Through this comparison it can evaluate the molar fractions of the different components present in the flow. This composition is shown in the machine interface, which is the "XStream" software, where it is also necessary to set the number and type of components of the input stream.

Heating of the furnace is carried out by means of resistors in which current is circulated. Current regulation is performed via a "power supply", which is external to the furnace itself and is shown in Figure 43.

Figure 43 – Power supply of furnace

The power supply is controlled by a software called "Euroterm iTools". This software defines:

- ramps
- ramp step (rate at which the temperature must be increased/decreased)
- ramp set point temperatures

Based on these data, the value of the current that should circulate in the resistances is evaluated to establish a certain production of thermal energy to maintain the furnace at the required temperature fixed by the set-point.

The controls of mass flow, gaseous and liquid flows circulating in the microreactor is performed by a SCADA-based system with a user interface (API M-IoT software)

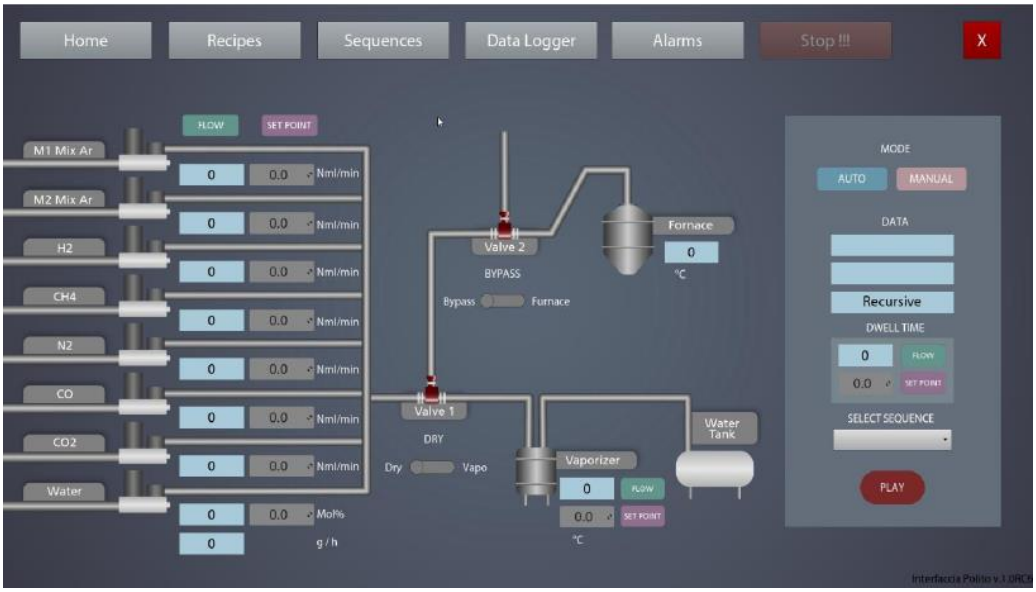

Figure 44 – Interface API M-IoT

The API M-IoT software also controls the switching on and off the two three-way valves included in the piping of the flows entering and leaving the microreactor.

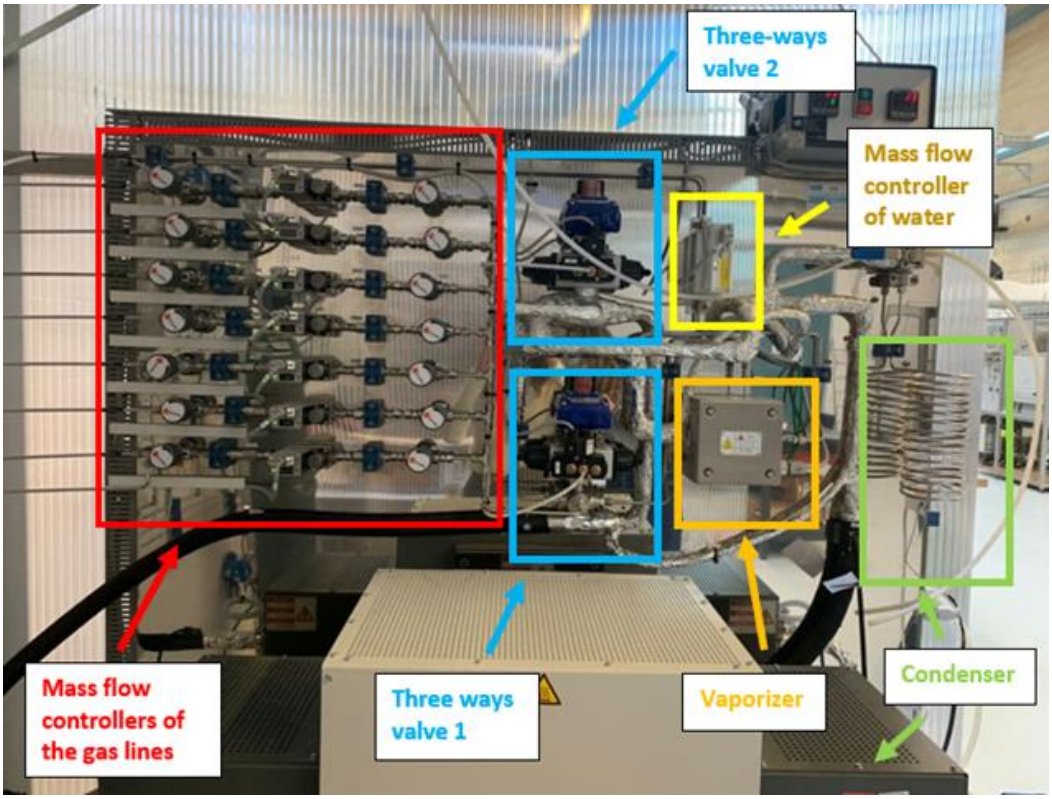

Figure 45 –Inlet and outlet pipeline to the furnace

The pipeline is characterized by a system to produce steam starting from demineralized water contained in a tank and seven gas lines:

- five lines connected directly to the laboratory gas lines (N_2, CH_4, CO, CO_2, H_2). This connection is made by means of pressure reducers installed on the wall (Figure 46), downstream of the reducers are the bench mass flow regulators;
- two lines connected to under-hood cylinders. These gases are made up of argon and gas mixtures and their pressure reducers are installed directly on the cylinder.

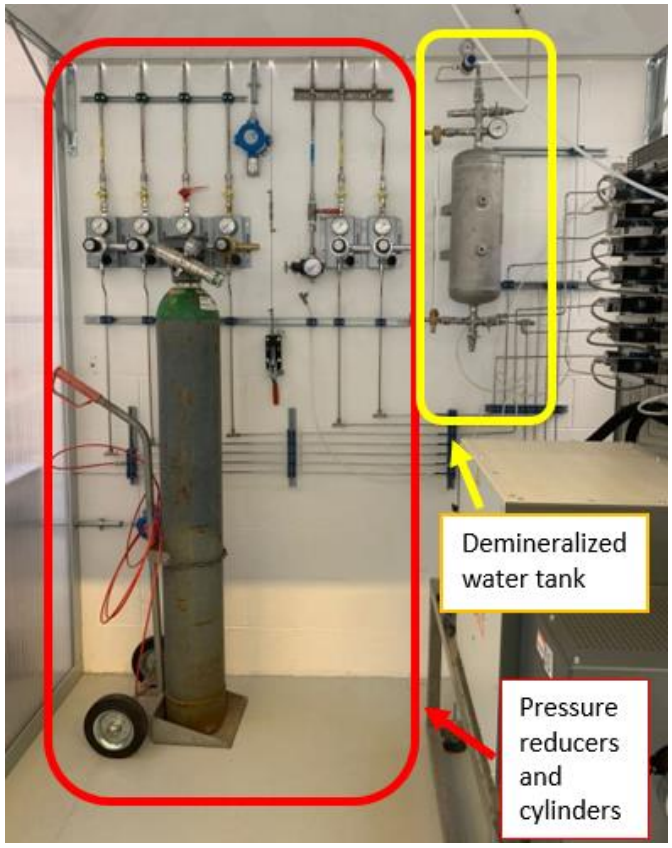

Figure 46 – Gas lines that feed the furnace

The pressure of the gas lines is 2.5 bar, even though the N_2 line is at 5 bar because this gas is also connected to the water tank to keep it under pressure. Downstream of the mass flow controllers, the seven gas lines converge to a single line, which is the dry mix line. The pressure of this line is roughly the atmospheric pressure. The line of the dry mixture of the seven gases is connected to the first three-way valve (shown the Figure 45), this valve is of the on-off type and allows you to choose to:

- feed the micro-reactor directly with the dry mixture.
- humidify the mixture. In this case the mixture is sent to the demineralized water evaporator where the gaseous mixture itself is mixed with the steam produced by the demineralized water. At the evaporator outlet there is a heated tube (it is heated to avoid water condensation) which connects to the cold line of the first section of the three-way valve. Downstream of the junction between the two lines, there is the power supply of the second three-way valve which allows you to choose between two heated lines:
    a. direct supply of the furnace.
    b. by-pass of the furnace.

These two lines converge at the outlet of the micro-reactor into a heated line. A manual valve allows you to choose to direct the mixture to the condenser or to the delivery line. Furthermore, both two lines can be connected to:

- exhaust line in the hood.
- gas analyzer. The outlet of this analyzer is connected to the exhaust line of the hood.

A more schematic representation of this architecture is given in Figure 47:

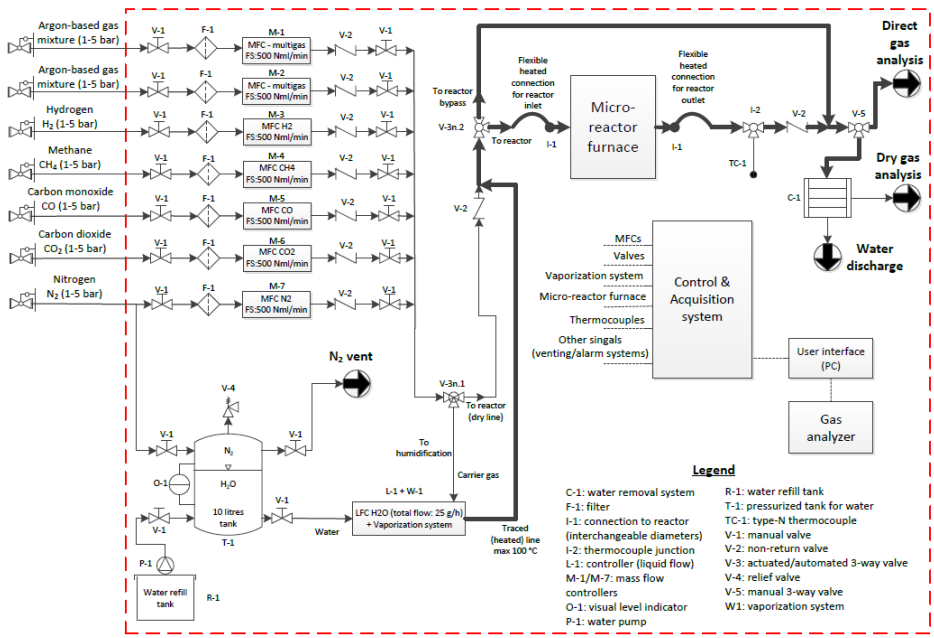

Figure 47 - Furnace pipeline scheme

During the test it is important that the iron particles remain in the position to ensure:

1) the correct execution of Chemical Looping.
2) the complete reduction/re-oxidation of the particles.
3) the production of a flow of "pure gas".

In the micro-reactor there are two different steady-state operations:

1) *REDUCTION OF IRON OXIDES.* During this phase, at the outlet of the micro-reactor, a gaseous flow consisting mainly of O_2 is obtained.
2) *OXIDATION OF IRON OXIDES.* In this step the reduced particles must remain in position to be invested by the flow of carbon dioxide for a certain time interval that allows the production of CO. Once the oxidation is over, the cycle starts all over again.

All tests were conducted using iron oxide samples, specifically hematite with spinel of both $MgAl_2O_4$ and Fe_2O_3, the percentages of particles contained within the sample are shown in Table 1, where it is possible to note the total absence of carbon, while Figure 48 shows XRD of the unused material.

Sample	Fe (wt%)	Mg (wt%)	Al (wt%)	C(wt%)	O (wt%)
Fresh OC	48.99	7.72	12.9	-	30.38

Table 1 - Percentages of particles contained in the sample

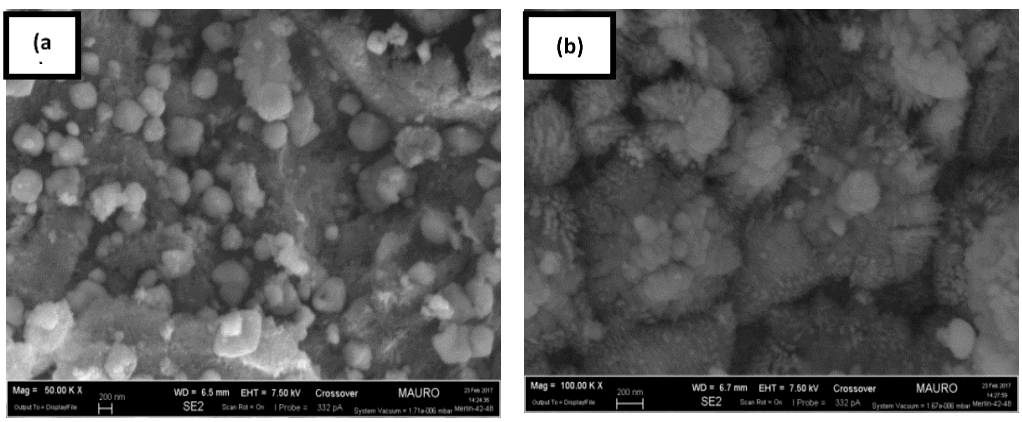

Figure 48 – XRD fresh OC a) 1 μm b) 400 nm

4.2. Experimental Test 1

In the first set of experimental data, an 8 mm tubular micro-reactor was used to perform the TPR and TPO in redox cycles with iron oxide powders. In the middle of the micro-reactor 200 mg of iron oxides powder was incorporated, blocked on both sides with quartz wool while a second 6.4 mm tubular reactor was introduced on the outlet side to prevent the movement of the mass.

The total gas flow rate was set at 200 Nml/min both during the reduction phase and during the oxidation phase. The reduction phase was carried out at a temperature of 1350°C with N_2, while the oxidation in two sets of temperatures, 800°C and 900°C, with CO_2 concentrations of 20%, 25%, 30% and 40% in volume, balanced with N_2.

The gas analyzer measured the CO data output during oxidation. Each experiment included four cycles. Each cycle consisted of a ramp up from 30°C/min to 1350°C, a reduction in nitrogen for 30 min, a ramp down at 6°C/min to 800°C or 900°C, a isotherm for 10 min to

stabilize the temperature and 15 min oxidation with the various percentages of carbon dioxide balanced with nitrogen.

The CO rate production measurement during the oxidation phase, which was considered for the analysis of the reactivity of the material, was calculated according to the following equation:

$$\dot{\omega}_{CO,oxi} = \frac{X_{CO,out}\,\dot{n}_{oxi,in}}{m_{OC}} = \frac{X_{CO,out}}{m_{OC}}\,\frac{P^0\dot{V}^0_{oxi,in}}{R\,T^0} \tag{4.1}$$

Where $X_{CO,out}$, is the mole fraction CO, $\dot{n}_{oxi,in}$ is the molar inflow of the gas mixture during the oxidation phase while P^0, T^0, and $\dot{V}^0_{oxy,in}$ are the pressure, temperature and volume flow at standard conditions (STP).

We show in the graphs shown below, as a representative example, the CO production rate during CO_2 splitting on the oxygen vector sample, as a function of time for four chemical cycles.

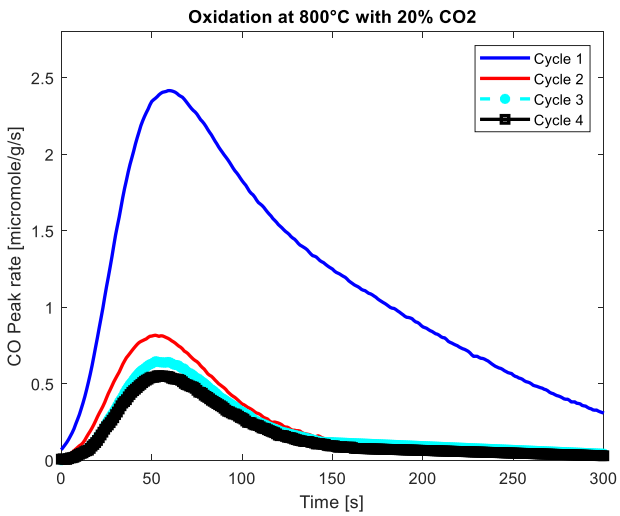

Figure 49 - Production rate of CO at 800 °C and CO_2: 20% for four cycles

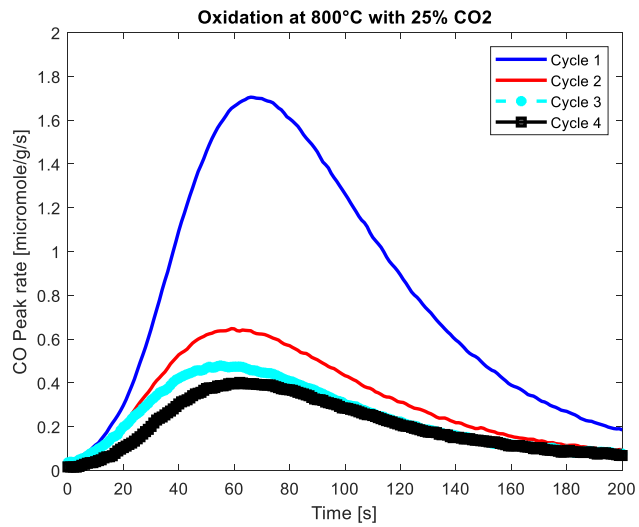

Figure 50 - Production rate of CO at 800 ° C and CO_2: 25% for four cycles

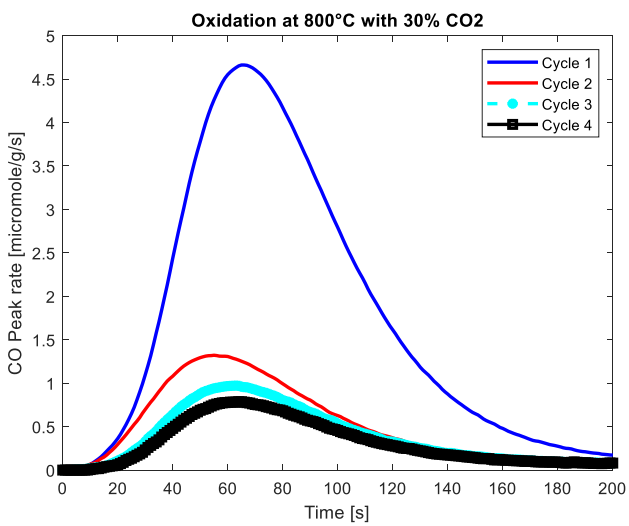

Figure 51 - Production rate of CO at 800 ° C and CO_2: 30% for four cycles

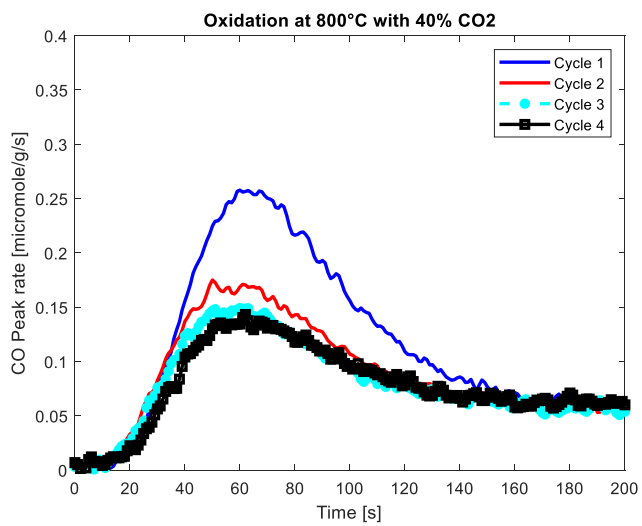

Figure 52 - Production rate of CO at 900 ° C and CO_2: 40% for four cycles

By observing the graphs above it is possible to observe that in the four data sets reported there is a lowering of the CO production rate peak, probably because following the first reduction and oxidation inside the oxygen vector there was carbon deposition which leads to deactivation of the material and consequently to a lower CO yield.

Comparing the Figure 51, with the other graphs shown in the other figures, it is noted that the maximum CO peak occurs following oxidation at 800°C with a CO_2 concentration equal to 30 vol%, it is clearly shown in the Figure 53.

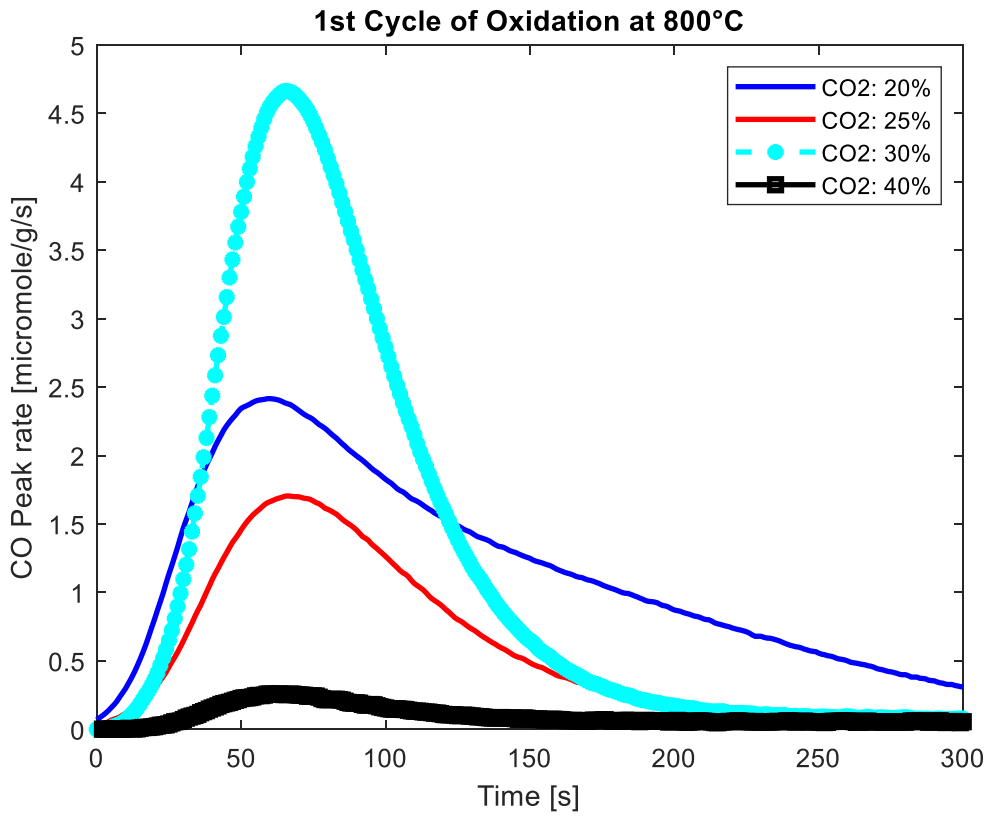

Figure 53 - CO production rate at 800 °C as the CO_2 concentration varies

From the Figure 53, where only the first cycles of each test are represented, it is noted that there is no linearity in the behavior of the material, what was expected was an increase in CO production as the CO_2 concentration increases. A peak is obtained at a concentration of 30 vol% and a minimum at a value of 40 vol%.

Further tests were carried out to better understand the phenomenon and the behavior of the material at the oxidation temperature of 900°C was analyzed.

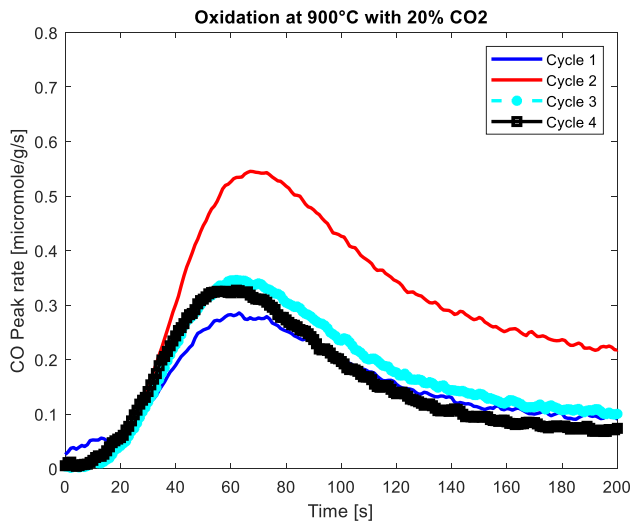

Figure 54 - Production rate of CO at 900 °C and CO_2: 20% for four cycles

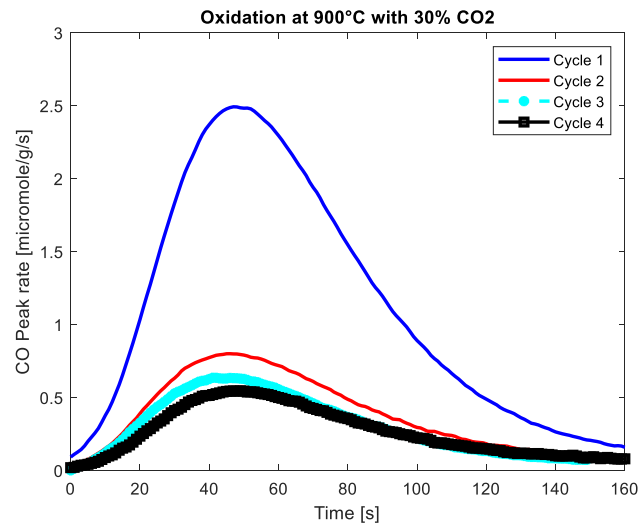

Figure 55 - Production rate of CO at 900 °C and CO_2: 30% for four cycles

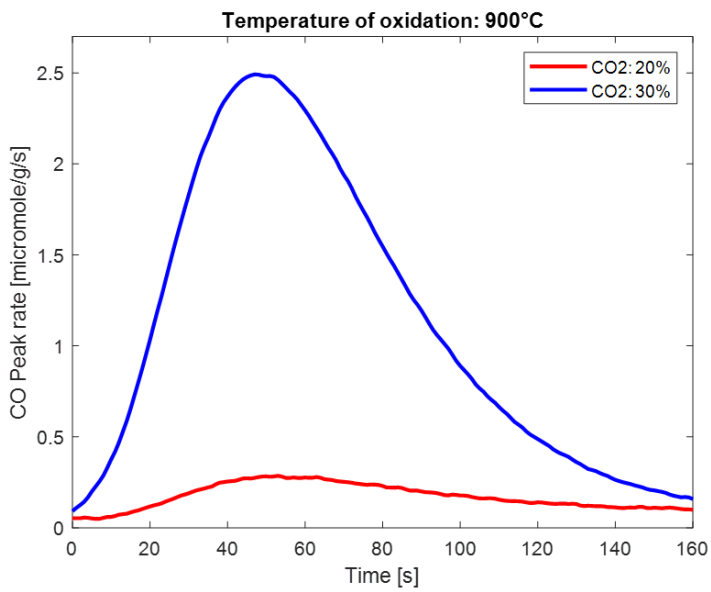

Figure 56 - CO production rate (µmol/g/s) during the oxidation phase at 900 °C with CO_2 concentration of 20 vol% and 30 vol%

Looking at the graph in Figure 54, it is noted that in this case a clear improvement is obtained for second cycle, negating what occurred during the test with the oxidation at 800°C.

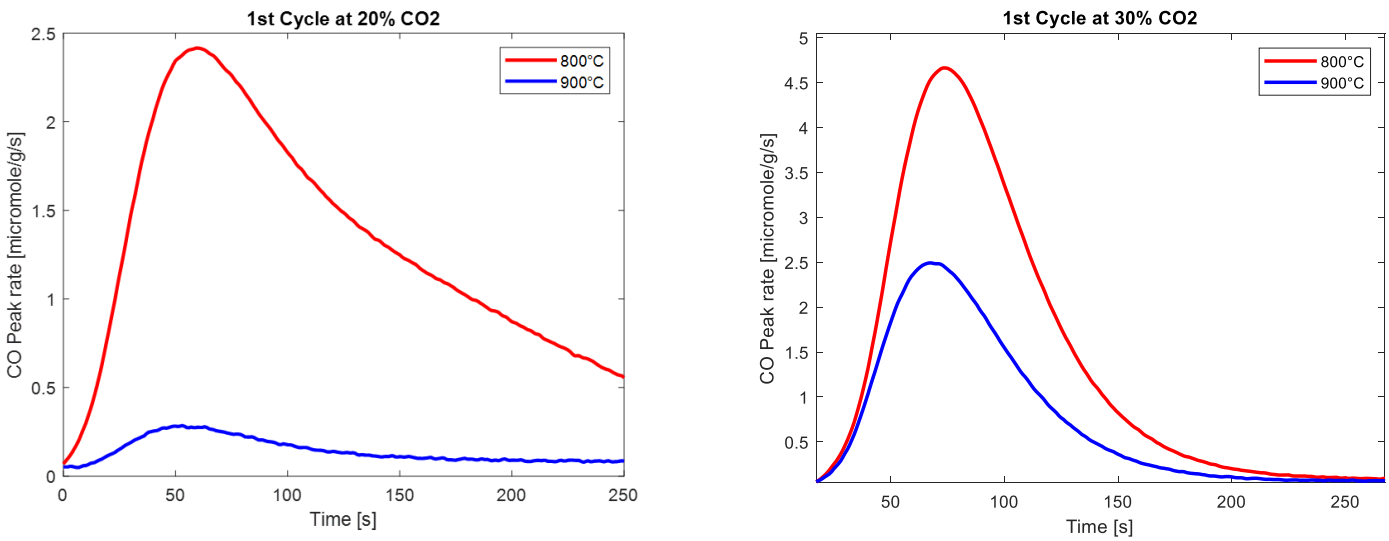

a) *b)*

Figure 57 - CO production rate (µmol/ g / s) during the oxidation phase with feeding temperatures of 800 °C and 900 °C to CO2 of a) 20 vol% and b) 30 vol%

In conclusion, observing the data obtained, the kinetics of the system is not very clear, but it is deductible that under these conditions of reduction in temperature with nitrogen, there is evidently a lot of carbon deposition formation which leads the material to have unpredictable behaviors, probably also due to the presence of traces of Mg inside the Fe_2O_3 powders. The phenomenon of carbon deposition in this experiment is evident from the moment after the first cycle when the peaks collapse, after the first cycle the sintering phenomenon has occurred, thus preventing the escape of oxygen. For this reason, in the subsequent tests, we opted for the use of H_2 which tends to reduce the formation of carbon.

4.3. Experimental Test 2

In the second set of experimental data, an alumina boat reactor was used to carry out TPR and TPO in redox cycles with iron oxide powders. At the bottom of the reactor 200 mg of iron oxide powder were incorporated.

Based on the reported studies, Al_2O_3 support is selected because it has strong resistant mechanical properties. Implementation various tests to increase the maximum oxygen transport capacity with different iron oxides charged at high temperatures. It is observed that with multiple redox cycles at high temperatures, the alumina interacts with the iron and the structure forms a spinel phase so that the sample does not oxidize to produce CO. Therefore, the alumina support must be pre-treated with a divalent cation such as magnesium to avoid spinel formation. [27]

In our case, a pre-treatment of the boat reactors at a high temperature of 1350 °C was carried out. In the first experimental test, since there had been too much carbon deposition inside the tubular reactors, it was necessary to perform a high temperature pre-treatment, 1000 °C with 10 vol% of H_2.

4.3.1. Thermodynamic Analysis

Wanting to do a thermodynamic analysis it must be said that oxidation is a single step or as a multi-phase reaction [28]. The thermal reduction of the material leads Fe/FeO to the next phase of Fe_3O_4 instead of Fe_2O_3. Precisely because of the thermodynamic constraints, the oxidation of Fe_3O_4 with CO_2 is almost impossible.

At 1173 K, for example, CO levels from 10 ppm (K_p <10-5, where K_p represents the equilibrium constant of the reaction) prevent the transition from Fe_3O_4 to Fe_2O_3. Since the oxygen storage capacity of Fe_2O_3/Fe and Fe_2O_3/FeO are 0.3 and 0.1 respectively while Fe_3O_4/FeO is 0.069, this implies that the metal oxide works in a restricted region of the storage capacity of oxygen by dissociation of CO_2. Further oxidation of Fe_3O_4/Fe_2O_3 in air or oxygen can be performed. [29] [30].

However, it has been shown that particle agglomeration can occur in CL systems and leads to more complex three-step redox reaction system. From Figure 58, the equilibrium diagram of the CO_2 oxidation of iron oxides in the atmosphere is shown.

$$R1:\ \ CO_2(g) + 3FeO \rightarrow Fe_3O_4 + CO(g) \tag{4.2}$$

$$R2:\ \ CO_2(g) + 3.807Fe_{0.947}O \rightarrow 1.202Fe_3O_4 + CO(g) \tag{4.3}$$

$$R3: CO_2(g) + Fe \rightarrow FeO + CO(g) \tag{4.4}$$

$$R4: C +\ CO_2(g) \rightarrow 2CO(g) \tag{4.5}$$

$$R5: 3FeO + 5CO \rightarrow Fe_3C + 4CO_2(g) \tag{4.6}$$

$$K_p = exp\left(\frac{-\Delta G_T^0}{RT}\right) = \frac{P_{CO}}{P_{CO_2}} = \frac{P_{total}\, X_{CO}}{P_{total}\, X_{CO_2}} = \frac{X_{CO}}{X_{CO_2}} = \frac{1 - X_{CO_2}}{X_{CO_2}} \tag{4.7}$$

$$X_{CO_2} = \frac{1}{1 + K_p} \tag{4.8}$$

The equilibrium constants of the reactions (R1) - (R5) share the same formulation, given by equation (4.7), which shows the pressure ratio of carbon monoxide to that of carbon dioxide.

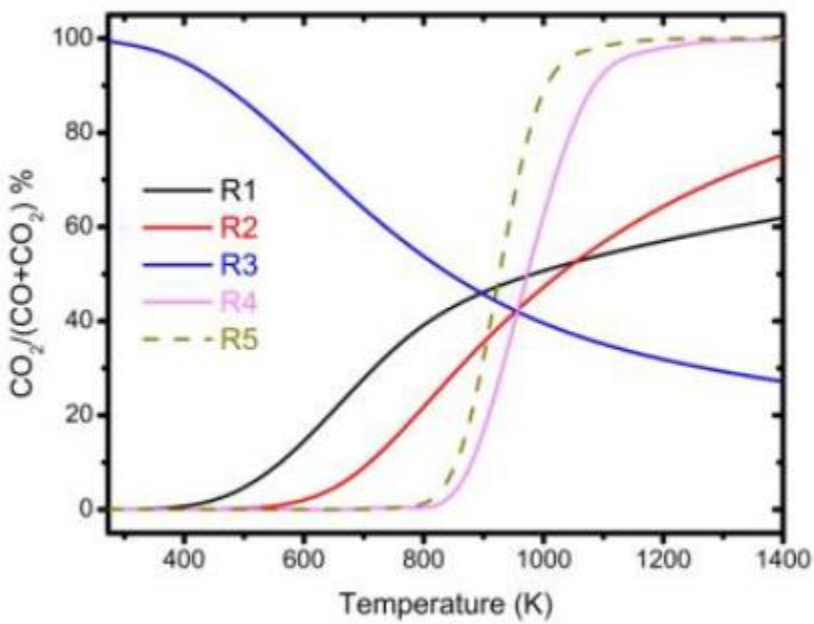

Figure 58 - Thermodynamic equilibrium of the sample oxygen vector of CO_2

The Figure 58, shows the equilibrium diagram of the CO_2 oxidation of iron oxides in the atmosphere, R1-R5 represent the reactions described by equations (4.2) - (4.6) respectively. The lines representing R1 and R2 increase with temperature, such as the oxidation of FeO

and non-stoichiometric from wustite to magnetite, are endothermic reactions. Instead, the R3 line decreases with temperature, which indicates that the reaction of metallic Fe to wustite is an exothermic reaction. Line R4 considers the Boudouard reaction relating to Fe/FeO oxidation with the formation of CO at high temperatures (> 973 K).

The above reaction is possible because iron acts as a catalyst leading to further carbon formation when it is transformed into iron carbide to deactivate the oxygen carrier as can be seen in the R5 line.

The Figure 58, shows that the R4 reaction tends to increase at higher temperatures and the equilibrium between reactant (CO_2) and production (CO) is sensitive below 900°C. For this reason, the kinetic investigation was carried out considering the temperatures of 700°C, 800°C, 900°C and 1000°C.

4.3.2. Experimental set up

To perform the test, a total gas flow rate was set at 200 Nml/min both during the reduction phase and during the oxidation phase. The reduction step was performed at a temperature equal to that of oxidation and with at 5 vol% of H_2, balanced with N_2. The oxidation was done with CO_2 concentrations of 20 vol% and 40 vol%, balanced with N_2. The tests were conducted considering a set of temperatures of 700°C, 800°C, 900°C and 1000°C.

The gas analyzer measured the CO data output during oxidation. Each experiment comprised five cycles. Each cycle consisted of an ramp up of 20°C/min to the set temperature, 700°C, 800°C, 900°C or 1000°C, a reduction with 5 vol% H_2 balanced with nitrogen for 30 min, a 10 min isotherm with only N_2 to clean up any residues of other gases, an oxidation of 15 min with the various percentages of carbon dioxide balanced with nitrogen and, finally, a second isotherm of 10 min with only N_2 to then start the cycle all over again.

The CO measurement during the oxidation phase, which was considered for the analysis of the reactivity of the material, was calculated according to the following equation:

$$\dot{\omega}_{CO,oxi} = \frac{X_{CO,out}\,\dot{n}_{oxi,in}}{m_{OC}} = \frac{X_{CO,out}}{m_{OC}}\,\frac{P^0\dot{V}^0_{oxi,in}}{R\,T^0} \tag{4.9}$$

Where $X_{CO,out}$, is the mole fraction CO, $\dot{n}_{oxi,in}$ is the molar inflow of the gas mixture during the oxidation phase while P^0, T^0, and $\dot{V}^0_{oxi,in}$ are the pressure, temperature and volume flow at standard conditions (STP).

4.4. Results and Discussion

We show in the graphs shown below, as a representative example, the CO production rate during CO_2 splitting on the oxygen vector sample, as a function of time for five chemical cycles.

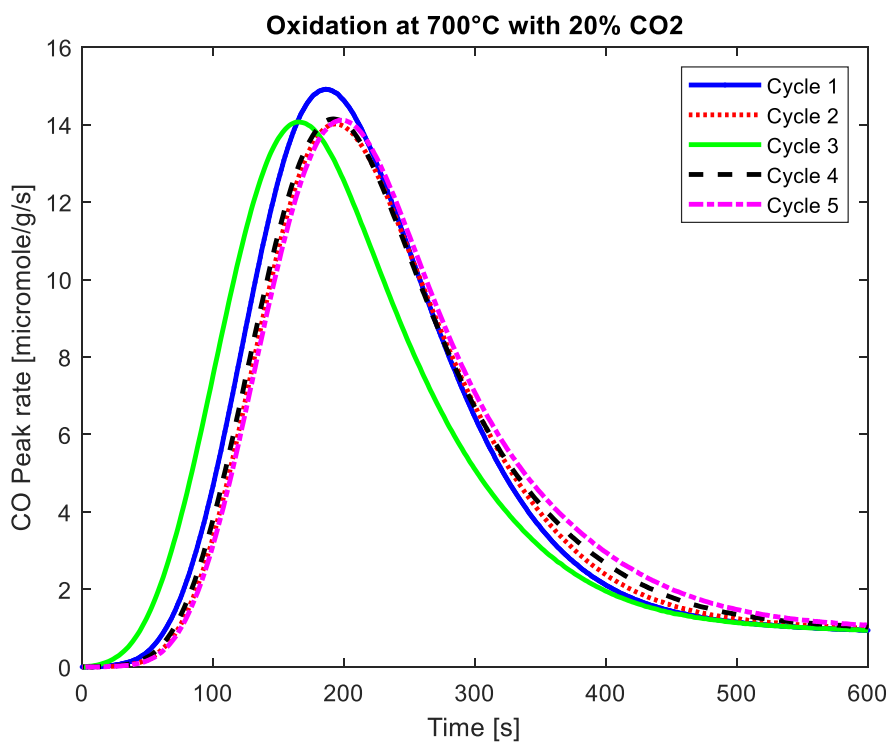

Figure 59 - Production rate of CO at 700 ° C and CO_2: 20% for five cycles

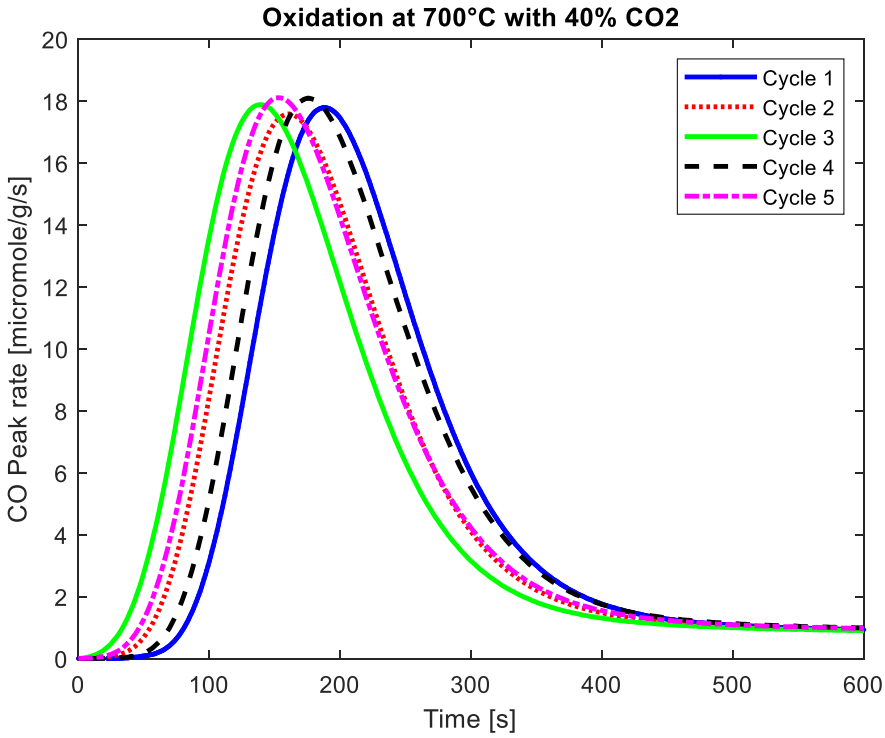

Figure 60 - Production rate of CO at 700 ° C and CO_2: 40% for five cycles

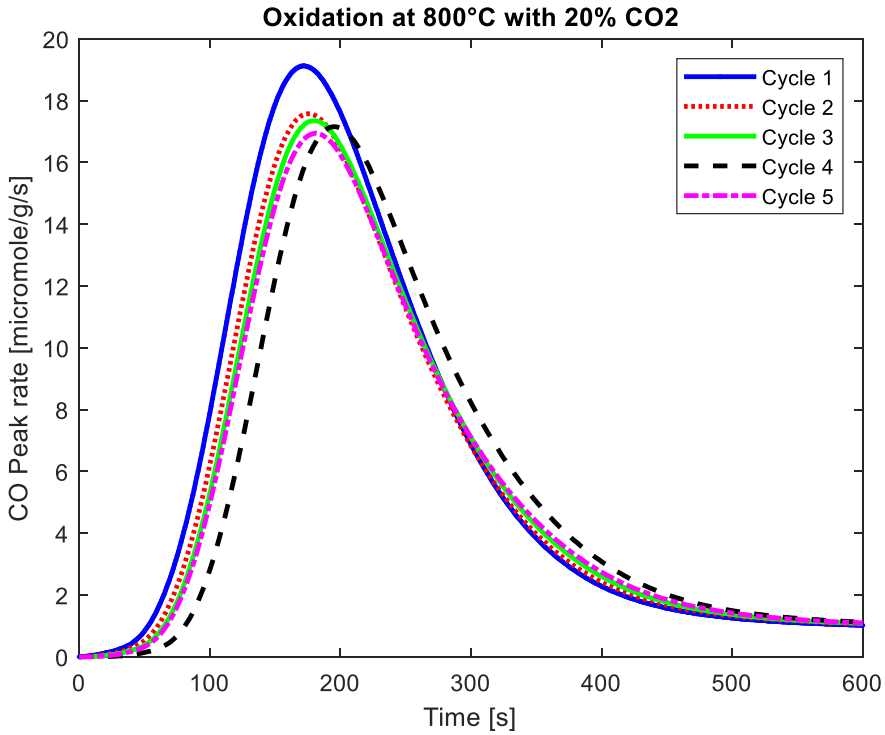

Figure 61 - Production rate of CO at 800 ° C and CO_2: 20% for five cycles

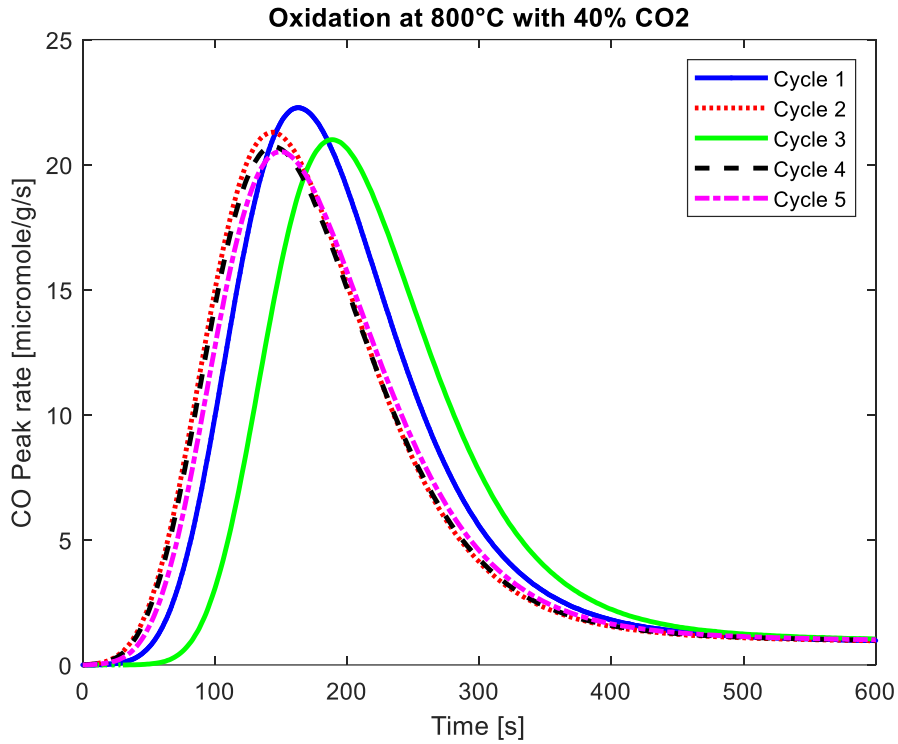

Figure 62 - Production rate of CO at 800 ° C and CO_2: 40% for five cycles

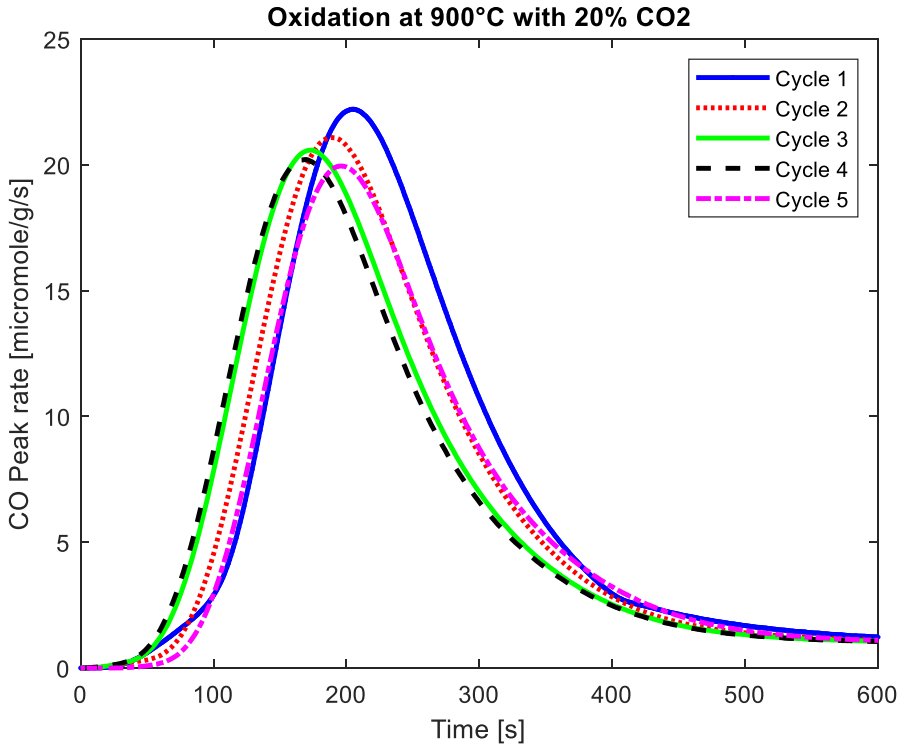

Figure 63 - Production rate of CO at 900 ° C and CO_2: 20% for five cycles

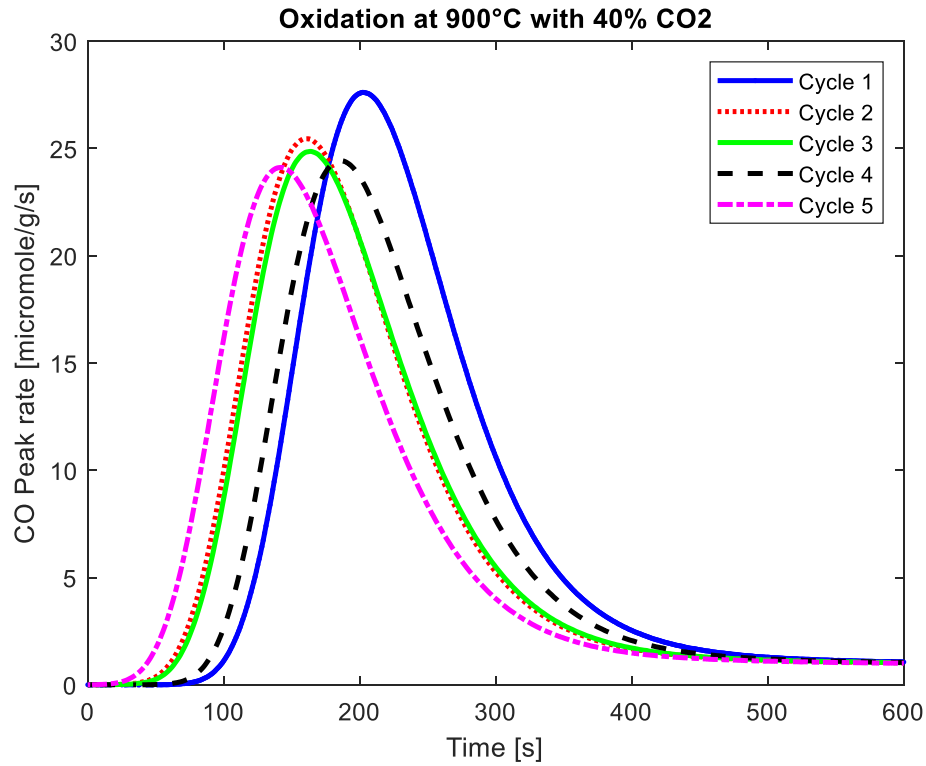

Figure 64 - Production rate of CO at 900 ° C and CO_2: 40% for five cycles

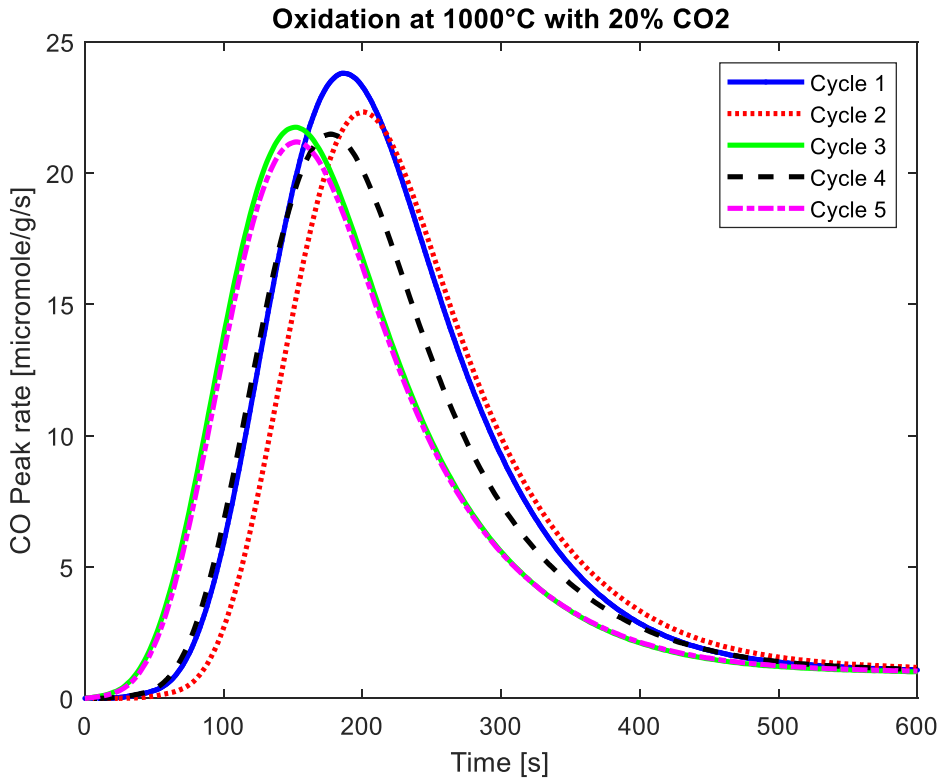

Figure 65 - Production rate of CO at 1000 ° C and CO_2: 20% for five cycles

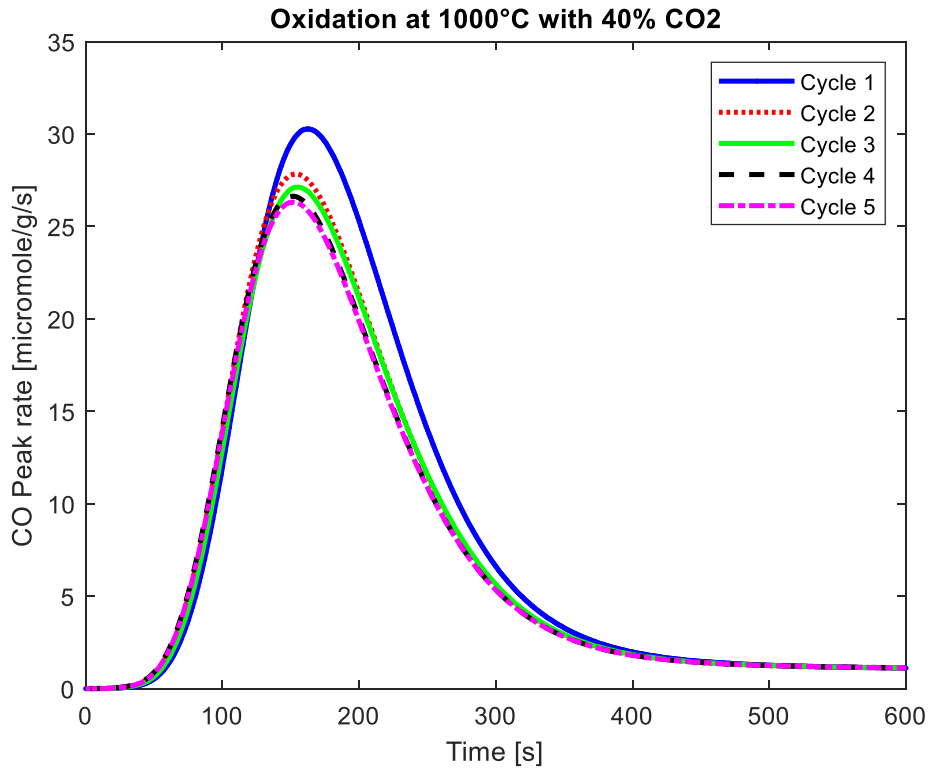

Figure 66 – Production rate of CO at 1000 ° C and CO_2: 40% for five cycles

Observing the graphs shown above, it is noted that there is a minimum decrease in the CO peak starting from the first cycle up to the fifth. In this case the effect of carbon deposition appears very slight since during the reduction phase, hydrogen is sent which "cleans" the dust by reacting with the carbon.

Also in this case, as in the previous one, the peak of the CO production rate of the various cycles is in the initial phase of oxidation, this depends on the presence of greater vacancies in the initial phase, which therefore create faster kinetics.

Looking the Figure 66, is shown the CO production rate during CO_2 splitting on the sample oxygen carrier as a function of time for five isothermal chemical cycles, a 10% decrease in the maximum production rate between the first and second cycle can be noted, but this decrease it dissolves by the third cycle and there is no change in CO production behavior from the fourth to the fifth cycle. There is no significant difference between the maximum CO production rate in the fourth and fifth cycle for the oxygen carrier.

Similarly, in Figure 67 (a-d), the total production in *μmol/g/s* of oxygen carrier was shown for the five cycles for each temperature and CO_2 concentration considered in the present study. It is observed that the production of CO from the third cycle becomes stable.

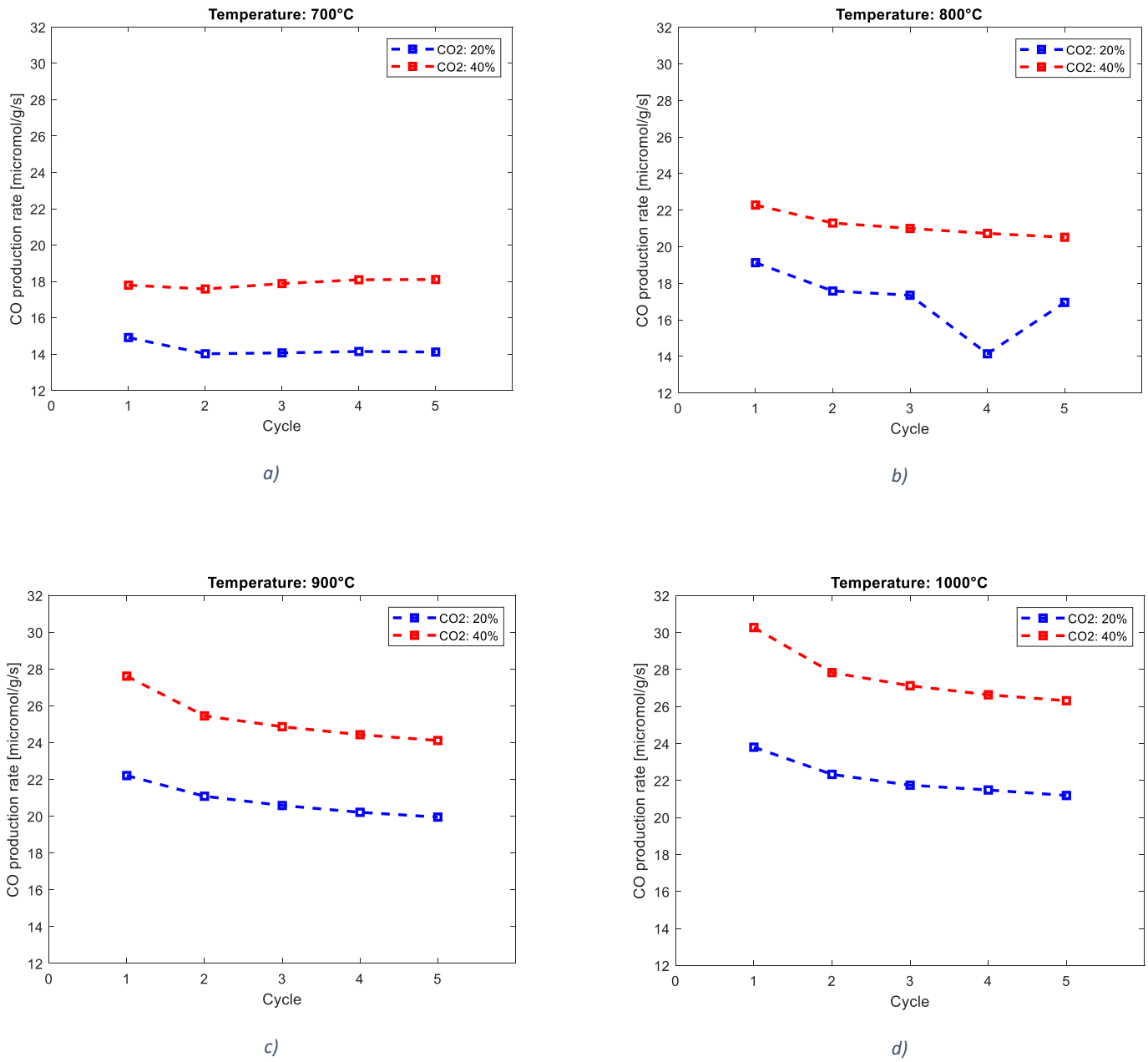

Figure 67 - Specific production of specific CO for different temperatures and CO_2 concentration in the different cycles

4.4.1. Effect of Temperature and CO_2 Concentration

The Figure 68 shows the CO production rate profile (*µmol/g/s*) at different temperatures from 700°C to 1000°C at different CO_2 concentrations. It is observed that at beginning the rate of CO is fast due to the more rapid absence of oxygen and the incorporation of ions, while subsequently the rate of CO production decreases as the oxygen gaps remaining in the reticulum of the sample are filled.

The concentration of the reactants and the oxidation temperature are decisive for the maximum CO peak rate.

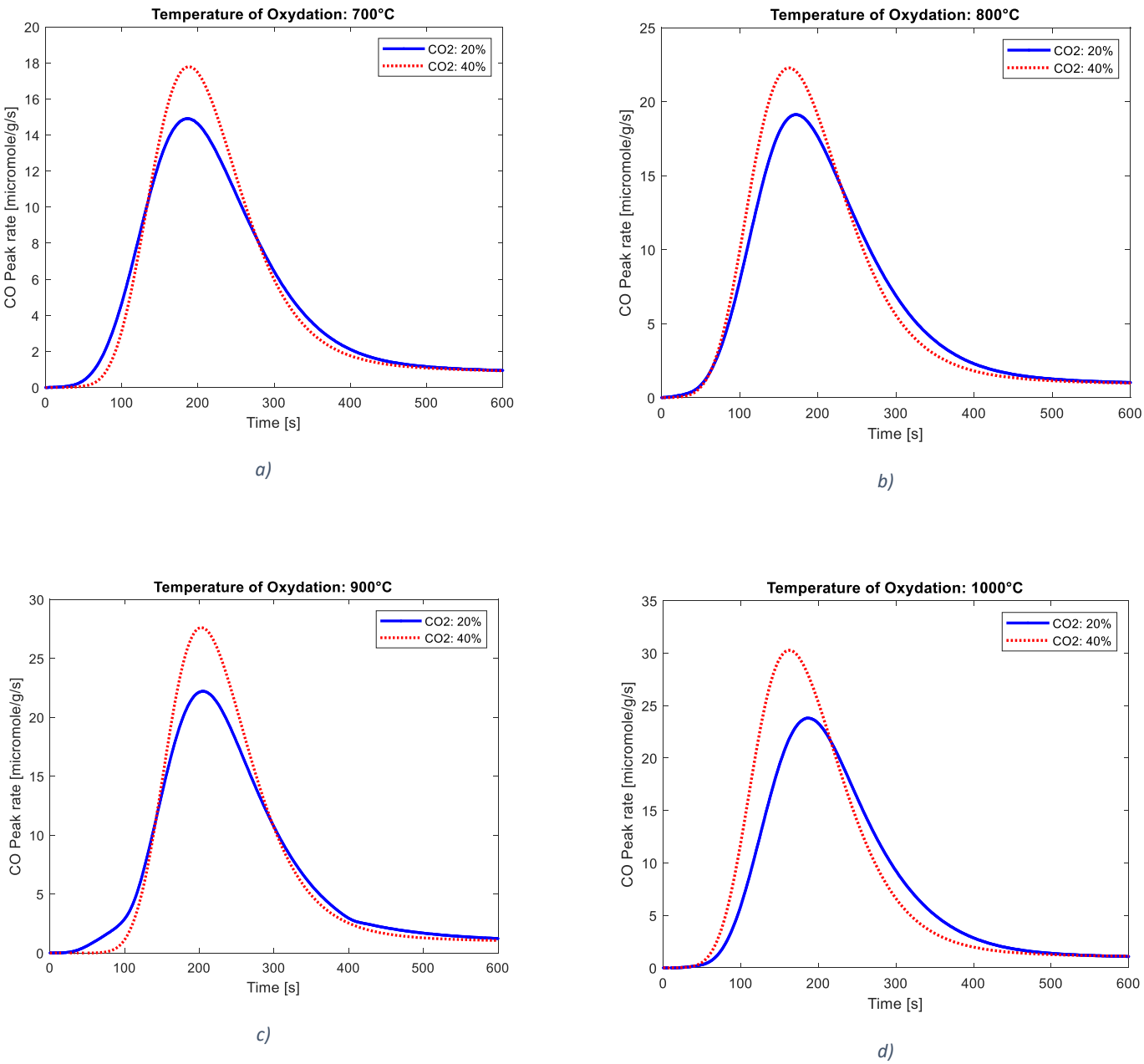

Figure 68 - CO production rate (µmol/g/s) during the oxidation phase with CO_2 supply of 20 to 40 vol% (a) 700 °C (b) 800 °C (c) 900 °C (d) 1000 °C

It is easy to observe, how at a temperature of 700°C, CO production is limited due to the fewer oxygen vacancies created during the reduction phase and this is confirmed precisely because by reducing at higher temperatures, CO production increases. It is noted, in fact, that the increase in the temperature to 1000°C showed a significant improvement in the peak production rates, more than two times higher.

It can also be observed that CO production rates peaked in about 100-125 seconds and the peak amplitude increases at higher temperatures due to higher oxygen sites created. CO_2

splitting rates decrease after peaking, for all reported temperatures, and reach zero between 500-630 seconds depending on temperature and of CO_2 concentration.

The Figure 69 (a) and (b) represents the CO production peaks at different temperatures between 700-1000°C, with a CO_2 concentration of 20 vol% and 40 vol%. CO_2 splitting rates show a profile with a rapid increase around the temperature of 1000°C and drops to 700°C.

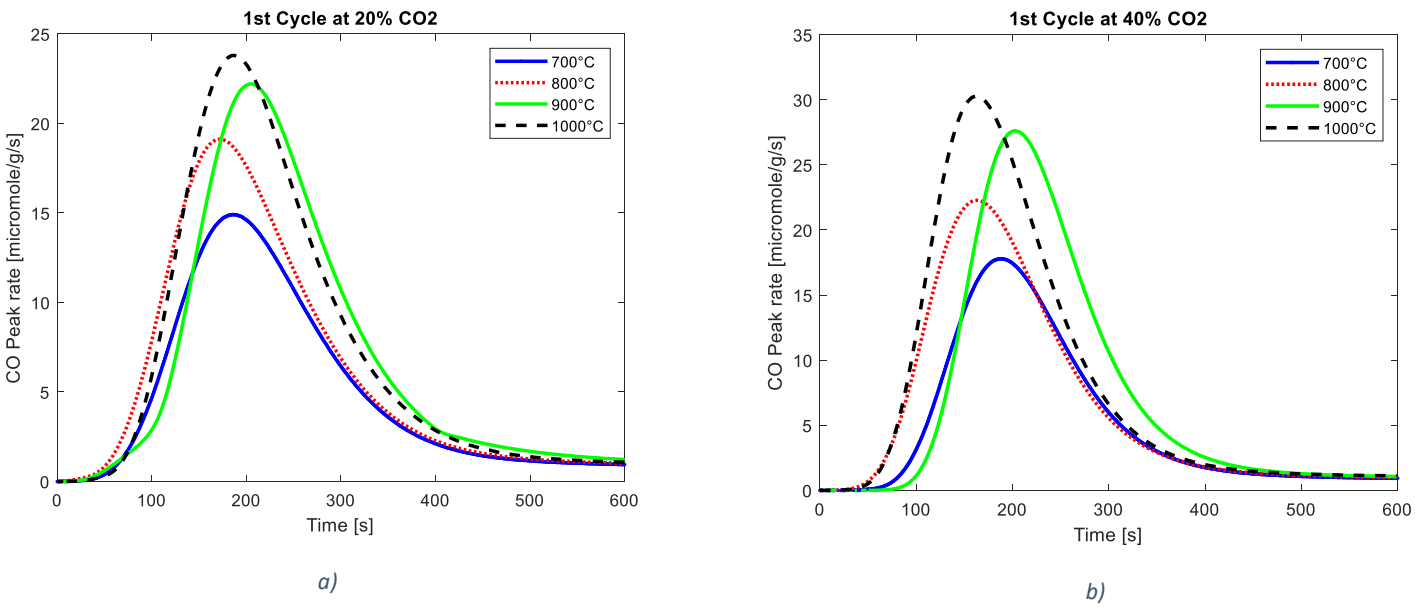

Figure 69 - CO peak production rate as the concentration of a) 20% CO_2 and b) 40% CO_2 varies

The increase in CO production rates is greater for a higher CO_2 concentration. The maximum CO production rate achieved for CO_2: 20 vol% and 700 °C was about 15 µmol/g/s while at 1000 °C it was found to be almost double with a production rate of 24 µmol/g/s. There is also an appreciable increase in the rate of CO production with increasing temperatures.

With increasing the CO_2 concentration to 40 vol%, the increase in the CO production rate has been seen to be exponential up to 1000°C.

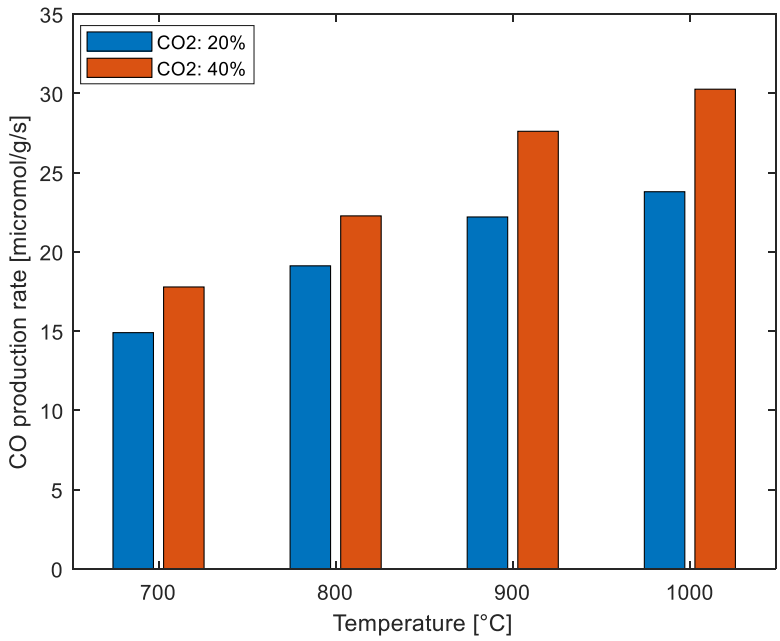

Figure 70 - Production speed of the CO peak with different temperatures

From the total CO production and the peak rate of CO, the influence of CO_2 concentration and temperature, are equally important for lower CO_2 concentrations. At a higher temperature, the effect of the CO_2 concentration replaces the influence of temperature on the production of CO, which means that the whole process of CO_2 splitting must be limited in the small temperature range between 900°C and 1000°C to have significant levels of CO production speed and the same time to avoid material deactivation.

In Chapter 3.1 we saw how the sintering effect on the material increases as the temperature, concentration and reduction times increase. In this work it was not possible to observe the sintering effect at higher temperatures, but in general it is expected, thanks to the CO yield studies conducted by Azharuddin E Farooqui on ceria using Chemical Looping process [27], that a reduction of the CO peak can probably be achieved at temperatures higher than 1000°C. For this reason, it is necessary to conduct further tests, at higher temperatures and varying the reduction times to understand the kinetics of the system and the phenomenon of carbon deposition.

4.5. Experimental Test 3

In the third experimental test an alumina boat was used to carry out the TPR and TPO in the redox cycles with 200 mg of iron oxides powder were incorporated into the bottom of the boat. The purpose of this test is to obtain syngas from the chemical looping process.

Significantly, the Steam Methane Reforming (SMR) based chemical looping process is a two-step method for generating syngas. In this process, methane is selectively converted to syngas by an oxygen carrier in the first reduction stage (methane conversion) [31]. In the second step, they are oxidized with carbon dioxide to obtain CO. Therefore, synthesis gas and pure CO can be produced by these redox reactions represented as follows:

Reduction →

$$MeO_x + \delta CH_4 \rightarrow MeO_{x-\delta} + \delta(2H_2 + CO) \tag{4.10}$$

Oxidation →

$$MeO_{x-\delta} + \delta CO_2 \rightarrow MeO_x + \delta CO \tag{4.11}$$

4.5.1. Experimental set up

To perform the test, a total gas flow rate was set at 200 Nml/min both during the reduction phase and during the oxidation phase. The reduction phase was carried out at a temperature equal to that of oxidation and was carried out at 30 vol% of CH_4, balanced with N_2. The oxidation was done with a CO_2 concentration of 40 vol%, balanced with N_2. The test was performed considering the temperature of 900°C.

The gas analyzer measured the CO and H_2 output data during oxidation. The experiment included five cycles. To perform the test it was necessary to impose an ramp up of 20 °C/min to the fixed temperature of 900°C, a reduction with 30 vol% of CH_4 balanced with nitrogen for 30 min, an isotherm of 10 min with only N_2 to clean up any residues of other gases, an oxidation of 15 min 40 vol% of carbon dioxide balanced with nitrogen and, finally, a second isotherm of 10 min with only N_2 and then start the cycle all over again.

The measure of H_2 during the reduction phase is given by:

$$\dot{\omega}_{H_2,red} = \frac{X_{H_2,out}\,\dot{n}_{red,in}}{m_{OC}} = \frac{X_{H_2,out}}{m_{OC}}\,\frac{P^0\dot{V}^0_{red,in}}{R\,T^0} \tag{4.12}$$

The CO measurements both during the oxidation and reduction phase which was considered for the assembly of the necessary kinetic model according to the following equations:

$$\dot{\omega}_{CO,red} = \frac{X_{CO,out}\,\dot{n}_{red,in}}{m_{OC}} = \frac{X_{CO,out}}{m_{OC}}\,\frac{P^0\dot{V}^0_{red,in}}{R\,T^0} \tag{4.13}$$

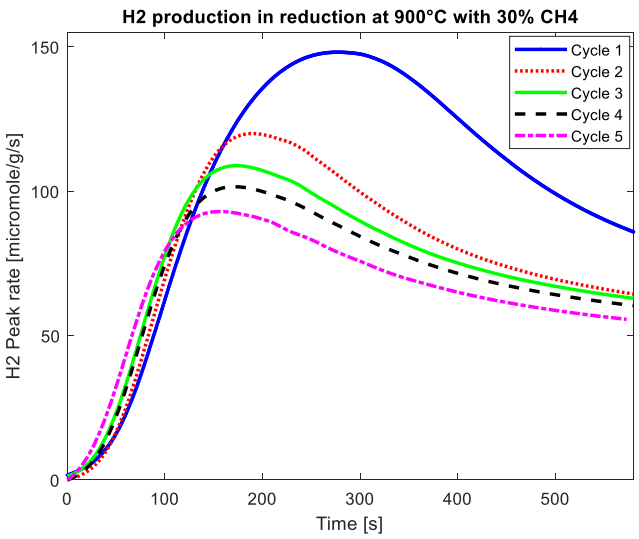

Figure 71 – H_2 production in reduction with 30 vol% CH_4

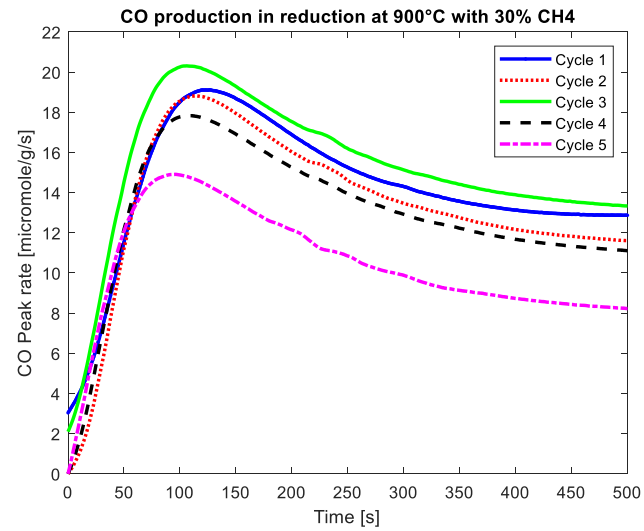

Figure 72 - CO production in reduction with 30 vol% CH_4

$$\dot{\omega}_{CO,oxi} = \frac{X_{CO,out}\,\dot{n}_{oxi,in}}{m_{OC}} = \frac{X_{CO,out}}{m_{OC}}\,\frac{P^0\dot{V}^0_{oxi,in}}{R\,T^0} \tag{4.14}$$

Where $X_{CO,out}$, is the mole fraction of CO, $X_{H_2,out}$ is the mole fraction of H_2, $\dot{n}_{oxi,in}$ and $\dot{n}_{red,in}$ is the molar inflow of the gas mixture during the oxidation and reduction phase, while P^0, T^0, $\dot{V}^0_{oxi,in}$ and $\dot{V}^0_{red,in}$ are the pressure, temperature and volume flow, in oxidation and reduction, at standard conditions (STP).

We show in the graphs shown below, as a representative example, the production rate of CO and H_2 that occur in the two phases.

As can be seen during the reduction phase we obtain very high H_2 producibility values but at the same time we obtain a good production of CO, in the oxidation phase we only get CO with a high peak of producibility.

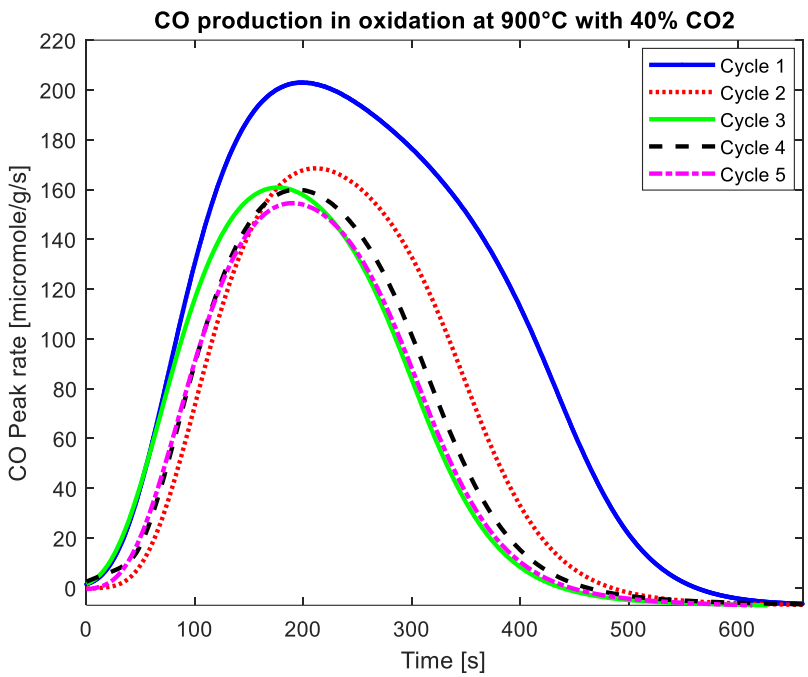

Figure 73 - CO production in oxidation with 40 vol% CO_2

It should be noted that the peaks in both the reduction and oxidation phases become lower as the cycles progress and this is always because of carbon deposition on the material.

This type of experiment is aimed at generating syngas, in fact, there are two moving bed reactors in chemical looping (CO_2) splitting unit that produces syngas that can be sent to a power plant. The reduction reactor produces syngas, using methane as a reducing agent, the iron oxides are then transported to the oxidation reactor where the carbon dioxide acts as an oxidant to produce CO.

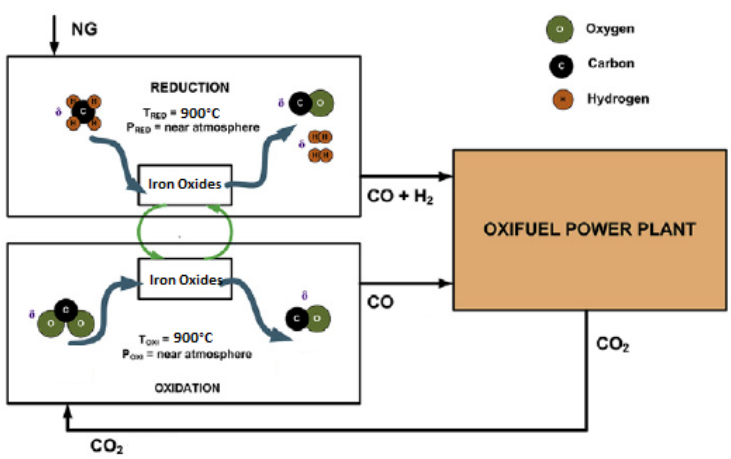

Figure 74 – SMR system diagram [32]

4.6. TGA Description

At the laboratory of the Energy Department of the Polytechnic of Turin, the continuous process of oxidation and thermochemical reduction of iron oxides was carried out, focusing mainly on the two-phase redox cycle for CO_2 splitting. To better understand the physics of the system and the effects of cyclicality, experiments were conducted under controlled conditions using a thermogravimeter, i.e. an instrument that detects the change in weight of a material according to temperature, as a result of the possible decompositions that it undergoes following the release of gaseous products. In general, thermogravimetric analysis (TGA) is a quantitative thermal analysis that allows to evaluate the thermal stability of a certain compound by measuring how much mass is lost from the sample at a certain temperature, without however distinguishing the nature of the species released. [33]

The results obtained consist of graphs, called thermogravimetric curves, which report the mass as a function of temperature and contain relevant information on thermal stability, reaction rates and processes and the composition of the sample. A typical example of thermogravimetric curves is shown in Figure 75.

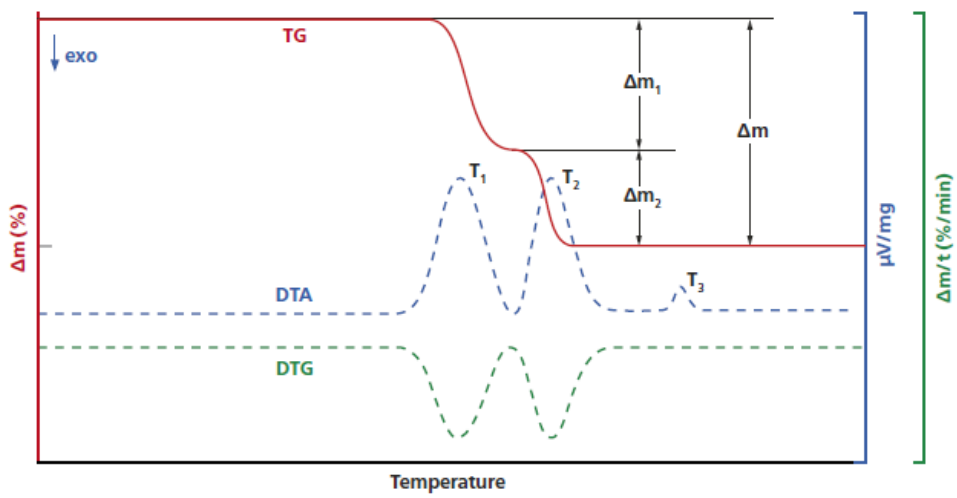

Figure 75 - TG thermogravimetric curve (phenomena accompanied by weight changes) combined with the differential thermal analysis DTA (thermal behavior following heating) as a function of temperature [34]

The TG reveals only phenomena accompanied by weight changes while the DTA also shows those (such as phase transitions) not accompanied by weight changes.

The DTG curve resembles the DTA curve and their comparison allows to distinguish the transformations that occur with changes in weight and enthalpy from those that occur with only a change in enthalpy.

The thermogravimeter used in the laboratory (model: NETZSCH STA 2500 Regulus) consists of:

- Thermal balance or thermobalance: it is an extremely precise balance in which the sample is progressively heated from the room temperature up to exceeding 1500°C with programmable thermal ascent/descent ramps. The available technology is based on the use of an electronic monitoring system with high sensitivity photodiodes, used for the continuous detection of the position of the two arms of the balance: one inserted in the furnace containing the sample and one on which an empty reference sample holder is placed. [35]
- Furnace: generally made of refractory material (alumina Al_2O_3 with T_{fusion}> 2000°C or quartz with T_{fusion}> 1700°C).
- Crucibles: containers intended for containing the sample and for the reference counterweight. They are manufactured with inert materials, such as steel (for applications at T<600-650°C), platinum or alumina.
- System with purge gas that guarantees a controlled atmosphere inside the furnace, maintaining proper ventilation and gas recirculation: in this way any gaseous substances released because of the decomposition of the analyzed material are expelled.
- Temperature monitoring system: essential to ensure the correct implementation of the thermal programs, from maintaining the temperature (isotherm) to transient heating/cooling actions (temperature ramp); the continuous measurement is carried out by means of platinum thermocouples coated with ceramic material and placed inside the furnace near the analyzed sample
- Digital interface for instrument control, data acquisition and display. [33]

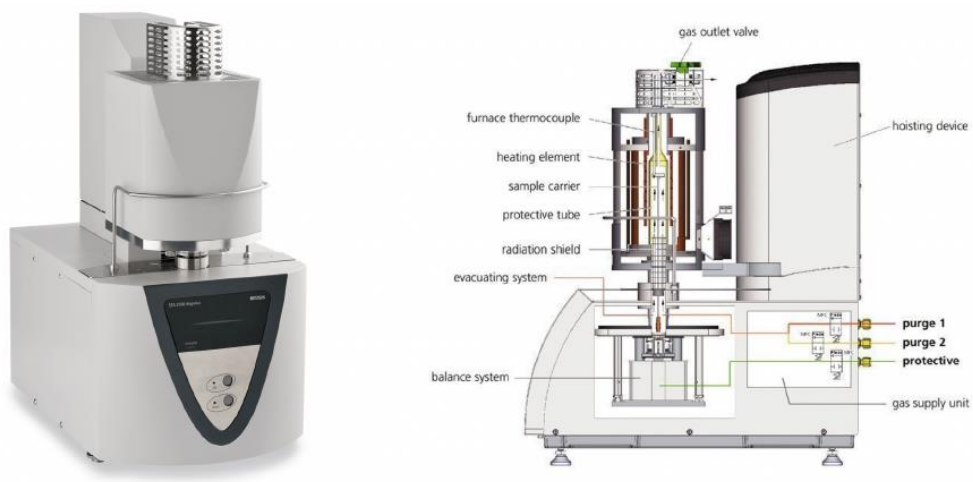

Figure 76 - NETZSCH STA 2500 Regulus thermogravimeter used for TGA analysis in the laboratory of the Energy Department. The image on the right shows the section view of the instrument with the main internal components indicated [36]

The main thermogravimetric effects that can be quantified thanks to the instrument described above concern the TGA curves as the absolute mass (mg) or relative mass (%)

varies, the phenomena of chemical dissociation, the thermokinetics of the reactions, the redox behavior and the chemical composition of the material. [36]

• **Temperatura max. campioni:** 1600°C (in base alla fornace, facilmente scambiabili)	• **Fornace I:** da TA a 1100°C (velocità di riscaldamento da 0,001 a 100 K/min) **Fornace II:** da TA a 1600°C (velocità di riscaldamento da 0,001 a 50 K/min)	• **Precisione di temperatura:** 0.3K
• **Range di pesata:** ± 250 mg	• **Carico campione:** 1 g max.	• **Risoluzione termogravimetrica:** 0.03 µg
• **Termocoppia:** tipo S	• **Sistema a tenuta di vuoto:** fino a 10^{-4} mbar (10^{-2} Pa)	• **Atmosfere gas:** inerte, ossidante, vuoto

Figure 77 - NETZSCH STA 2500 Regulus thermogravimeter technical specifications [36]

The STA 2500 thermogravimeter features a top load differential balance with extremely low thermogravimetric resolution. The self-compensating differential balance (Figure 78) operates thanks to two thin symmetrical arms, connected respectively to the rod on which the reference crucible is positioned and to the rod relating to the crucible containing the sample to be analyzed. Both rods with their respective crucibles are placed inside the oven. The compensation system, consisting of two magnetic coils, is controlled by a high precision optical sensor. This avoids shaft movements ensuring a stable and accurate balance with a weighing tolerance of ± 250 mg. The differential balance setting also serves to compensate for possible floating effects that could occur during variations in the gas flow. [34]

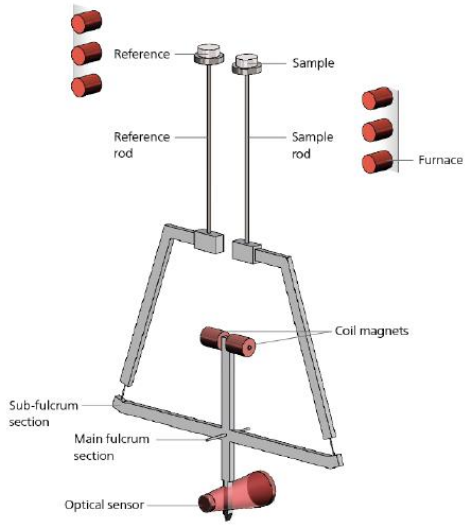

Figure 78 - Schematic representation of the top-loading differential scale of the STA 2500 Regulus [34]

The thermogravimetric (TGA) test of the iron oxides sample was conducted in the laboratory using the NETZSCH STA 2500 Regulus. Once the calibration of the thermogravimeter was completed, the tests were carried out to balance the sampling crucible with the reference.

4.6.1. Experimental Test 1

The first test was conducted by execution an oxidation with 20 vol% of CO_2 and a reduction in 1% of H_2 in an isotherm of 800°C.

The measurements were performed using an alumina crucible (Al_2O_3) having a mass of 100 mg and filled with iron oxide powder (about 28.02 mg) positioned to constantly expose the surface of the sample to the heated internal environment. Following the thermal stabilization performed for 5 minutes at 20°C, to remove residual moisture and constantly oxidize the sample before the reduction phase.

Each experimental cycle began with a heating phase of the powder subjected to a nitrogen gas flow rate of 80 ml/min, heating from 20°C to 800°C with a gradient of 20 K/min.

Subsequently the sample was kept at a constant 800°C for the entire duration of the test to obtain the thermal reduction of the sample when 1 vol% H_2 is injected with consequent release of O_2. Afterwards, there is a phase where 20 vol% of CO_2 is injected in which the thermal oxidation process takes place at 800°C, and relative production of CO.

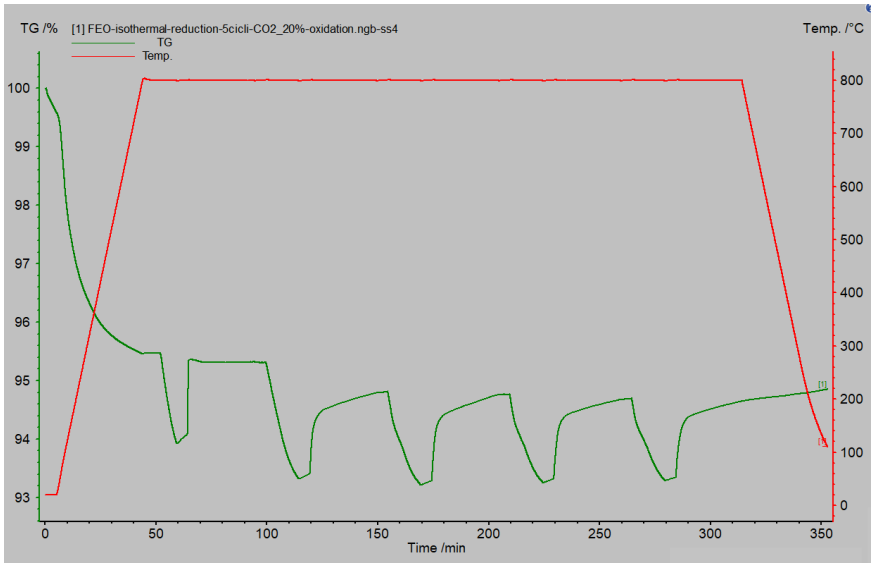

Figure 79 - Graph of the mass variation (TG) of the isothermal temperature at 800 ° C during the test

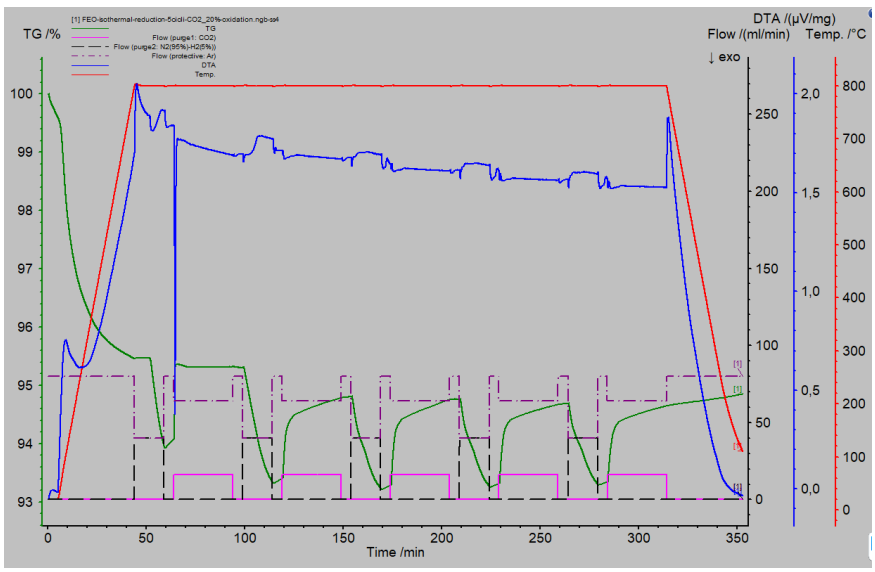

Figure 80 - TG, TGA and gas change during the test at 800°C

Below are the percentage values of the mass variation during the oxidation phase and during the reduction phase, provided by the instrument.

	Variation Mass [%]	
	Reduction	Oxidation
1	1.29951	1.41311
2	1.82509	1.1129
3	1.44023	1.15276
4	1.36565	1.07322
5	1.18769	1.06628

Table 2 - Percentage variation in mass in isothermal tests with reduction 1 vol% in H_2 and oxidation to 20 vol% CO_2

4.6.2. Experimental Test 2

The second test was conducted by carrying out an oxidation with 20 vol% of N_2/O_2 and a thermal reduction in nitrogen at 1350°C.

The sample was progressively heated from ambient temperature up to 1350°C by programming a thermal ramp of 20 K/min.

The measurements were performed using an alumina crucible (Al_2O_3) having a mass of 100 mg and filled with iron oxides powder (about 21.495 mg) positioned to constantly expose the surface of the sample to the heated internal environment. Following the thermal stabilization carried out for 5 minutes at 20°C, to remove residual moisture and constantly oxidize the sample before the reduction phase.

The experimental test began with a heating phase of the powder subjected to a nitrogen gas flow rate of 80 ml/min by heating from 20°C to 1350°C with a gradient of 20 K/min.

Subsequently, the sample was kept at a constant 1350°C for the entire duration of the test to obtain the thermal reduction of the sample resulting in the release of O_2 with only nitrogen. Following is a phase where 20 vol% of N_2/O_2 is injected in which the thermal oxidation process takes place at 1350°C, and relative production of CO.

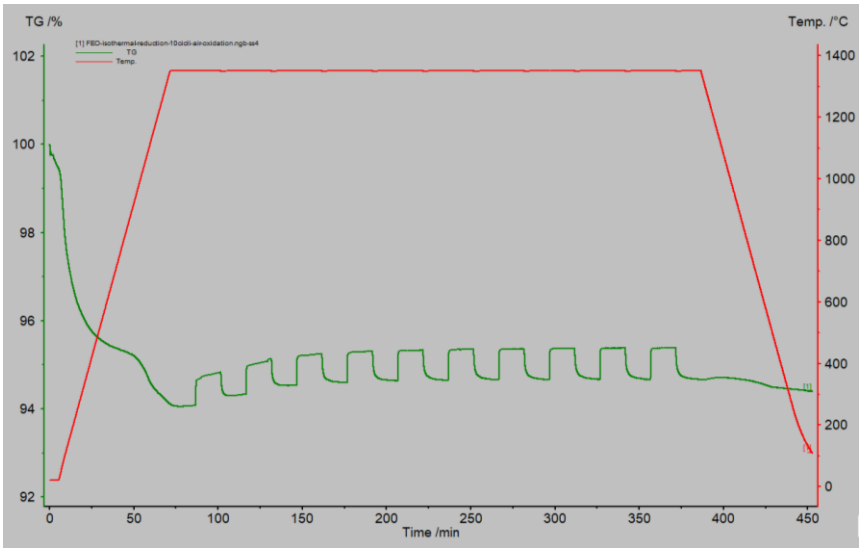

Figure 81 - Graph of the mass variation (TG) of the isothermal temperature at 1350°C during the test

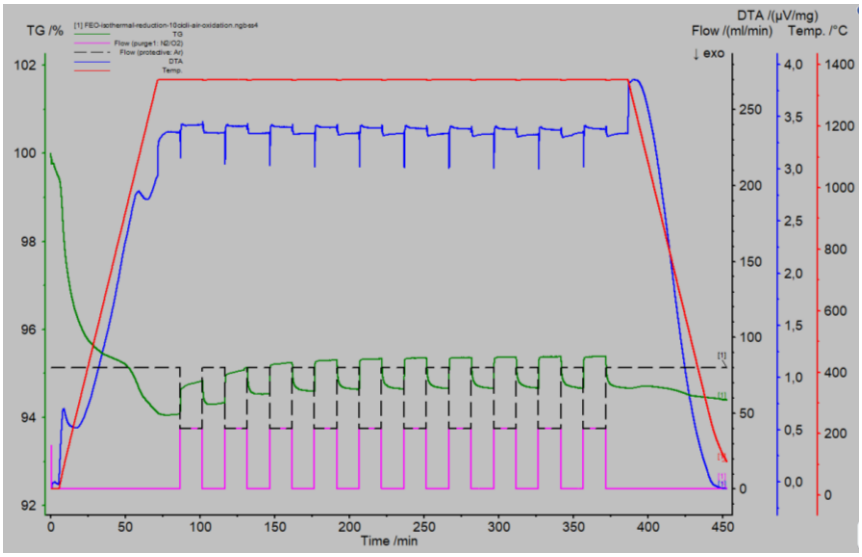

Figure 82 - TG, TGA and gas change during the test at 1350°C

The following are the percentage values of the mass variation during the oxidation and reduction phases, provided by the instrument.

	Variation Mass [%]	
	Reduction	Oxidation
1	0.9316	0.753782
2	0.51286	0.75059
3	0.52689	0.69607
4	0.61842	0.68609
5	0.68609	0.67088
6	0.67088	0.69384
7	0.67298	0.68622
8	0.68813	0.69993
9	0.6926	0.69594
10	0.6871	0.6909

Table 3 - Percentage variation in mass in isothermal tests with thermal reduction and oxidation to 20 vol% of N2/O2

4.7. Comparison of results

The two TGA tests can be compared with the test carried out in the furnace with microreactor and with the one using a boat with oxidation at 20 vol% CO_2.

To make a comparison, it is necessary to analytically calculate the mass variation that occurred with the use of the furnace, since this input is provided to us through the TGA thanks to the presence of the internal balance.

As already said before, the high temperature process heat allows to endothermically reduce the sample at high temperature and low partial pressure of O_2, producing gaseous O_2 that generate interstitial oxygen defects inside the solid phase of the material, these are called "vacancies". The empty oxygen positions are filled in the second phase, i.e. during oxidation, in which the sample is oxidized exothermally to extract oxygen from CO_2 and produce CO.

Precisely during the oxidation phase, the sample reacquires the oxygen released in the reduction step, increasing its weight in a sudden way by a value almost similar to the mass lost in the reduction, it is therefore possible to calculate the mass variation through the moles of O_2 acquired.

During oxidation we have the following reaction that describes the splitting of CO_2:

$$CO_2 \rightarrow \frac{1}{2}\, O_2 + CO \tag{4.15}$$

We already know the production rate (in $\mu mol/g/s$) we can then calculate the total specific production:

$$Total\ Specific\ Rate = \sum Rate\ production\ in\ oxidation\ phase \quad [\mu mol/g] \tag{4.16}$$

Then the mass variation will be given by:

$$Variation\ Mass = \left(\frac{1}{2} \cdot \frac{Total\ Specific\ Rate\ \cdot M_{Oxygen}}{10^6}\right) \cdot 100 \qquad [\%] \tag{4.17}$$

Where M_{Oxygen} represents the molecular weight of oxygen.

The results obtained are given in the following table:

	Variation Mass in Oxidation Phase [%]			
Cycle	*Reduction with 1% H_2, Oxidation with 20% CO_2 at 800°C*	*Reduction with N_2, Oxidation with 20% N_2/O_2 at 1350°C*	*Reduction with 5% H_2, Oxidation with 20% CO_2 at 800°C*	*Reduction with N_2 at 1350 °C, Oxidation with 20% CO_2 at 800°C*
1	1.413	0.754	5.431	0.571
2	1.113	0.751	4.995	0.096
3	1.153	0.696	4.912	0.072
4	1.073	0.686	4.808	0.069
5	1.066	0.671	4.819	
6		0.694		
7		0.686		
8		0.700		
9		0.696		
10		0.691		

Table 4 - Comparison of mass variation in different tests

Looking at the data, we see that we have greater mass variation when hydrogen is used in reduction and as the percentage of hydrogen increases, the mass also increases. When the reduction is carried out with argon alone, on the other hand, the mass variation is much less than in the previous cases and the values obtained from the test with reduction in N_2 and oxidation at 20 vol% N_2/O_2 at 1350°C and with reduction in N_2 at 1350°C and oxidation at 20 vol% CO_2 at 800°C can be considered approximately equal to each other, since they were made with two different tools and they use two different oxidants.

It is also worth noting, in all four cases shown, that the change in mass decreases as the cycle increases, this is due to the carbon deposition that accumulates from cycle to cycle and prevents the escape of oxygen to create vacancies during the thermal reduction.

4.8. Real Applications

As previously mentioned, to carry out the tests, illustrated in the previous paragraphs, an electric furnace was used which, by means of an electric resistance, provided the energy vector necessary to carry out the reduction and oxidation reactions at high temperatures. On an industrial scale, as mentioned above, this system is neither ecological nor convenient and for this reason we opt for the use of a solar reactor that can provide the energy vector necessary to make the reactions take place.

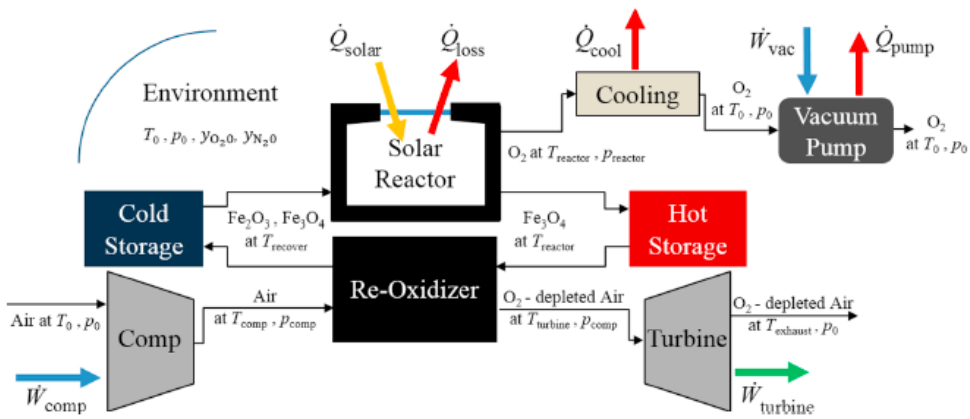

Figure 83 - System schematic of the Air Brayton cycle with an integrated two-step thermochemical energy storage cycle based on Fe_2O_3/Fe_3O_4 redox reactions with relevant mass and energy flows. [37]

The Figure 83 shows a diagram, of an Air Brayton cycle, of a chemical looping process plant that uses a solar reactor to do redox reactions on Fe_2O_3/Fe_3O_4.

The cycle uses a solar receiver/reactor which is irradiated to aid in the thermal reduction of the metal oxide particles at a temperature $T_{reactor}$. The reduced particles are then re-oxidized in a counter-current configuration with a pressurized air flow to P_{comp} supplied by a compressor High temperature and oxygen-deficient air the re-oxidant and expands through a turbine, while the re-oxidate particles are returned to the receiver/reactor to complete the cycle. [37]

Inside the Energy Center of the Polytechnic of Turin there is a solar disk concentrator to do laboratory experiments for research purposes and for temporary use that can be used to carry out chemical looping tests.

The disc parabolic concentrating system is composed of an aluminum paraboloid internally coated with a polymeric film characterized by high optical efficiency reflectivity. The plant has an automatic solar tracking system with two independent axes (azimuth and elevation) aimed at the automatic orientation of the parabolas in such a way as to receive solar radiation always with the best possible angle of incidence, developed and built entirely by El.Ma. The biaxial solar tracker allows you to orient the system for the production of energy in the direction of the sun instant by instant, by calculating the solar coordinates in real-

time according to time, date, latitude and longitude, with maximum theoretical precision (>0.015°).

The solar tracker is biaxial, i.e. it moves the two polar axes independently (azimuth and elevation), but it can be easily set to manage only one axis (azimuth for example) keeping the other fixed (constant tilt): in this case it is possible orient two different or linear parabolic concentrators with a single tracker.

The concentrator has an absorbing surface of 4.5 m^2 with an optical efficiency of 80% and an average direct radiation of 800 W/m^2, the concentrated power in optimal conditions is approximately 2.8 kW. At the fire point, temperatures above 1800°C can be reached, the ideal temperature to carry out the redox reactions in CL. [38]

Figure 84 - Solar Disk concentrator on the roof of the Energy Center

This solar disk concentrator can be used coupled with an aerosol solar reactor creating a thermochemical redox cycle for CO_2 splitting. The developed prototype consists of a cavity receiver inside which an alumina tube (Al_2O_3) is positioned vertically, crossed by a flow of solid iron particles directed downwards due to gravity. The counter-current flow that goes up the pipes is instead made up of inert gas, generally argon, to ensure the effective separation of the reduced oxides from oxygen and to reduce the thermal stress of the materials given the high operating temperatures. [39]

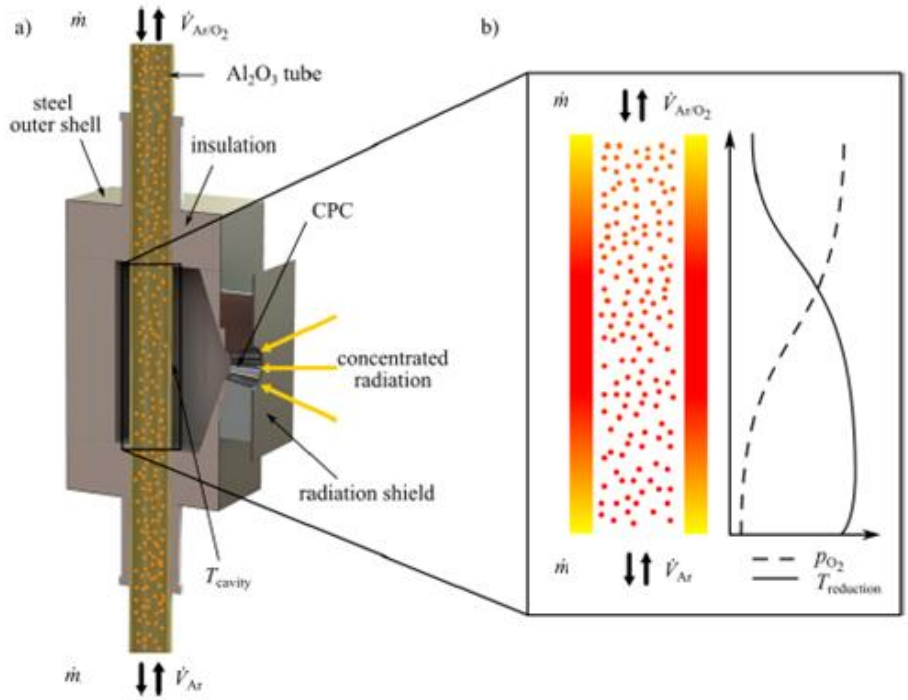

Figure 85 – a) Schematic representation of the solar receiver showing the main components and the flow rates together with a representation of the partial pressure profiles of O_2 and b) reduction temperature relating to the reaction zone [39].

5. Conclusions

Thanks to laboratory tests, it emerged that the producibility of CO is strongly linked to the oxygen exchange capacity of the iron oxide that occurs in the reduction phase. By oxidizing the Fe-based oxygen carrier with CO_2, the results have been examined to evaluate the effects of the re-oxidation conditions at different values of CO_2 concentration and temperature.

It has been possible to observe that high temperatures and CO_2 concentrations favor the oxidation of the material during repeated cycles with an increase in the CO yield, which tends to drastically decrease if a thermal reduction is carried out or a low concentration of hydrogen is used on the iron oxide. It has been shown that the yield of CO can also decrease due to the thermodynamic limitation and formation of iron carbide which leads to the deactivation of the sample, due to the sintering phenomena that occur on the material which prevent the leakage of O_2 and therefore the formation of vacancies during the reduction phase.

Wanting to obtain syngas through a Chemical Looping process, it was possible to demonstrate that it is possible to obtain it using methane as a reducing agent. In fact, reacting with the iron oxides generates CO and H_2, i.e. syngas, during the reduction phase, which can be directly used for various purposes, while during the oxidation phase very high values of the CO yield are obtained, to demonstrate as methane turns out to be an excellent reducing agent.

The only disadvantage that was found during the testing phase was the appearance of carbon residues in the material. It is possible to state, in fact, that when the oxygen carrier is treated with high temperatures and high concentrations of carbon dioxide, without the use of a gas that reduces the formation of carbon, the surface grains of the material become larger due to the process of sintering, consequently leading to the deactivation of the sample. In general, from the results obtained it is possible to observe a decrease in the yield of CO between the various cycles even when hydrogen or methane is used as a reducing agent, this demonstrates how it is impossible to avoid the formation of carbon deposition in the oxygen carrier, but it is possible to reduce its formation using suitable reducing agents.

To date, the Chemical Looping process is one of the most interesting in terms of research and development, it allows the reuse of CO_2 sequestered from the atmosphere to generate syngas which can be used to generate electricity or as fuel in cars, thus leading to creation of a closed cycle of carbon dioxide.

For the Chemical Looping process to be sustainable, there is no doubt that it must be used by coupling it to a solar concentrator to reduce the release of emissions into the atmosphere.

The costs for the construction of a Chemical Looping plant are around hundreds of thousands of euros, and the cost of H_2 and CO produced by this process is around 100 €/kg and 12 €/kg respectively. It is possible to notice how the price of hydrogen, obtained with this process, turns out to have a much higher cost than those in circulation (2-20 €/kg) where hydrogen is obtained with less sustainable processes. The estimates of these costs obtained from the CL process were carried out on plants not yet optimized and on an experimental basis for the purpose of research.

However, with the research and development of further prototypes, the goal of process optimization and cost reduction is still pursued, to make the entire system more competitive and can be designed on a large scale.

References

[1] G. Sammarco, «LA TRANSIZIONE ENERGETICA,» Editore Eni SpA.

[2] E. Montà, «Applicazioni ad alta temperatura per la realizzazione di cicli termochimici,» in *Realizzazione di processi di chemical looping e produzione di gas sintetico mediante solare termico a concentrazione*, 2020, pp. 93-120.

[3] A. B. Pittock, «Climate change matters,» in *Climate Change*, Routledge, 2005, pp. 1-15.

[4] A. B. Pittock, «Impacts: Why be concerned?,» in *Climate change*, Routledge, 2005, pp. 106-111.

[5] M. Santarelli, «Carbon capture and sequestration (CCS) processes,» in *Dispense del Corso PAES*, 2020.

[6] A. B. Pittock, «Mitigation: limiting climate change,» in *Climate change*, Routeldge, 2005, pp. 150 -155.

[7] E. F. Azharuddin, «Carbon capture and sequestration,» in *Solar-Fuels via two-steps termochemical redox cycles for power and fuel production*, 2018, pp. 20-25.

[8] G. Girardi, «Tecnologie di sequestro e cattura della CO2,» 2011.

[9] F. Nocito e A. Dibenedetto, «Atmospheric CO2 mitigation technologies: carbon capture utilization and storage,» *Green and Sustainable Chemistry,* pp. 34-43, 2020.

[10] E. F. Azharuddin, «Carbon capture and utilization,» in *Solar-Fuels via two-steps termochemical redox cycles for power and fuel production* , 2018, pp. 23-24.

[11] E. F. Azharuddin, «CO2 utilization using chemical looping processes,» in *Solar-Fuels via two-steps termochemical redox cycles for power and fuel production*, 2018, pp. 25-32.

[12] A. Lyngfelt, «Chemical-looping combustion of solid fuels – Status of development,» *Applied Energy,* pp. 1-2, 2014.

[13] N. G. a. A. S. Fanxing Li, «Mixed Metal Oxide-Based Oxygen Carriers for Chemical Looping Applications,» in *Handbook of Chemical Looping Technology*, Wiley-VCH, pp. 229-243.

[14] M. R. C. S. Christos Agrafiotis, «A review on solar thermal syngas production via redox pair-based water/carbon dioxide splitting thermochemical cycles,» *Renewable and Sustainable Energy Reviews,* pp. 10-11, 2014.

[15] E. Pirone, «STUDIO E DIMENSIONAMENTO DI UN IMPIANTO SOLARE TERMODINAMICO CON MICROTURBINA A GAS E TORRE SOLARE,» 2016, p. 23.

[16] F. Uras, «Ricevitore solare,» in *ANALISI DELLE TECNOLOGIE SOLARI TERMODINAMICHE A CONCENTRAZIONE*, 2014, pp. 44-47.

[17] H. P. G. B. M. C. D. S. K. V. V. G. Jiawei Hu, «FeO controls the sintering of iron-based oxygen carriers in chemical looping CO2 conversion,» *Journal of CO2 Utilization,* pp. 1-6, 2020.

[18] 05 Febbraio 2021. [Online]. Available: https://www.google.com/url?sa=i&url=https%3A%2F%2Fit.dreamstime.com%2Ffotografia-stock-minerale-di-ferro-image99606930&psig=AOvVaw3mm7BUk8oBfpwVEV_QHF5k&ust=1612609372824000&source=images&cd=vfe&ved=0CAIQjRxqFwoTCIC_itXR0u4CFQAAAAAdAAAAABAD.

[19] 05 Febbraio 2021. [Online]. Available: https://it.m.wikipedia.org/wiki/File:Iron(III)-oxide-sample.jpg.

[20] M. R. C. S. Christos Agrafiotis, «A review on solar thermal syngas production via redox pair-based water/carbon dioxide splitting thermochemical cycles,» *Renewable and Sustainable Energy Reviews,* pp. 260-261, 2014.

[21] 05 Febbraio 2021. [Online]. Available: https://it.wikipedia.org/wiki/Sinterizzazione.

[22] R. X. L. C. Zhong Ma, «Kinetics of sintering induced surface area decay of iron oxide in the reduction process of chemical looping combustion,» *Fuel Processing Technology,* pp. 23-25, 2017.

[23] A. M. P. P. M. D. F. A. L. S. F. J. L. M. S. A.E. Farooqui, «Assessment of kinetic model for ceria oxidation for chemical-looping CO2 dissociation,» *Chemical Engineering Journal,* pp. 1-6, 2018.

[24] «Ossidi di cerio (IV),» 06 Febbraio 2021. [Online]. Available: https://it.wikipedia.org/wiki/Ossido_di_cerio(IV).

[25] «Perovskite,» 07 Febbraio 2021. [Online]. Available: https://it.wikipedia.org/wiki/Perovskite.

[26] M. H. R. A. N. J. G.-P. F. R.-L. R. M. MH Imanieh, «Novel perovskite ceramics for chemical looping combustion application,» *Journal of CO2 Utilization,* pp. 95-104, 2016.

[27] J. L. M. S. Azharuddin E Farooqui, «Reactivity assessment and oxidation kinetic model for CO2 splitting on Fe-based oxygen carrier,» *ResearchGate,* pp. 1-10, 2019.

[28] L. Fan, «Iron-based chemical looping processes Iron-based Chemical Looping Processes CO2 Summit II : Technologies and Opportunities,» p. 113, 2016.

[29] R. B. R. S. E.R. Monazam, «Kinetics of magnetite (Fe3O4) oxidation to hematite (Fe2O3) in air for chemical looping combustion,» *Ind. Eng. Chem. Res,* p. 53, 2014.

[30] E. M. R.W. Breault, «Fixed bed reduction of hematite under alternating reduction and oxidation cycles,,» *Appl. Energy.,* p. 180–190, 2015.

[31] M. R. K.-N. A. S. Seyyed Yaghoob Hosseini, «Production of hydrogen and syngas using chemical looping technology via cerium-iron mixed oxides,» *Chemical Engineering & Processing: Process Intensification,* pp. 20-33, Marzo 2019.

[32] A. B. M. B. J. L. M. S. Azharuddin Farooqui, «Assessment of integration of methane-reduced ceria chemical looping CO2/H2O splitting cycle to an oxy-fired power plant,» *International Journal of Hydrogen Energy,* pp. 1-23, 2020.

[33] «Analisi termogravimetrica,» 12 Febbraio 2021. [Online]. Available: https://www.chimicamo.org/chimica-analitica/analisi-termogravimetrica.html..

[34] Netzsch, *STA 2500 Regulus Simultaneous Thermal Analysis - Technique, Instrument, Applications.*

[35] «Termogravimetria,» 12 Febbraio 2021. [Online]. Available: https://it.wikipedia.org/wiki/Termogravimetria.

[36] «STA 2500 Regulus,» 14 febbraio 2021. [Online]. Available: https://www.netzsch-thermal-analysis.com/it/prodotti-soluzioni/termogravimetria-calorimetria-differenziale-a-scansione-in-simultanea/sta-2500-regulus/.

[37] P. G. L. H. Evan Bush, «Solar electricity via an Air Brayton cycle with an integrated two-step thermochemical cycle for heat storage based on Fe2O3/Fe3O4 redox reactions: Thermodynamic and kinetic analyses,» *Solar Energy,* pp. 617-627, 2018.

[38] E. s. a. s. u. E. Machine, «Manuale uso e Manutenzione Concentratore Solare a Disco,» 2019.

[39] R. B. A. Z. J. R. S. e. A. S. M. Welte, «Experimental Demonstration of the Thermochemical Reduction of Ceria in a Solar Aerosol Reactor,» *Industrial & Engineering Chemistry Research,* p. 10618−10625, 2016.

[40] M. V. K. D. L.-S. F. Andrew Tong, «Chemical Looping Process Concepts,» in *Handbook of Chemical Looping Technology*, Weinheim, Germany, Wiley-VCH, 2019, p. 475.